2.1 THICKNESS OF THE SEISMOGENIC CRUST

The maximum thickness of the brittle crust (with assigned probability) is interpreted to be: 12 km (0.2), 15 km (0.7), and 20 km (0.1) (Figure RYA-1b). These depths represent the limits observed for both small- and large-magnitude earthquakes (e.g., Rogers *et al.*, 1987, 1991; K. Smith, SSC Workshop 2; Harmsen and Bufe, 1991; and Doser and Smith, 1989). The largest earthquakes in the southern Great Basin occur to depths of 20 km; smaller earthquakes tend to occur above about 10 and 12 km (with some exceptions). The assessment of seismogenic crustal depth is independent of the other source interpretations, and the ensuing source characteristics for the Yucca Mountain area depend on this quantity; therefore, the depth of the brittle crustal is the first assessment on the logic tree.

2.2 AREAL OR BACKGROUND SOURCES

The region within a 100-km radius surrounding the Yucca Mountain site has been divided into three zones, which are defined by different rates of seismicity and structural characteristics (Figure RYA-2). Zone A encloses the local Yucca Mountain area. It is characterized by low seismicity; Quaternary volcanism; northerly trending, anastomosing, and branching faults that appear to belong to the same structural domain; and a basement graben structure illuminated by a gravity low that may extend south into the Amargosa trough. Zone B, which surrounds Zone A, includes the Basin and Range and parts of the Walker Lane tectonic provinces. Seismic rates in Zone B are higher than those in Zone A. Structurally, Zone B is highly complex, consisting of mixed zones of volcanism; northerly trending, block-bounding faults; and northeast-trending, left-lateral and northwest-trending, right-lateral faults. Zone C consists of the Death Valley-Furnace Creek fault zone and faults to the west, such as the Hunter Mountain and Panamint fault zones. It is characterized by long faults having higher rates of slip than the faults of Zones A or B.

2.2.1 Recurrence

In our analysis, background seismicity was interpreted to be non-uniform or uniform. In the non-uniform case, the observed seismicity was smoothed in a manner similar to that described by Frankel (1995). This method was applied to preserve the observed spatial characteristics of the historical earthquake record while including a degree of geographical

variation through spatial smoothing. Spatial seismicity smoothing is assigned a weight of 0.6, because short-term seismicity patterns are considered good predictors of future short-term seismicity (McGuire and Barnhard, 1981). A Gaussian smoothing function was applied to the cumulative gridded earthquake counts for two correlation distances: 5 and 15 km. The relatively shorter h-values were used to retain the spatial concentrations of seismicity. We assign the highest weight to the short-wavelength smoother on the basis that the accuracy of earthquake location is closer to ± 5 km than to ± 15 km, on average (K. Smith, SSC Workshop 2; Rogers *et al.*, 1987). Smoothing was conducted within the boundaries of each source zone shown on Figure RYA-2, considered a hard boundary for the spatial smoothing model. The derived rates were used with a truncated Gutenberg-Richter recurrence relationship for earthquakes below the threshold magnitude of surface faulting, discussed below.

In the uniform smoothing interpretation (weight 0.4), Zones A, B, and C are modeled as equivalent to having faults that are distributed uniformly throughout each zone. This interpretation smooths the observed seismic rate uniformly across each zone. Hence, historical seismicity is interpreted to be spatially stationary only on a zonal basis, and individual seismic clusters are assumed to be possible anywhere within the zone. The modeled faults are distributed with a uniform 1-km spacing within Zone A so that fault spacing does not artificially induce geographic variation in the computed hazard. The faults can have any length, although the rupture areas depend on the magnitude. The square rupture patches are distributed randomly on the faults. The rupture areas are constrained below the near-surface Tertiary rocks, because we assume that faults penetrating these rocks do not store significant shear strain when slip propagates from the deeper parts of the fault toward the surface; fault segments in the Tertiary sedimentary section are modeled as passive slip without significant energy release through shaking. Hence, in the model the faults are constrained below a depth of 2 km.

The seismicity rates on faults within zones A, B, and C were calculated by fitting truncated exponential relationships (e.g., Youngs and Coppersmith, 1985) to declustered catalog versions 5 and 7 within 100 km of Yucca Mountain. In this analysis, we used the Weichert maximum likelihood method (Weichert, 1980). Earthquake aftershocks were removed from the version 5 catalog using a declustering routine developed by Youngs *et al.*, 1987;

aftershocks also were removed from the version 7 catalog using a declustering technique, termed the Veneziano method, developed for EPRI (McGuire, 1985). We give equal weight to the catalogs, because we have no basis for preferring one to the other. We determined a- and b-values from the catalogs using these techniques and the following procedures. Figures RYA-3 and RYA-4 show maps of the declustered catalogs used in our analyses. Figures RYA-5 and RYA-6 show modified Stepp plots (Stepp, 1972) used to calculate the period of complete detection and reporting of earthquakes as a function of magnitude bin. If the rate of earthquake occurrence is constant over the long term, then, as the historical period increases, these curves should approach a constant annual rate; however, if detection and reporting of earthquakes becomes incomplete as the historical period increases, these curves will show a negative slope. The point at which the slope of these curves changes from zero to negative is termed the completeness time. Based on the spacing of these curves, we judged that the earthquake magnitude range of 1.5 to 2.0 is incompletely reported for all times. Although this bin could be complete for the Yucca Mountain region, it likely is incomplete for the 100-km circle. We exclude it from our calculations for this reason. Table RYA-1 shows the preferred completeness times and the ranges we inferred from these plots. We randomly selected from within these completeness ranges the corresponding annual earthquake rate from the Stepp plots. In separate trials, we used either uniform sampling or truncated normal distributions having a mean at the preferred values and a standard deviation of five years. The randomly selected annual rates were fit with a truncated Gutenberg-Richter relationship to obtain a- and b-values for each random selection. This procedure was repeated for 200 trials. Histograms of the resulting b-values are shown on Figures RYA-7, -8, -9, and -10. These figures show that the b-values have narrow distributions; modal values for catalog 5 range from 1.08 (normal distribution) to 1.09 (uniform distribution). For catalog 7, b-values of about 1.16 (normal distribution) to 1.17 (uniform distribution) were determined. We used the uniform distribution because it expresses the greatest uncertainty, as might be expected.

The consistently higher b-values for catalog 7 may be related to less complete removal of aftershocks. Typical recurrence curves for the modal b-value are shown on Figures RYA-11 (catalog 5) and RYA-12 (catalog 7). These figures show that the fitting technique weights the low- to mid-magnitude range most heavily; the largest-magnitude bin has little influence, but it also has the fewest earthquakes and, consequently, the largest expected error in the annual rate. For each b-value bin, we can assign a corresponding a-value based on the

correlation between a- and b-values observed in the Monte Carlo simulation. This correlation is shown on Figures RYA-13 and RYA-14. Based on this analysis, we used the b- and a-value pairs and their respective probabilities shown in Table RYA-2. (Note that the bin probabilities were determined using larger bins than shown on the figures.)

A proportioning process was applied to the a- and b-value pairs for the 100-km circle in each distribution above to compute corresponding distributions for each subzone. The total number of earthquakes greater than or equal to magnitude 3 in each subzone were counted in each magnitude bin over the preferred completeness time for that bin. These binned earthquake counts were summed separately for each zone and for the 100-km circle to obtain the cumulative number of earthquakes above this magnitude for the entire zone and its subzones. The ratio of counts in each zone to the total count in the 100-km circle then was computed. These ratios were used to proportion the anti-logarithm of the a-values, given above, to obtain cumulative earthquake counts for each subzone. The corresponding b-values and probability levels are carried along with their proportioned a-values. These proportioned counts and corresponding b-values were used to compute truncated recurrence relationships for each subzone.

2.2.2 Maximum Magnitude

We interpret background earthquakes to be caused by ruptures that do not intersect the Earth's surface. Based on the work of S. K. Pezzopane and T. E. Dawson (USGS, written communication, 1996), Pezzopane (SSC Workshop 3), and dePolo (1994), we consider the maximum background earthquake magnitude to be Mw = 6.3 ±0.3. We use weights (0.185, 0.63, and 0.185) to simulate the 5th percentile, mean, and 95th percentile in a normal distribution.

2.3 LOCAL FAULT SOURCES

Within Zone A (the local Yucca Mountain area), we consider three alternative structural models: pure planar faults that behave independently, faults that lie above a detachment or zone of decoupling and respond passively to slip on a buried fault, and faults that are planar to listric but that coalesce downdip. In the planar fault model, each fault identified at Yucca Mountain is considered seismogenic and is modeled as an independent seismic source that exists from the surface downdip through the entire seismogenic crust. In the detachment or

decoupled model, the surface faults could be seismic sources, but they more likely represent a relatively passive response to earthquakes occurring on buried sources below the detachment. In the coalescing fault model for Yucca Mountain, individual faults mapped at the surface are assumed to merge or coalesce downdip and along strike and, as such, to operate as a group or groups of faults in generating earthquakes. Various groups of faults, therefore, are considered synchronous seismic sources (Figure RYA-1b).

The coalescing model is our preferred model because it is the only one that appears to account for most of the spatial and temporal fault characteristics at Yucca Mountain; that is, the close fault spacing, the merging and bifurcating of faults, and the very short mapped length for some faults that have large single-event displacements. Further, the coalescing fault model explains the apparent synchroneity of faulting on multiple Yucca Mountain faults at about 70 ka (i.e., the ash event; S. K. Pezzopane *et al.*, USGS, 1996a; Figure RYA-15). In the planar fault model, this apparently synchronous event would be considered the result of the coincidental rupture of multiple, independent faults, some of which are relatively short. We do not consider this interpretation to be geologically plausible. Some investigators have discussed the possible presence in the Yucca Mountain area of a buried strike-slip fault or a seismogenic detachment fault (e.g., Wernicke, 1995; Scott, 1990; Schweickert and Lahren, 1997; J. Bell and R. Schweickert, SSC Workshop 3; Wernicke, SSC Workshop 4). In these models the faults above a detachment or zone of decoupling may be seismogenic or nonseismogenic, and the primary seismogenic source(s) lie below the detachment or zone of decoupling. Such models commonly require unlikely fault geometry, such as a long but narrow fault, produced because the fault is constrained below a detachment and above the brittle-ductile boundary. Furthermore, our coalescing sources include as end members both the independent fault treatment and the fault truncation-detachment model. Hence, we eliminated these models and included only the coalescing sources in our logic tree.

2.3.1 Coalescing Fault Structure

Seismogenic fault sources are defined as faults capable of generating earthquakes of magnitude ≥ 5. Criteria for evaluating whether a fault is seismogenic include evidence for Quaternary displacement, a minimum length of 5 km measured along scarps of equivalent age, paleoseismic displacements of at least tens of centimeters (i.e., not a cracking event), and a possible spatial association of the fault with observed seismicity. The primary independent

seismogenic sources considered for Yucca Mountain are the Windy Wash, Solitario Canyon, and Paintbrush Canyon faults (Table RYA-3). The Fatigue Wash, Iron Ridge, Bow Ridge, and Stagecoach Road faults are not considered independent sources because of their short lengths and spatial association to other nearby faults. The maximum northern extent of the Paintbrush Canyon fault is taken from the map of Frizzell and Shulters (1990). For the Solitario Canyon and Windy Wash faults, the northern extent is taken to be the bedrock ridge south of Yucca Wash (Simonds *et al.*, 1995; A. R. Ramelli and J. W. Bell, Nevada Bureua of Mines and Geology, written communication, 1997). The maximum southern extent of the Windy Wash and Stagecoach Road faults is taken from A. R. Ramelli and J. W. Bell (Nevada Bureau of Mines and Geology, written communication, 1996). The lack of Quaternary geomorphic expression in Amargosa Valley suggests that the Yucca Mountain faults do not extend south of the Lathrop Wells cone.

The Crater Flat fault system is not considered a seismic source because of the short lengths of its features and the absence of significant mid- to late Quaternary displacement on those features (see S. K. Pezzopane *et al.*, USGS, written communication, 1996a). Further, the short distance between the Crater Flat faults and the faults of the Windy Wash system suggest that the Crater Flat faults are antithetic to the Windy Wash system.

Except for the Bare Mountain (BM) fault, all the faults near Yucca Mountain are interpreted to merge downdip at relatively shallow depths (2 to 5 km) and to rupture in groups of two or more faults during individual earthquakes. The groups of faults therefore are considered to represent individual seismic sources, with the Paintbrush Canyon (PBC), Solitario Canyon (SC), and Windy Wash (WW) faults representing the primary seismogenic structures in the three-fault system (Figure RYA-16). The combinations of faults in each group are shown in the logic tree and in Tables RYA-4, RYA-5, and RYA-6.

The Bare Mountain fault always behaves independently in this model, although synchronous, secondary fault rupture could occur on some of the westernmost faults at Yucca Mountain, such as the Windy Wash. Faults in the Yucca Mountain site vicinity are considered to coalesce at depth, forming one to three groups. The branch in the logic tree that represents only one group of faults is assigned a relatively low weight (0.1 to 0.3 depending on crustal thickness) because of the large spacing between the faults (10 km across all of the mapped

faults). Given their steep dips at the surface, it appears unlikely that all the faults coalesce downdip into a single structure within the 12 to 20 km thickness of the seismogenic crust. If they did, the Paintbrush Canyon fault (PBC) would be the primary rupture source in this interpretation. The principal evidence favoring a single group of faults is the apparent contemporaneous surface rupture among several faults, which is represented by the 70-ka ash event. On the branch that has two fault groups, the east group is composed of the Paintbrush Canyon (PBC)-Stagecoach Road (SR)-Bow Ridge (BWR) faults (Paintbrush Canyon fault is primary rupture source); the west group consists of the Windy Wash (WW)-Fatigue Wash (FW)-Solitario Canyon (SC)-Iron Ridge (IR) fault systems (Solitario Canyon fault being the primary rupture source). On the branch that is composed of three groups, the east group is PBC-SR-BWR, and the west side of Yucca Mountain comprises two groups, WW-FW and SC-IR.

We consider the faults at Yucca Mountain to coalesce at variable depths. This assessment is based on the pattern of fault spacing shown on maps and geologic cross sections that suggests that many of the Yucca Mountain fault systems intersect at some depth. Coalescing faults can be modeled by allowing each mapped fault trace to intersect the master fault(s) at some depth. We assume that for magnitudes smaller than the maximum, the rupture patch is distributed uniformly on each individual fault combination. For example, a magnitude 6 rupture patch on the east fault group could occur on the Paintbrush Canyon-Stagecoach Road combination or the Paintbrush Canyon-Bow Ridge combination with equal probability; however, for the maximum magnitude (M_{max} ±1/4), we consider that all faults in a group undergo slip.

The Ghost Dance fault has no record of displacement in the past approximately 400 ka. Because of its location within the Yucca Mountain block, its short length, and its lack of Quaternary geomorphic expression, it is not considered a seismogenic source; however, the fault may experience secondary faulting or fracturing. This is discussed in Section 3.

2.3.2 Maximum Magnitude Approach

Several alternative approaches and data sets were considered to assess the maximum magnitude of each local fault source (Wells and Coppersmith, 1994; Mason, 1996; Anderson *et al.*, 1996). We used the Wells and Coppersmith regressions because: (1) the Mason data

are considered more appropriate to the longer faults of the northern Basin and Range (30 to 50 km); and (2) the approach of Anderson *et al.* is untested. In addition, many of the low slip-rate faults used in the analysis of Anderson *et al.* (1996) are thrust faults in Japan. We evaluated maximum magnitudes using rupture length (RL) and rupture area (RA) from the regressions of Wells and Coppersmith (all fault slip styles; the difference between magnitudes for all slip styles versus normal slip faults is small, and more data are used in the regressions for all slip styles), as these are the parameters that have been or can be measured with some confidence. The regressions for RA and RL have smaller standard deviations than the relationships for maximum and average displacement; the range in magnitude value for any measured displacement is approximately ± 1.0 magnitude unit. The displacement relationships also tended to produce unreasonably high stress drops for the shorter faults. For these reasons, we did not use magnitudes based on maximum and average displacement. We give weights of 0.5 each to RA and RL magnitude estimates, because we have no basis for preferring one relationship over the other.

Computation of the maximum magnitude from the fault area relationship of Wells and Coppersmith (1994) was complicated by variability in downdip fault width. Fault width is dependent on the depth of the seismogenic crust, fault dip, and the depth of intersection with the Bare Mountain fault. We calculated the extreme and preferred fault widths based on the extreme and preferred fault dips both for Bare Mountain faults (55, 60, and 65 degrees) and Yucca Mountain faults (60, 67.5, and 75 degrees), and the extreme and preferred depths for the seismogenic crust (12, 15, and 20 km). The middle of each range is the preferred value. Fault width was taken as the downdip distance to the seismogenic zone or the Bare Mountain fault, whichever was shortest. The extreme and preferred magnitudes computed from these widths are shown in Tables RYA-3, 4, and 5. (Note that the PSHA analysis uses the full distribution for fault dip, crustal thickness, and maximum rupture length to develop the distribution for maximum magnitude). Because of the uncertainties in assessing maximum magnitude, we consider the magnitudes computed from the various empirical relationships to be uncertain by ±0.5 magnitude units. The ±0.5 magnitude values are considered to represent 5- and 95-percentile values. The assigned weights are 0.63 assigned to the estimate from the empirical relationships and 0.185 assigned to the ±0.5 magnitude values, which are the appropriate weights for a three-point representation of a normal distribution (Keefer and Bodily, 1983).

2.3.3 Recurrence Approach

We assessed earthquake recurrence rates for each local fault source based on trench data (time between events) (Figure RYA-15) and on fault slip rate information and average displacement values from USGS (written communication, 1996). We give a higher weight to the slip rate (0.7) than to recurrence interval (0.3) because use of recurrence alone appears to overestimate the total slip in the Yucca Mountain area. Slip rates and their associated uncertainties are provided in Tables RYA-3, -4, -5, and -6. We consider slip of greater than 20 cm to represent earthquake occurrence at or above the threshold magnitude for surface faulting. The seismicity on mapped faults was modeled separately with both truncated-exponential (e.g., Anderson, 1979; Youngs and Coppersmith, 1985) and characteristic recurrence relationships (Schwartz and Coppersmith, 1984). The relative weights given to the two recurrence models depend on the degree to which we consider the faults to coalesce; i.e., greater coalescence suggests that the faults behave in a more exponential manner. Thus, for the one-fault system model the exponential model was given a weight of 0.9, whereas it was given 0.1 for the characteristic model. More weight was given the characteristic model in the two-fault system (0.3) and three-fault system (0.5) models. For the characteristic model, the maximum magnitude is considered to lie uniformly in the range M_{max} -1/2 to M_{max}.

2.4 POSSIBILITY OF A BURIED SEISMIC SOURCE

Within the resolution of the data, we consider it possible that a seismic source (possibly strike-slip), buried beneath cover rocks and with no direct surface manifestation, exists within Zone A; however, we conclude that this source is incapable of generating an earthquake larger than the background earthquake, or an earthquake larger than that produced by any other source

considered. Such a buried source, if it exists, is decoupled from surface faults, in that faults at depth may behave differently from faults near the surface, and the boundary between these different faulting styles may be anything from a simple low-angle fault to a zone of transition between passive and active faulting. This region of decoupling, whether a simple plane or a thicker zone, is not considered a seismic source. The surface faults above the decoupled boundary, thought to be seismic sources in the coalescing model discussed above, here are considered nonseismogenic, responding passively to earthquakes generated along a buried, near-vertical source.

The principal evidence for the decoupled structural model is the discrepancy between the earthquakes recorded in the Yucca Mountain region that have normal focal mechanisms at shallow crustal levels and those that have the more common strike-slip mechanisms recorded at depth. Further, megaton nuclear tests at Pahute Mesa produced normal faulting at the ground surface (Bucknam, 1969; McKeown and Dickey, 1969; Maldonado, 1977a, b; Orkild *et al.*, 1969; Snyder, 1971, 1973; Morris, 1971), but modeling of the ground motions from these tests (Aki and Tsai, 1972; Aki *et al.*, 1969; Lay *et al.*, 1984; Wallace *et al.*, 1983, 1985, 1986) indicated energy release consistent with right-lateral slip on north-trending faults at depth. Additional evidence is provided by geologic mapping in the Specter Range east of Yucca Mountain (Burchfiel, 1965), which shows a structural style in the Paleozoic cover that is interpreted as deformation above a buried strike-slip fault.

Two depths of decoupling (5 and 10 km) are considered. The shallower depth is considered a minimum for decoupling, because the seismic reflection data indicate that upper crustal, high-angle faults penetrate beneath the Paleozoic-Tertiary contact at least to this level. Also, the upper depth limit of aftershocks from the Little Skull Mountain earthquake was approximately 5 km (K. Smith, SSC Workshop 2). The greater decoupling depth is considered the maximum that might produce a significant buried earthquake, given the thicknesses considered for the seismogenic crust.

Estimates of M_{max} for the buried source are derived from the rupture area versus maximum magnitude relationship developed by Wells and Coppersmith (1994). Length of the buried source is considered to be 30 km. Thirty kilometers, which is slightly greater than the maximum fault lengths for the main faults at Yucca Mountain, is approximately the length of the north-trending gravity gradients that bound either side of the Amargosa trough. Fault width is estimated by the limits set by the various combinations of seismogenic crustal thickness at depth of decoupling (Table RYA-7). The buried source is considered to have vertical dip.

A 30-km-long buried source would produce an earthquake having a magnitude at or above the background magnitude of 6.3 ±0.3 only for a decoupling depth of 5 km and a thick (20-

km) seismogenic crust. We conclude, therefore, that a buried source is adequately included in our interpretation of the background source and the coalescing fault sources.

2.5 VOLCANIC SOURCE

The eruption of basaltic volcanoes in the site vicinity may be associated with seismicity. Based on observed eruptions within similar volcanic fields, we assess the probability that a volcanic source exists to be 0.7. This seismic source is assessed to be independent of the other seismic sources. The spatial location of future volcanic seismic sources and the recurrence rate are taken from the results of B. M. Crowe *et al.* (LANL, written communication, 1995). Of the numerous results described by B. M. Crowe *et al.* (LANL, written communication, 1995), return periods of 2×10^{-5} to 2×10^{-6} are preferred. The maximum magnitude associated with a volcanic eruption is assessed based on the studies by S. M. Jackson (INEL, written communication, 1994), which consider the largest observed earthquakes associated with the intrusion and eruption of small- to moderate-volume basaltic magmas. An upper limit of $M_{max} = 5.5$ is used based on this work.

2.6 REGIONAL FAULT SOURCES

Eleven regional fault sources in Zones B and C (Figure RYA-17) are identified primarily through our analysis of the data in Piety (1994) and Anderson *et al.* (1995a, b; See Table RYA-8). The eleven sources we identified are considered relevant due to their distance to Yucca Mountain, their length, high slip rates, evidence for late Quaternary surface rupturing earthquakes, or because they have not been studied in enough detail to preclude or adequately characterize their Quaternary activity (i.e., Wahmonie or Cane Spring faults). Several of the faults that H. L. McKague *et al.* (CNRWA, written communication, 1996) consider Type I faults (for example, Keane Wonder, Oasis Valley, Rocket Wash-Beatty Wash, Sarcobatus Flat, and Kawich Range) are not considered relevant to our analysis because of their short length, distance from Yucca Mountain, and studies such as those by Anderson *et al.* (1995a, b) that show that some of these faults either have no significant Quaternary displacement or are much shorter than previously thought. In addition, the so-called Carrara fault (memoranda from D.B. Slemmons, February 3 and 16, 1997, to R. Quittmeyer) is not considered a potential seismic source. Interpretation of aerial photographs and

reconnaissance geologic mapping by L.W. Anderson (unpub. mapping) found no evidence of late Quaternary fault activity in the area of the suspected fault. Our interpretation is that the features cited as evidence for Quaternary fault activity are instead normal fluvial terraces and terrace scarps produced by the southeast-flowing streams that drain the south flank of Bare Mountain (also see mapping of Swadley and Carr, 1987).

Faults within Zones B and C are considered to have the simple planar shape, with downdip widths that penetrate to mid-crust. The faults are assumed to be either near vertical (faults that display primarily strike-slip displacement) or steeply dipping (~60°; faults that display primarily normal or dip-slip displacement). For computing fault rupture areas, we have assumed a 15 km thick seismogenic crust. Estimates of surface rupture length, maximum displacement per event (if available), and slip rate are from the work of Piety (1994), Anderson *et al.* (1995a, b), R. E. Klinger and L. A. Piety (USBR, written communication, 1996), and J. A. Coe *et al.* (USGS, written communication, 1996).

2.6.1 Maximum Magnitude Approach

Empirical relationships developed by Wells and Coppersmith (1994) between magnitude and fault length, fault area, and maximum fault displacement (if available) were used to estimate the maximum magnitudes for the regional faults (Table RYA-8). Equal weights were applied to the computed magnitudes. That is, when three magnitudes were computed, weights of about 1/3 were used and when two magnitudes were computed, weights of 1/2 were used. As was done for the local faults, we consider the magnitudes computed from the various empirical relationships to be uncertain by ±0.5 magnitude units, representing 5- and 95-percentile values.

2.6.2 Recurrence Approach

The slip rates in Table RYA-8 were converted to estimated seismic recurrence rates using estimated displacement per event [the methods indicated by Anderson (1979) and Youngs and Coppersmith (1985)], and using an average b-value from the two catalogs of 1.12 (0.63), with 5 percent and 95 percent distribution values of 1.07 (0.185) and 1.20 (0.185), respectively, based on the distributions developed above.

3.0
FAULT DISPLACEMENT CHARACTERIZATION

3.1 INTRODUCTION

Two types of fault displacement are of potential concern to the Yucca Mountain Controlled Area (the proposed repository block and the associated access and waste handling facilities): (1) **principal** (or primary) faulting and (2) **distributed** (or secondary) faulting. Principal faulting is defined as the displacement along the main fault plane (or planes) responsible for the release of seismic energy during an earthquake. When the fault rupture extends to or near the ground surface, displacement may be represented by a zone of deformation up to several meters wide with measured amounts of fault offset (slip) ranging from several tens of centimeters to several meters. The amount of slip is dependent on the location along the fault and the magnitude of the earthquake. Within the site area, two possible sources of primary faulting have been identified, the Solitario Canyon-Iron Ridge fault system and the Paintbrush Canyon-Stagecoach Road-Bow Ridge fault system (Figure RYA-16 and Table RYA-4).

Distributed faulting is defined as displacement (measured slip as opposed to fracturing; based on our personal experience in the Yucca Mountain area, with the presence of suitable stratigraphic horizons, the uncertainty in the measurement of displacement or non-displacement is about $\pm$ 2.5 cm - anything less than that is essentially zero) that occurs on adjacent or nearby faults (or fractures) in response to an earthquake on another fault. If it occurs at all, distributed faulting is by nature discontinuous and can occur up to several kilometers from the principal fault rupture. Several factors influence the occurrence or non-occurrence of secondary faulting along a pre-existing fault or fracture (S. K. Pezzopane and T. E. Dawson, USGS, written communication, 1996; H. L. McKague *et al.*, CNWRA, written communication, 1996). Among them are: (1) location with respect to the principal fault rupture (hanging wall verses foot wall; (2) fault orientation; (3) sense of previous slip; and, (4) distance to the principal fault rupture or earthquake epicenter. A primary fault also can

undergo distributed displacement or fracturing in response to a nearby earthquake. Paleoseismic trench data probably cannot differentiate between principal and distributed faulting except by size of the measured displacement. However, we believe that displacement from a distributed event will always be smaller than that from a primary event. In our team's review of the Yucca Mountain paleoseismic data (Figure RYA-15), we considered all events in the trenches with less than 20 cm of displacement to represent "cracking" events. Thus, our interpretation is that most of these cracking events are the probable surface representation of distributed faulting events due to strong ground shaking.

The teams were asked to characterize fault displacement potential at nine sites within the controlled area of Yucca Mountain. The nine sites are located:

(1) Along the Bow Ridge fault where it crosses the ESF;

(2) Along the Solitario Canyon fault near the proposed repository block;

(3) Along the Drill Hole Wash fault where it crosses the ESF;

(4) Along the Ghost Dance fault;

(5) Along the Sundance fault west of the ESF;

(6) On a minor unnamed fault west of Dune Wash;

(7) 100 m east of the Solitario Canyon fault that has:

a. a small fault with 2.0 m cumulative slip;
b. a shear with about 10 cm of cumulative displacement;
c. a fracture having no measurable displacement; and
d. intact rock;

(8) Midway between the Solitario Canyon and Ghost Dance faults that has:

a. a small fault with 2.0 m cumulative slip;
b. a shear with about 10 cm of cumulative displacement;
c. a fracture having no measurable displacement; and
d. intact rock; and

(8) Along the Exile Hill fault in Midway Valley.

Two of the study sites (1 and 2) are on faults which are considered to be primary fault sources in our assessment of seismic sources. For the other 7 sites, all are considered to be potential sites for secondary displacement because of their location within an area of Quaternary faulting. However, the relative probability of activity is weighted depending on whether there is evidence for Quaternary (past 1.6 million years) activity associated with the feature, the known length of the feature, amount of total post-Tiva Canyon bedrock displacement, the orientation of the feature, whether there is an existing fault or fracture, or whether the site is on intact bedrock.

3.2 APPROACH

For either primary or secondary displacement, an assessment of the probability of fault displacement requires an assessment of the frequency of occurrence and the amount of displacement if it occurs. The fault displacement hazard at any location can be characterized in terms of the expression:

$$\nu(d) = P(C) \cdot \lambda_{DE} \cdot P(D_E > d) \qquad (1)$$

where $P(C)$ is the probability that the feature can slip in the present tectonic regime, δ_{DE} is the frequency of occurrence of displacement events on the feature, and $P(D_E > d)$ is the probability that a displacement event will exceed a slip of d. The general logic structure for characterizing the parameters of Equation (1) is shown on Figures RYA-18 and RYA-19. Figure RYA-18 shows the approaches appropriate for sites where Quaternary data are available for frequency and size of displacement events and Figure RYA-19 shows the approaches appropriate for sites where paleoseismic data are absent. The components of these approaches are discussed below.

3.2.1 Probability Slip can Occur

The probability that slip can occur on a feature in the present tectonic regime is assessed based on the evidence for recency of slip on the feature and its relationship to the structural elements of Yucca Mountain.

3.2.2 Frequency of Displacement Events

Two approaches are considered for the assessment of the frequency of displacement events: the paleoseismic recurrence intervals and the long-term fault slip rate. For sites where paleoseismic data are available, we believe that the displacement hazard at any of the various sites within the Controlled Area can best be assessed using paleoseismic data for recurrence rates (intervals) (Figure RYA-18). The alternative approach for such locations is to use the estimates of Quaternary slip rates and compute the frequency of displacement events using the expression:

$$\lambda_{DE} = SR / \bar{D}_E \qquad (2)$$

where SR is slip rate and $\bar{D}_E$ is the average displacement per event. This approach is given a weight of 0.2. The procedures used to assess the average displacement per event are described below in Section 3.2.4.

For those sites where direct paleoseismic data is lacking, a slip rate approach is used with a weight of 1.0 (Figure RYA-19). The slip rates are estimated from the total slip of the fault since eruption of the Tiva Canyon Tuff (12.7 ± 1.3 Ma).

Without paleoseismic data or total slip information; i.e., for sites located on fractures showing no displacement or for sites located in unfractured rock, a negligibly low probability of displacement is considered. We consider that: (1) displacement from a future earthquake will be in the same sense as shown by slip indicators from the last displacement event; and (2) displacement on a fault will be confined to the fault's present length; that is, faults do not generally increase in length with each new event.

3.2.3 Estimation of Slip Rate

For those locations where data are available to estimate Quaternary slip rates, these rate estimates are used to assess displacement event frequency (Figure RYA-18). For bedrock faults that either lack specific evidence for Quaternary slip or have no specific paleoseismic data, but that show post-Miocene (post-Tiva Canyon Tuff) displacement, three alternative approaches are considered for assessing the fault slip rate (Figure RYA-19). In the first approach, the total measured cumulative post-Miocene slip is divided by the age of the Miocene rocks (12.7 Ma) . This assumes a uniform slip rate through time. However, the tectonic history of the region suggests that the assumption of uniform rate over time is incorrect. Many data indicate that extensional deformation in the region has waned with time. Therefore, the assumption of uniform slip rate is given a low weight of 0.1. A second alternative is to develop a slip history that follows Fridrich *et al.*'s (1997) regional extensional history. Their analysis suggests that nearly all the regional extension was accomplished in the Crater Flat region by 11 Ma, leaving only small additional extension during Quaternary time. We estimate that 2 percent of the regional extension occurred during the past 1.6 Ma, which is consistent with Fridrich *et al.*=s interpretation. Using this approach, a slip rate for the Quaternary period is calculated on representative faults, applying 2 percent of the observed cumulative slip to estimate the Quaternary rates. This approach is given a weight of 0.6, because it accounts for what appears to be the waning tectonic activity in the region. In a third approach, the time history of Fridrich *et al.* is modified to account for the onset of volcanism in Crater Flat beginning at about 3.7 Ma. This volcanic episode may indicate an increase in tectonic rates in the region since mid-Pliocene. We allow for 20 percent of the measured fault slip to occur within the past 3.7 Ma (weight of 0.3).

3.2.4 Estimation of Average Slip Per Event

For sites where paleoseismic data are available, the average slip per event is estimated from these data (Figure RYA-18). For faults without direct paleoseismic data, analogies to other faults both locally and world wide must be made. The AAR Team at Workshop 6 (June

1997) presented data relating average displacement, $\bar{D}_E$, to total fault length, L or cumulative fault displacement D_{cum}. The AAR Team reanalyzed the data and developed new relations in their draft summary in terms of parameter MD^{max} (the expected maximum displacement in a maximum event). These relationships are:

$$MD^{max} = 1.32 \times 3.69 \times 10^{-5} \times L \text{ (in m)} \quad \textbf{(3)}$$

and

$$MD^{max} = 1.32 \times \beta \times D_{cum} \text{ (m)} \quad \textbf{(4)}$$

where β is a constant that varies for smaller faults (L < 3 km and Dcum < 75 m) between 1.40×10^{-3} (weight of 0.3) and 1.85×10^{-2} (weight of 0.3) with their preferred value of 5.59×10^{-3} (weight of 0.4). For faults with L >3 km and Dcum > 75 m, $B = 1.40 \times 10^{-3}$. We find these results to be reasonable and adopt them to characterize the uncertainty in estimating MD^{max}. They also find that the mean value of $\bar{D}_E / MD^{max} = 0.83$. Thus, to find an estimate of $\bar{D}_E$ simply multiply relations (3) and (4) by 0.83.

$$\bar{D}_E = 0.83 \times 1.32 \times 3.69 \times 10^{-5} \times L \text{ (in m)} \quad \textbf{(5)}$$

and

$$\bar{D}_E = 0.83 \times 1.32 \times \beta \times D_{cum} \text{ (m)} \quad \textbf{(6)}$$

We adopt these approaches for our assessment of sites without paleoseismic data (Figure RYA-19) and give equal weight to the assessments based on the length of the fault, (5) and the cumulative offset (6).

3.2.5 Distribution for Displacement Per Event

Trenching data from Yucca Mountain indicate that displacement per event on a fault varies greatly both at individual sites and along strike (see Figure RYA-15). Recurrence intervals between earthquakes or displacement events also vary greatly. We consider two approaches for assessing the distribution for slip per event. Both approaches are based on analyses of data from trenching studies at Yucca Mountain.

The Doser-Fridrich-Swan (DFS) team developed a distribution for the ratio of $D/\bar{D}_E$ by normalizing data from each trenching site by the average displacement at that location. Figure RYA-20 shows the resulting empirical distribution. The Facilitation Team analyzed these data and indicate that a good fit is obtained by a gamma distribution (see Appendix H, Section H.2.1). We adopt the distribution given in Appendix H for $D/\bar{D}_E$. The Arabasz-Andreson-Ramelli (AAR) team normalized the displacement data by the estimate of MD^{max} for each fault and observed that the ratio of D/MD^{max} could be represented by the exponential distribution shown on Figure RYA-21. We consider these two approaches to be equally applicable to assessing the variability in displacement from event to event and give them equal weight (Figures RYA-18 and RYA-19).

3.3 DATA FOR CHARACTERIZATION OF DISPLACEMENT HAZARD AT THE NINE TEST CALCULATION SITES

Site 1 - Bow Ridge fault where it crosses the ESF

The Bow Ridge fault is about 7 km long and is both a site for primary and secondary faulting as the fault is interpreted to be a splay of the Paintbrush Canyon- Stagecoach Road fault system. Given the evidence for Quaternary displacement, the probability of activity is considered 1.0. Cumulative slip estimated at site 1 is about 100 m (USGS, written communication, 1996, chapter 2). Paleoseismic information (Figure RYA-15) from trenches near site 1 indicate that the average recurrence for surface rupturing, displacement events is

about 75 ka (Table RYA-3) and the Quaternary slip rate for the fault is estimated to be 0.003 mm/yr. Using the Quaternary slip rate and recurrence information yields a average displacement value of 22.5 cm which is just larger than the 20 cm value we use as a break between faulting and cracking events (Table RYA-5). The trench data also indicate that the average displacement is about 21 cm, but the largest measured displacement is 44 cm in one trench (T-14D) and there was only fracturing observed in another nearby trench (T-14). The 44 cm value is our preferred maximum displacement from paleoseismic data. Relation (4) suggests that the maximum displacement for the Bow ridge fault could be about 18 cm whereas relation (3) indicates 34 cm. Relation (7) using the 1.73 factor indicates 49 cm, and relation (6) using the 1.73 factor suggests 26 cm for maximum displacement. The resulting parameters are

$P(C) = 1.0$
$SR = \{0.001 \text{ mm/yr } (0.15), 0.003 \text{ mm/yr } (0.7), 0.006 \text{ mm/yr } (0.15)\}$
$RI_{DE} = \{25 \text{ ka } (0.15), 75 \text{ ka } (0.7), 140 \text{ ka } (0.15)\}$
$\bar{D}_E = \{21 \text{ cm } (1.0)\}$
$MD^{max} = \{44 \text{ cm } (1.0)\}$

Site 2 - Solitario Canyon fault near the proposed repository block

The Solitario Canyon fault is one of the major block bounding faults at Yucca Mountain and is both a primary and a secondary fault displacement source because of the evidence for Quaternary displacement events. Therefore, the probability of activity is considered 1.0. Paleoseismic information (Figure RYA-15) indicates that the recurrence for surface rupturing events (displacement > 20 cm) ranges between 50-130 ka with a preferred value of 75 ka (Table RYA-3). However, a fracturing event that could be the result of secondary faulting apparently occurred on the fault about 25 ka. The paleoseismic Quaternary slip rate for the fault is estimated to be 0.01 mm/yr, and the post-Tiva Canyon cumulative slip estimated at site 2 is 230 m (estimated from cross section of W.C. Day *et al.*, USGS, written communication, 1996a). Although we generally prefer the 2% rule for calculating the Quaternary slip rate, the Solitario Canyon fault is the one fault we know of for which a large difference exists between the paleoseismic Quaternary slip rate estimate and the calculated

Quaternary rate. This suggests, at least for the Solitario Canyon fault, that there has been an increase in activity in the last 2-4 Ma. Be that as it may, we have used the paleoseismic Quaternary slip rate and recurrence information to calculate an average displacement value of 75 cm. Also, our analysis of data in U.S.Geological Survey (written communication, 1996) and shown in Figure RYA-15 indicates that the average displacement is about 75 cm from four trenches. However, at T-4, just to the south of the test site, the displacement during the last event was 30 cm. Since site 2 is near the northern end of the fault where displacement appears to be dying out, one would expect the average slip per event to be less than it is to the south. In addition, the slip rate also is probably less than the 0.01 mm/yr used in the calculations. Relation (4) suggests a maximum displacement of 43 cm, and relation (3) suggests 88 cm. The resulting parameters are:

$P(C) = 1.0$
SR = {0.005 mm/yr (0.15), 0.01 mm/yr (0.7), 0.02 mm/yr (0.15)}
RI_{DE} = {50 ka (0.15), 75 ka (0.7), 130 ka (0.15)}
$\bar{D}_E$ = {30 cm (1.0)}
MD^{max} = {75 cm (1.0)}

Site 3 - Drill Hole Wash fault where it crosses the ESF

The Drill hole Wash fault is considered a possible source for secondary fault displacement only. Although there is no direct paleoseismic information for the fault, given the apparent lack of evidence for Quaternary activity and the northwest strike , the probability of future slip is considered low (0.1). Available information (W. C. Day *et al.*, USGS, written communication, 1996a) indicates that the fault is about 4 km long with maximum displacement of 15 m. Thus, the estimated Quaternary (2%) slip rate is about 0.0002 mm/yr. Using relations (5) and (6) suggests that the average displacement per event could be in the range of 9 to17 cm. These values appear large in comparison to those for other short faults. However, using these displacement values and the slip estimate of 0.0002, the recurrence for such displacement events is on the order of 650 ka. Maximum displacement values are 11 and 20 cm using relations (3) and (4) and they increase to 16 and 29 cm using relations (7) and (8) and the 1.73 factor. The resulting parameters are:

$P(C) = 0.1$
D_{cum} = {5 m (0.15), 15 m (0.7), 25 m (0.15)}
L = {3 km (0.15), 4.2 km (0.7), 5.5 km (0.15)}

Site 4 - Ghost Dance fault

The Ghost Dance fault is considered a source for secondary fault displacement only. Although paleoseismic data indicates that the fault has not experienced unequivocal (>5 cm) surface rupture since the middle Quaternary, the north-south strike of the fault, the same as active faults in the site area indicates that the fault could have potential for future slip. We believe the probability of activity is 0.5. Total length of the fault is about 3 km (W. C. Day *et al.*, USGS, written communication, 1996) and the total displacement at the site is about 25 m. The Quaternary paleoseismic slip rate for the fault has been estimated to be <0.0005 mm/yr, which agrees well with the Quaternary (2%) bedrock slip estimate of 0.0003. The age of the last displacement event appears to be at least 200 ka and may be over 1 Ma (E. M. Taylor *et al.*, USGS, written communication, 1996a). Using the 200 ka age as an average recurrence and a slip rate of 0.0005 suggests average displacements of about 10 cm and 20 cm for maximum displacement (weight of 0.8; Figure RYA-18). Using relations (3) and (4) suggests slightly higher displacement values. The resulting parameters are:

$P(C) = 0.5$
D_{cum} = {20 m (0.15), 25 m (0.7), 30 m (0.15)}
L = {2.5 km (0.15), 3 km (0.7), 5 km (0.15)}

Site 5 - Sundance fault west of the ESF

The Sundance fault is a source for secondary fault displacement only. However, given its northwest strike, short length, and the lack of evidence for Quaternary activity the probability of activity is considered low (0.1). Total mapped length of the fault is only about 600 m (W.C., Day *et al.*, USGS, written communication, 1996) and total displacement is about 8.5 m (E. M. Taylor *et al.*, USGS, written communication, 1996a). Use of relations (5) and (6) suggests that the average displacement for this fault should be on the order of 2-5 cm. This value, in conjunction with an estimated Quaternary (2%) slip rate of 0.00001 yields a recurrence of 3.5 Ma. The resulting parameters are:

$P(C) = 0.1$
D_{cum} = {6 m (0.15), 8.8 m (0.7), 11 m (0.15)}
L = {0.2 km (0.15), 0.6 km (0.7), 1.0 km (0.15)}

Site 6 - Minor unnamed fault west of Dune Wash

Any unnamed fault west of Dune Wash is considered a source for secondary fault displacement only. Without site specific paleoseismic data and without knowing the strike, sense of slip for the fault, and length, the probability of activity is considered to be 0.2. We have assumed total slip at the site to be about 4 m (slightly less than the tunnel diameter) and an unknown length of about 1 km. Our preferred slip rate for the fault is 0.00005 mm/yr. Using relations (5) and (6) suggest an average displacement of 2-4 cm. This yields a recurrence of about 600 ka. The resulting parameters are:

$P(C) = 0.2$
D_{cum} = {2 m (0.15), 4 m (0.7), 6 m (0.15)}
L = {0.5 km (0.15), 1.0 km (0.7), 1.5 km (0.15)}

Site 7 - 100 m east of the Solitario Canyon fault

Four situations or conditions are evaluated for site 7. (a) A small fault with 2.0 m cumulative slip, (b) a shear with about 10 cm of cumulative displacement, (c) a fracture having no measurable displacement, and (d) intact rock. For example 7a adjacent to the Solitario Canyon fault, the potential for activity is considered higher than for site 8a (0.5 verses 0.3). For example 7a and the purpose of our analysis, we have assumed that the total displacement at the site is 1.25 m, yielding a preferred Quaternary (2%) slip rate of 0.00002 mm/yr. We do not know the length of the fault but comparison to site 6 and the Ghost Dance fault suggests the length is probably less than 1 km. From this, we estimate the average displacement to be about 1cm. This would equate to a recurrence of 500 ka. For example 7b, the fault length is probably insignificant given a total displacement of 10 cm. The Quaternary (2%) slip rate for this feature would be 0.000001 mm/yr. We assume displacement per event of 1 cm (essentially at or below the level of detection). This would indicate a recurrence of 1 Ma. For examples (c) and (d) there is an essentially 0 probability of displacement. The resulting parameters are:

Point 7a: cumulative offset 2 m
$P(C) = 0.5$
D_{cum} = {2 m (1.0)}
L not known

Point 7b: cumulative offset 10 cm
$P(C) = 0.3$
D_{cum} = {0.1 m (1.0)}
L not known

Point 7c: fracture with no measurable cumulative offset
$P(C) = 0$

Point 7d: intact rock
$P(C) = 0$

Site 8 - Midway between the Solitario Canyon and Ghost Dance faults

The same four situations used for site 7 were evaluated for site 8. The only difference between this site and site 7 is the increased distance to a potentially active fault. Thus, we have given this fault a low activity weight. The resulting parameters are:

Point 8a: cumulative offset 2 m

$P(C) = 0.3$
D_{cum} = {2 m (1.0)}
L not known

Point 8b: cumulative offset 10 cm
$P(C) = 0.1$
D_{cum} = {0.1 m (1.0)}
L not known

Point 8c: fracture with no measurable cumulative offset
$P(C) = 0$

Point 8d: intact rock
$P(C) = 0$

Site 9 - Along the Exile Hill fault in Midway Valley

The Exile Hill fault is an approximately 3 km long, north-south striking fault in Midway Valley. Work by F. H. Swan *et al.* (Geomatrix Consultants, written communication, 1995) indicates that essentially no detectable displacement has occurred on the fault in the middle to late Quaternary (limits of detection essentially 0-5 cm) although at least two fracturing events may have occurred. Because Quaternary fracturing may have been associated with this fault, the probability of activity is considered 0.7. Slip rate has been estimated to be similar to the Ghost Dance fault, <0.0005, although total slip is less than half that of the Ghost Dance (10 m). Considering the evidence for no measurable displacement in at least the last several hundred thousand years and the limited amount of total slip, the average slip per event must be small. Thus, the estimate of about 5 cm for average slip per event which is near the detection level. This leads to an estimate of >100 ka for displacement events. Using relations (5) and (6) suggests 6 and 13 cm for average displacements. Relations (3) and (4) suggest 7 and 16 cm for maximum displacement and (5) and (6) and the 1.73 factor suggest 10 and 22 cm for maximum displacement. The resulting parameters are:

$P(C) = 0.7$
D_{cum} = {5 m (0.15), 10 m (0.7), 15 m (0.15)}
L = {2 km (0.15), 3.2 km (0.7), 4.4 km (0.15)}

REFERENCES

Aki, K., Reasenberg, P., DeFazio, T., and Tsai, Y., 1969, Near-field and far-field seismic evidences for triggering of an earthquake by the Benham explosion: Seismological Society of America Bulletin, v. 59, p. 2197-2207.

Aki, K., and Tsai, Y., 1972, Mechanism of long-wave excitation by explosive sources: Journal of Geophysical Research, v. 77, p. 1452-1475.

Anderson, J.G., 1979, Estimating the seismicity from geological structure for seismic risk studies: Bulletin of the Seismological Society of America, v. 69, p. 135-158.

Anderson, R.E., Bucknam, R.C., Crone, A.J., Haller, K.M., Machette, M.N., Personius, S.F., Barnhard, T.P., Cecil, M.J., and Dart, R.L., 1995a, Characterization of Quaternary and suspected Quaternary faults, regional studies, Nevada and California: U.S. Geological Survey Open-File Report 95-599, 56 p.

Anderson, R.E., Crone, A.J., Machette, M.N., Bradley, L., and Diehl, S.F., 1995b, Characterization of Quaternary and suspected Quaternary faults, Amargosa area, Nevada and California: U.S. Geological Survey Open File Report 95-613, 41 p.

Anderson, J.G., Wesnousky, S.G., and Stirling, M.W., 1996, Earthquake size as a function of fault slip rate: Bulletin of the Seismological Society of America, v. 86, p. 683-690.

Bucknam, R.C., 1969, Geologic effects of the Benham underground nuclear explosion: Bulletin of the Seismological Society of America, v. 59, p. 2209-2220.

Burchfiel, B.C., 1965, Structural geology of the Specter Range quadrangle, Nevada, and its regional significance: Geological Society of America Bulletin, v. 76, p. 175-192.

Carr, W.J., 1982, Volcano-tectonic history of Crater Flat, southwestern Nevada, as suggested by new evidence from Drill Hole USW-VH-1: U.S. Geological Survey Open-File Report 82-457, 53 p.

Carr, W.J., 1990, Styles of extension in the Nevada Test Site region, southern Walker Lane Belt—an integration of volcano-tectonic and detachment fault models, *in* Wernicke, B.P., ed., Basin and Range Extensional Tectonics Near the Latitude of Las Vegas, Nevada: Geological Society of America Memoir 176, p. 283-303.

Carr, W.J., Byers, F.M.J., and Orkild, P.P., 1986, Stratigraphic and volcano-tectonic relations of Crater Flat tuff and some older volcanic units: U.S. Geological Survey Professional Paper 1321, 23 p.

DePolo, C.M., 1994, The maximum background earthquake for the Basin and Range province, western North America: Bulletin of the Seismological Society of America, v. 84, p. 466-472.

Doser, D.I., and Smith, R.B., 1989, An assessment of source parameters of earthquakes in the Cordillera of the Western United States: Bulletin of the Seismological Society of America, v. 79, p. 1383-1409.

Frankel, A., 1995, Mapping seismic hazard in the Central and Eastern United States: Bulletin of the Seismological Society of America, v. 66, p. 8-21.

Fridrich, C. J., Whitney, J. W., Hudson, M. R., and Crowe, B. M., 1997, Space-time patterns of late Cenozoic extension, vertical-axis rotation, and volcanism in the Crater Flat basin, Nevada, *in* Wright, L. A. and Troxel B. W., eds., Cenozoic Basins of the Death Valley Region, California and Nevada: Geological Society of America Special Paper 1996 (in press).

Frizzell, V.A. Jr., and Shulters, J., 1990, Geologic map of the Nevada Test Site, southern Nevada: U.S. Geological Survey Miscellaneous Investigations Map I-2046, scale 1:100,000.

Hamilton, W.B., 1988, Detachment faulting in the Death Valley region: U.S. Geological Survey Bulletin 1790, p. 51-85.

Harmsen, S.C., and Bufe, C., 1991, Seismicity and focal mechanisms for the southern Great Basin of Nevada and California, 1987 through 1989: U.S. Geological Survey Open-File Report 91-572, 208 p.

Jackson, J.A., 1987, Active normal faulting and crustal extension, *in* Coward, M.P., Dewey, J.F., and Hancock, P.L., eds., Continental-Extensional Tectonics: Geological Society of London Special Publication No. 28, p. 3-17.

Keefer, D.L., and S.E. Bodily, 1983, Three-point approximations for continuous random variables: Management Science, v 29, p 595-609.

Lay, T., Wallace, T.C., and Helmberger, D.V., 1984, The effects of tectonic release on short-period P-waves from NTS nuclear explosions: Bulletin of the Seismological Society of America, v. 74, p. 819-842.

Maldonado, F., 1977a, Composite postshot fracture map of Pahute Mesa, Nevada Test Site, June 1973 through March 1976, Nevada Operations Office, U.S. Energy Research and Development Administration: U.S. Geological Survey, Denver, USGS-474-243, 11 p.

Maldonado, F., 1977b, Results from fault-monitoring stations on Pahute Mesa, Nevada Test Site, from July 1973 through December 1976, Nevada Operations Office, U.S. Energy Research and Development Administration: U.S. Geological Survey, Denver, USGS-474-242, 32 p.

Mason, D.B., 1996, Earthquake magnitude potential of the Intermountain seismic belt, USA, from surface-parameter scaling of late Quaternary faults: Bulletin of the Seismological Society of America, v. 86, p. 1487-1506.

McGuire, R.K., 1985, Seismic hazard methodology for nuclear facilities in the Eastern United States: Dames and Moore, Golden, Vol. 2, Appendix A, EPRI Research Project Number P101-29.

McGuire, R.K., and Barnhard, T.P., 1981, Effects of temporal variations in seismicity on seismic hazard: Bulletin of the Seismological Society of America, v. 71, p. 321-334.

McKeown, F.A., and Dickey, D.D., 1969, Fault displacements and motion related to nuclear explosions: Bulletin of the Seismological Society of America, v. 59, p. 2253-2269.

Morris, R.H., 1971, Geologic effects, *in* Geologic and Hydrologic Effects of the Handley Event, Pahute Mesa, Nevada Test Site: U.S. Geologic Survey USGS-474-95, Denver, Colorado, p. 7-26.

Orkild, P.P., Sargent, K.A., and Snyder, R.P., 1969, Geologic map of Pahute Mesa, Nevada Test Site and vicinity, Nye County, Nevada: U.S. Geological Survey Miscellaneous Geologic Investigations Map I-567, scale 1:48,000.

Piety, L.A., 1994, Compilation of known and suspected Quaternary faults within 100 km of Yucca Mountain, Nevada and California: U.S. Geological Survey Open-File Report 94-112.

Rogers, A.M., Harmsen, S.C., Corbett, E.J., Priestley, K., and dePolo, D., 1991, The seismicity of Nevada and some adjacent parts of the Great Basin, *in* Slemmons, D.B., Engdahl, E.R., Zoback, M.D., and Blackwell, D.D., eds., Neotectonics of North America: Geological Society of America, p. 153-184.

Rogers, A.M., Harmsen, S.C., and Meremonte, M.E., 1987, Evaluation of the seismicity of the southern Great Basin and its relationship to the tectonic framework of the region: U.S. Geological Survey Open-File Report 87-408, 196 p.

Schwartz, D.P., and Coppersmith, K.J., 1984, Fault behavior and characteristic earthquakes—examples from the Wasatch and San Andreas fault zones: Journal of Geophysical Research, v. 89, p. 5681-5698.

Schweickert, R.A., and Lahren, M.M., 1997, Strike-slip fault system in Amargosa Valley and Yucca Mountain, Nevada: Tectonophysics, v. 272, p. 25-41.

Scott, R.B., 1990, Tectonic setting of Yucca Mountain, southwest Nevada, in Basin and Range extensional tectonics near the latitude of Las Vegas, Nevada: Geological Society of America Memoir 176, p. 251-282.

Simonds, F.W., Fridrich, C.J., Hoisch, T.D., and Hamilton, W.B., 1995, A synthesis of detachment fault studies in the Yucca Mountain region, *in* Topical Meeting on Methods of Seismic Hazards Evaluation—Focus '95, Las Vegas, Nevada: American Nuclear Society, p. 107-114.

Snyder, R.P., 1971, Composite postshot fracture map of Pahute Mesa, Nevada Test Site; Energy Research Development Administration, U.S. Geologic Survey, Denver, USGS-474-100, 17 p.

Snyder, R.P., 1973, Recent fault movement on Pahute Mesa, Nevada Test Site, from May 1970 through June 1973: Energy Research and Development Administration, U.S. Geological Survey, Denver, USGS-474-137, 32 p.

Stepp, J.C., 1972, Analysis of completeness of the earthquake sample in the Puget Sound area and its effects on statistical estimates of earthquake hazard: Proceedings, First Microzonation Conference, Seattle, Washington, p. 897-909.

Swadley, W.C., and Carr, W.J., 1987, Geologic map of the Quaternary and Tertiary deposits of the Big Dune quadrangle, Nye County, Nevada, and Inyo County, California: U.S. Geological Survey Miscellaneous Investigations Series Map I-1767.

Wallace, T.C., Helmberger, D.V., and Engen, G.R., 1983, Evidence of tectonic release from underground nuclear explosions in long-period P-waves: Bulletin of the Seismological Society of America, v. 73, p. 593-613.

Wallace, T.C., Helmberger, D.V., and Engen, G.R., 1985, Evidence of tectonic release from underground nuclear explosions in long-period S-waves: Bulletin of the Seismological Society of America, v. 75, p. 157-174.

Wallace, T.C., Helmberger, D.V., and Lay, J., 1986, Reply to comments by A. Douglas, J.B. Yolong, and N.S. Lyman and a note on the revised moments for Pahute Mesa tectonic release: Bulletin of the Seismological Society of America, v. 76, p. 313-318.

Weichert, D.H., 1980. Estimation of the earthquake recurrence parameters for unequal observation period for different magnitudes: Bulletin of the Seismological Society of America, v. 70, p. 1337-1346.

Wells, D.L., and Coppersmith, K.J., 1994, New empirical relationships among magnitude, rupture length, rupture width, rupture area, and surface displacement: Bulletin of the Seismological Society of America, v. 84, p. 974-1002.

Wernicke, B., 1995, Low-angle normal faults and seismicity—a review: Journal of Geophysical Research, v. 100, p. 20,159-20,174.

Youngs, R.R., and Coppersmith, K.J., 1985, Implications of fault slip rates and earthquake recurrence models for probabilistic seismic hazard estimates: Bulletin of the Seismological Society of America, v. 75, p. 939-964.

Youngs, R.R., Swan, F.H., III, Power, M.S., Schwartz, D.P., and Green, R.K., 1987, Probabilistic analysis of earthquake and ground shaking hazard along the Wasatch Front, Utah, *in* Gori, P.O., and Hays, W.W. eds., Assessment of Regional Earthquake Hazards and Risk Along the Wasatch Front, Utah: U.S. Geological Survey Open File Report 87-585, p. M-1 to M-100.

TABLE RYA-1
COMPLETENESS TIMES

VERSION 5 CATALOG (YEARS)			
MW Magnitude Bin	**Lower Limit**	**Preferred Value**	**Upper Limit**
1.5-2.0	2.6	2.8	7.7
2.0-2.5	1.4	8.3	12.0
2.5-3.0	9.3	11.2	18.9
3.0-3.5	7.4	8.2	12.9
3.5-4.0	8.2	16.6	29.7
4.0-4.5	19.6	26.1	44.6
4.5-5.0	empty	Empty	Empty
5.0-5.5	51.2	85.8	85.8
5.5-6.0	85.8	85.8	85.8
VERSION 7 CATALOG (YEARS)			
1.5-2.0	3.0	6.0	6.0
2.0-2.5	6.0	8.0	16.0
2.5-3.0	6.5	11.0	17.0
3.0-3.5	9.5	25.0	37.0
3.5-4.0	15.7	37.0	40.0
4.0-4.5	35.4	47.0	55.0
4.5-5.0	57.2	62.0	62.0
5.0-5.5	empty	Empty	empty
5.5-6.0	85.6	85.6	85.6

TABLE RYA-2
INTERVAL RECURRENCE PARAMETERS

VERSION 5 CATALOG		
b-Value	**a-Value**	**Probability**
-1.088	4.13	0.020
-1.065	4.15	0.065
-1.075	4.17	0.215
-1.085	4.22	0.215
-1.095	4.24	0.285
-1.105	4.26	0.155
-1.115	4.28	0.040
-1.125	4.32	0.005
VERSION 7 CATALOG		
-1.125	4.24	0.010
-1.135	4.36	0.020
-1.145	4.38	0.060
-1.155	4.41	0.125
-1.165	4.44	0.175
-1.175	4.46	0.167
-1.185	4.48	0.167
-1.195	4.51	0.125
-1.205	4.53	0.075
-1.215	4.56	0.075
-1.225	4.58	0.005

TABLE RYA-3
FAULT SOURCES PARAMETERS, AREA A

Fault [1]	Fault Length (km) [2]	Max.; Average Disp./Event (cm) [3]	Maximum Magnitude (Mw) [4]	Age Most Recent Event (ka) [5]	Estimated Recurrence (kyr) [6]	Late Quaternary Slip Rate (mm/yr) [7]
BM	11-40; 23	150; 100	(6.3, 6.6., 6.9) (RL) (6.2, 6.6, 7.1) (RA)	40 ± 20	80-150 100	0.01
PBC	13-28; 13	100; 50	(6.4, 6.4, 6.8) (RL) (6.2, 6.4, 6.8) (RA)	13 ± 3 (c)	37-75 50	0.005-0.013
SR	4-9; 7	67; 55	(5.8, 6.1, 6.2) (RL) (5.7, 6.1, 6.3) (RA)	13 ± 3	15-40; 25	0.02
BWR	4-10; 7	44; 21?	(5.8, 6.1, 6.2) (RL) (5.7, 6.1, 6.4) (RA)	75 ± 10	75?	0.003
WW	12-26; 23	88; 50	(6.3, 6.7, 6.7) (RL) (6.1, 6.5, 6.6) (RA)	6 ± 4 (c) 40 + 20	30-100; 46	0.01
FW	7-16; 11	105; 61	(6.1, 6.3, 6.5) (RL) (6.0, 6.3, 6.6) (RA)	40 ± 20 (c) 75 ± 10	30-100; 46	0.002
SC	12-21; 18	120; 75	(6.3, 6.5, 6.6) (RL) (6.2, 6.5, 6.7) (RA)	25 ± 10	50-130; 90	0.01
IR	6-9; 8	130; 100	(6.0, 6.1, 6.2) (RL) (5.9, 6.1, 6.3) (RA)	25 ± 10	?	?

[1] Named faults that comprise the fault systems are: BM, Bare Mountain; PBC, Paintbrush Canyon; SR, Stagecoach Road; BWR, Bow Ridge; WW, Windy Wash; FW, Fatigue Wash; SC, Solitario Canyon; and IR, Iron Ridge. Bare Mountain fault data from L. W. Anderson and R. E. Klinger (USBR, written communication, 1996a), all other fault data (displacement, age of most recent event, recurrence, and slip rate) based on review and analysis of data in USGS (written communication, 1996). Bare Mountain fault assumed to dip 55, 60, or 65 degrees to the east; Yucca Mountain faults assumed to dip 60, 67.5, or 75 degrees to the west. Faults are assumed to have pure normal to normal-oblique slip.

[2] Minimum and maximum fault lengths; preferred estimate. Distance measured along strike of fault system, primarily from Simonds *et al.* (1995). Maximum lengths from A. R. Ramelli and J. W. Bell (Nevada Bureau of Mines and Geology, written communication, 1996) and Frizzell and Shulters (1990). Maximum fault areas can be calculated by multiplying fault length by fault width (fault width calculated using dip of fault and seismogenic depth of 12, 15, or 20 km).

[3] Maximum displacement is largest single-event displacement measured or calculated from trench exposure. Average displacement represents average of all displacement values from the various trenches on the specific fault.

[4] (RL) indicates magnitudes calculated from the "all faults" Mw-fault length relationship of Wells and Coppersmith (1994). The three magnitudes given are computed from the minimum, preferred, and maximum fault length values. (RA) indicates magnitudes calculated from the "all faults" Mw-fault area relationship of Wells and Coppersmith (1994). The three magnitudes given are computed from the smallest, preferred, and largest areas for a fault given that the Yucca Mountain faults may dip between 60 and 75 degrees; Bare Mountain may dip between 55 and 65 degrees; and the thickness of the seismogenic crust is 12, 15, or 20 km (see text for a discussion of the magnitudes and weights used in the PSHA). Relative weights are 0.5 for RL and 0.5 for RA.

[5] "Cracking" event (displacement less than 20 cm) indicated by (c).

[6] Upper numbers represent elapsed time between faulting events as interpreted from trench data (USGS, written communication, 1996; Figure RYA-15). Lower number is an estimate of average recurrence using slip rate and average displacement per event. Preferred recurrence model is the "characteristic model" of Schwartz and Coppersmith (1984), assigned a relative weight of 0.9, and applied to the estimate of average recurrence only.

[7] Uncertainty probably ± 0.005 mm/yr.

TABLE RYA-4
COALESCING FAULT SOURCE MODEL, AREA A
THREE YUCCA MOUNTAIN FAULT SYSTEMS

Fault System [1]	Max. Fault Length (km) [2]	Max. Combined Disp/Event (m) [3]	Maximum Magnitude (M_w) [4]	Age Most Recent Event (ka)	Estimated Avg. Recurrence (kyr) [6]	Late Quaternary Slip Rate (mm/yr) [7]
BM (planar)	11-40; 23	1.5; 1.0	(6.3, 6.6, 6.9) (RL) (6.2, 6.6, 7.1) (RA)	40 ± 20	80-150; 100	0.01
PBC-SR-BWR	7-35; 20	1.0; 0.5	(6.1, 6.5, 6.8) (RL) (6.0, 6.5, 6.9) (RA)	13 ± 3	15-75; 25	0.005-0.02; 0.01
WW-FW	11-25; 23	1.13; 0.46	(6.3, 6.7, 6.7) (RL) (6.0, 6.5, 6.6) (RA)	6 ± 4; [5] 40 ± 20	30-100; 46	0.01
SC-IR	8-21; 20	1.2; 0.75	(6.1, 6.6, 6.6) (RL) (6.0, 6.5, 6.7) (RA)	25 ± 10	50-130; 75	0.01

TABLE RYA-5
COALESCING FAULT SOURCE MODEL, AREA A
TWO YUCCA MOUNTAIN FAULT SYSTEMS

Fault System [1]	Max. Fault Length (km) [2]	Max. Combined Disp/Event (m) [3]	Maximum Magnitude (M_w) [4]	Age Most Recent Event (ka)	Estimated Avg. Recurrence (ka) [8]	Late Quaternary Slip Rate (mm/yr) [7]
BM (planar)	11-40; 23	1.5; 1.0	(6.3, 6.6, 6.9) (RL) (6.2, 6.6, 7.1) (RA)	40 ± 20	80-150; 100	0.01
East Side (SR-PBC-BWR)	7-35; 20	1.0; 0.5	(6.1, 6.5, 6.8) (RL) (6.0, 6.5, 6.9) (RA)	13 ± 3	15-75 50	0.005-0.02; 0.01
West Side (WW-FW-SC-IR)	8-26; 23	2.3; 1.8	(6.1, 6.7, 6.7) (RL) (5.9, 6.5, 6.6) (RA)	6 ± 4; [5] 40 ± 20	30-130 90	0.02-0.03; 0.025

---

[1] Named faults that comprise the fault systems are: BM, Bare Mountain; SR, Stagecoach Road; PBC, Paintbrush Canyon; BWR, Bow Ridge; WW, Windy Wash; FW, Fatigue Wash; SC, Solitario Canyon; and IR, Iron Ridge. Bare Mountain fault data from L. W. Anderson and R. E. Klinger (USBR, written communication, 1996a); all other fault data (displacement, age of most recent event, recurrence, and slip rate) based on review and analysis of data in USGS (written communication, 1996). Bare Mountain fault assumed to dip 55, 60, or 65 degrees to the east; Yucca Mountain faults assumed to dip 60, 67.5, or 75 degrees to the west. In this model, all sources are considered seismogenic. Bare Mountain fault is always an independent source. Faults are assumed to have pure normal to normal-oblique slip.

[2] Minimum and maximum rupture lengths; preferred estimate. Distance measured along strike of fault system, primarily from Simonds *et al.* (1995). Minimum rupture length assumes rupture only of preferred length of shortest part of fault system. Maximum rupture includes possible southern projections from A. R. Ramelli and J. W. Bell (Nevada Bureau of Mines and Geology, written communication, 1996) and northern bedrock projections from Frizzell and Shulters (1990). Probabilities for each rupture scenario are minimum (0.15), maximum (0.15), and preferred (0.7).

Notes for Tables RYA-4 and RYA-5 (Cont'd.):

[3] Maximum displacement is largest single-event displacement measured or calculated from trench exposure. Because the Windy Wash and Fatigue Wash fault systems are parallel, the maximum is the sum of the maximum displacement values for each fault. Average displacement represents the average of all displacement values from the various trenches on the specific fault.

[4] (RL) indicates magnitudes calculated from the all faults" Mw-fault length relationship of Wells and Coppersmith (1994). The three magnitudes given are computed from the minimum, preferred, and maximum fault length values. (RA) indicates magnitudes calculated from the "all faults" Mw-fault area relationship of Wells and Coppersmith (1994). The three magnitudes given are computed from the smallest, preferred, and largest areas for a fault given that the Yucca Mountain faults may dip between 60 and 75 degrees; Bare Mountain may dip between 55 and 65 degrees; and the thickness of the seismogenic crust is 12, 15, or 20 km (see text for a discussion of the magnitudes and weights used in the PSHA). Relative weights are 0.5 for RL and 0.5 for RA.

[5] 6 ± 4 ka age is for 6-cm "cracking" event on Windy Wash fault. 40 ± 20 ka age is for penultimate 35-cm displacement event also on Windy Wash fault.

[6] Upper numbers represent time between faulting events as interpreted from trench data (USGS, written communication, 1996; Figure RYA-15). Lower number is an estimate of average recurrence for maximum magnitude events using slip rate and average displacement per event. No preferred recurrence model. The "characteristic model" of Schwartz and Coppersmith (1984) is given a weight of 0.5, and the exponential magnitude distribution model also is given a weight of 0.5. This applies to the average recurrence only.

[7] Ranges and preferred slip rate. Relative weights are 0.15 for maximum and minimum and 0.7 for preferred estimate. Uncertainty in slip rate estimates probably ± 0.005 mm/yr.

[8] Upper numbers represent elapsed time between faulting events as interpreted from trench data. Lower number is an estimate of average recurrence for maximum magnitude events using slip rate and average displacement per event. Preferred recurrence model is the exponential magnitude distribution, using the average recurrence estimates, and is assigned a weight of 0.7.

TABLE RYA-6
COALESCING SOURCE MODEL, AREA A
ONE FAULT SYSTEM[1]

Fault System [1]	Maximum Fault Length (km) [2]	Maximum Combined Disp./Event (m) [3]	Age Most Recent Event (ka)	Estimated Average Recurrence (kyr) [4]	Slip Rate (mm/yr) [5]	Maximum Magnitude (M_W) [6]
BM (planar)	11-40; 23	1.5; 1.0	40 ± 20	80-150; 100	0.01	(6.3, 6.6, 6.9) (RL) (6.2, 6.6, 7.1) (RA)
PBC/SR (master fault)	25	3.3	75 ± 10	73.3-94.3; 82.5	0.35-0.45; 0.4	6.7 (RL) (6.1, 6.6, 6.9) (RA)

---

1 Bare Mountain fault remains independent source. (See Table RYA-3 or RYA-4.) The Paintbrush Canyon/Stagecoach Road (PBC/SR), fault is the master fault. Other named faults within the fault system are the Bow Ridge, Windy Wash, Fatigue Wash, Solitario Canyon, and Iron Ridge. All fault data (displacement, age of most recent event, recurrence, and slip rate) based on review and analysis of data in USGS (written communication, 1996). Faults are assumed to have pure normal to normal-oblique slip.

2 Distance measured along strike of Windy Wash-Solitario Canyon fault system, primarily from Simonds *et al.* (1995). Maximum rupture includes possible southern projections from A. R. Ramelli and J. W. Bell (Nevada Bureau of Mines and Geology, written communication, 1996).

3 Maximum displacement for the fault system is the sum of the largest single-event displacements measured or calculated from all the trench exposures of all the faults.

4 Recurrence estimate (range and preferred) for maximum magnitude events calculated from maximum displacement and slip rate estimates. Preferred recurrence model is the exponential magnitude distribution, assigned a weight of 0.9. The characteristic earthquake recurrence model is given a weight of 0.1.

5 Range and preferred slip rates. Based on the sum of late Quaternary slip rates for the major parallel faults; uncertainty probably ±0.02 mm/yr.

6 (RL) indicates magnitudes calculated from the "all faults" Mw-fault length relationship of Wells and Coppersmith (1994). The three magnitudes given are computed from the minimum, preferred, and maximum fault length values. (RA) indicates magnitudes calculated from the "all faults" Mw-fault area relationship of Wells and Coppersmith (1994). The three magnitudes given are computed from the smallest, preferred, and largest areas for a fault given that the Yucca Mountain faults may dip between 60 and 75 degrees; Bare Mountain may dip between 55 and 65 degrees; and the thickness of the seismogenic crust is 12, 15, or 20 km (see text for a discussion of the magnitudes and weights used in the PSHA). Relative weights are 0.5 for RL and 0.5 for RA. Historical analogs may be the 1932 Cedar Mountain earthquake of M7.2 and the 1959 Hebgen Lake earthquake of M7.4.

TABLE RYA-7
M_{max} FOR HYPOTHESIZED BURIED SEISMIC SOURCE 30 KM LONG
(M_{max} DERIVED FROM M = 4.04+0.98 LOG [RUPTURE AREA])
(WELLS AND COPPERSMITH, 1994)

Decoupled Depth (km)	Thickness of Seismic Crust (km)	Rupture Area (km^2)	M_{max}
5	12	210	6.3
5	15	300	6.5
5	20	450	6.7
10	12	60	5.8
10	15	150	6.2
10	20	300	6.5

TABLE RYA-8
SIGNIFICANT REGIONAL FAULT SOURCE PARAMETERS, AREAS B and C

FAULT[1]	Fault Rupture Length (km); Max. Disp/Event (m)[2] Dip (deg.) & Direction	Maximum Magnitude (M_W)[3]	Age Most Recent Event (ka)	Estimated Recurrence (ka)[4, 5]	Slip Rate (mm/yr)[5]	Reference[6]
Wahmonie (WAH; 22)	15; ? 90	6.4 (RL) 6.3 (RA)	<180	90?	0.02	1, 6
Rock Valley (RV; 25)	30 (20-40); 2.5-3.9 90	6.8 (RL) 7.3 (MD) 6.7 (RA)	<10	25-195	0.02-0.1	1, 5
Cane Spring (CS; 28)	20 (14-27); ? 90	6.6 (RL) 6.5 (RA)	<1.8 Ma ?	?	0.02	1
Ash Meadows (AM; 30)	40 (34-47); 1.8 90	6.9 (RL) 6.9 (MD) 6.8 (RA)	>10	>120-180	< 0.01	1, 3
Yucca Flat (YC; 40)	25; ? 90	6.7 (RL) 6.6 (RA)	<10	?	0.08	1, 6
Furnace Creek (FC; 52)[7]	105 (100-111); 4.5 90	7.4 (RL) 7.2 (MD) 7.2 (RA)	>0.2	0.6 - 0.8	4-8	4
Death Valley (DV; 54)[7]	60 (45-76); 3.5 60 W	7.2 (RL) 7.1 (MD) 7.0 (RA)	>0.2	0.5-1.0	3-5	4
West Spring Mts (WSM; 56)	36 (30-56); 2.0 60 W	6.9 (RL) 6.9 (MD) 6.8 (RA)	10	28-124	0.02-0.07	1, 2
Belted Range (BLR; 64)	30 (20-51); 0.9 60 W	6.8 (RL) 6.7 (MD) 6.7 (RA)	<10	9-90	0.01-0.1	1, 2
Pahrump-Stewart Valley (PSV; 65)	35 (18-42); 2.0 90	6.9 (RL) 6.9 (MD) 6.7 (RA)	<10	100-167	0.009-0.02	1, 3
West Pintwater (WPR; 76)	55 (55-60); ? 60 W	7.1 (RL) 7.0 (RA)	>10	?	0.01-0.1	1

Notes for Table RYA-8

[1] Letters and numbers in parentheses are fault abbreviations and distance in kilometers to Yucca Mountain; distance measured from Piety (1994).

[2] Preferred estimate of surface fault rupture length based on review and analysis of mapped scarp and fault length from cited references (weight 0.7). Numbers in parentheses indicate minimum and maximum values (weight 0.15 each). Where no range given, assumes rupture of entire mapped trace. Displacement estimates are from profile or trench data in cited reference. 90 degree dip assumes sense of displacement primarily strike-slip, 60 degree assumes displacement primarily dip-slip.

[3] Magnitudes estimated from regressions of Wells and Coppersmith (1994) for all faults using preferred estimated surface rupture length (RL), maximum displacement (MD), and rupture area (RA). Relative weights are 0.35 for SRL, 0.35 for RA, and 0.3 for MD or 0.5 for RL and 0.5 for RA depending on available data. Magnitudes estimated to be $\pm$ 0.5 magnitude units for RL and RA.

[4] Recurrence estimates calculated from displacement and slip rate estimates. Characteristic recurrence model given weight of 0.9; truncated exponential recurrence model is given weight of 0.1.

[5] Where a range of values is given, equal weight is assigned to end member values.

[6] References:

(1) Piety (1994).
(2) Anderson (1995a).
(3) Anderson (1995b).
(4) R. E. Klinger and L. A. Piety, USBR, written communication, 1996.
(5) J. A. Coe *et al.* USGS, written communication, 1996.
(6) Yount, J., unpub. mapping.

Simultaneous rupture of Death Valley and Furnace Creek faults would result in M_W 7.7 earthquake; however, the probability of this event is low, 10%.

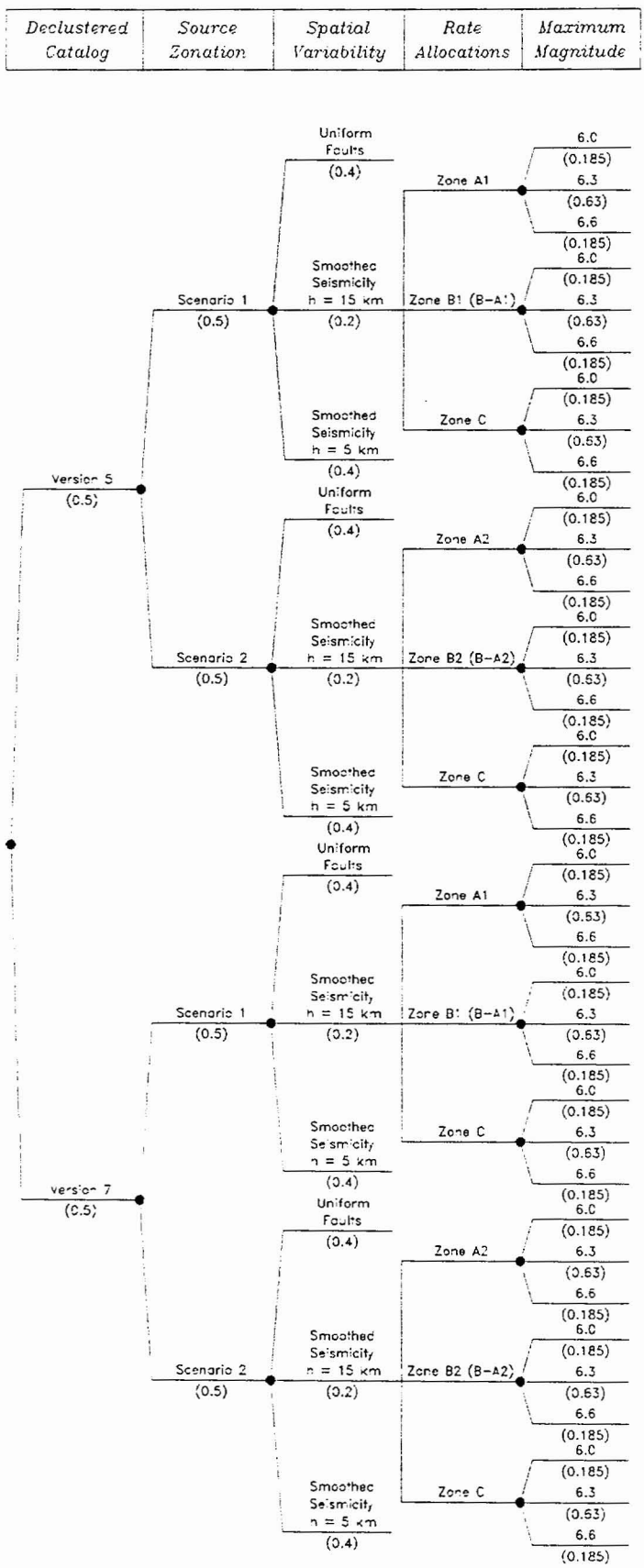

Figure RYA-1a Logic tree for background source zones

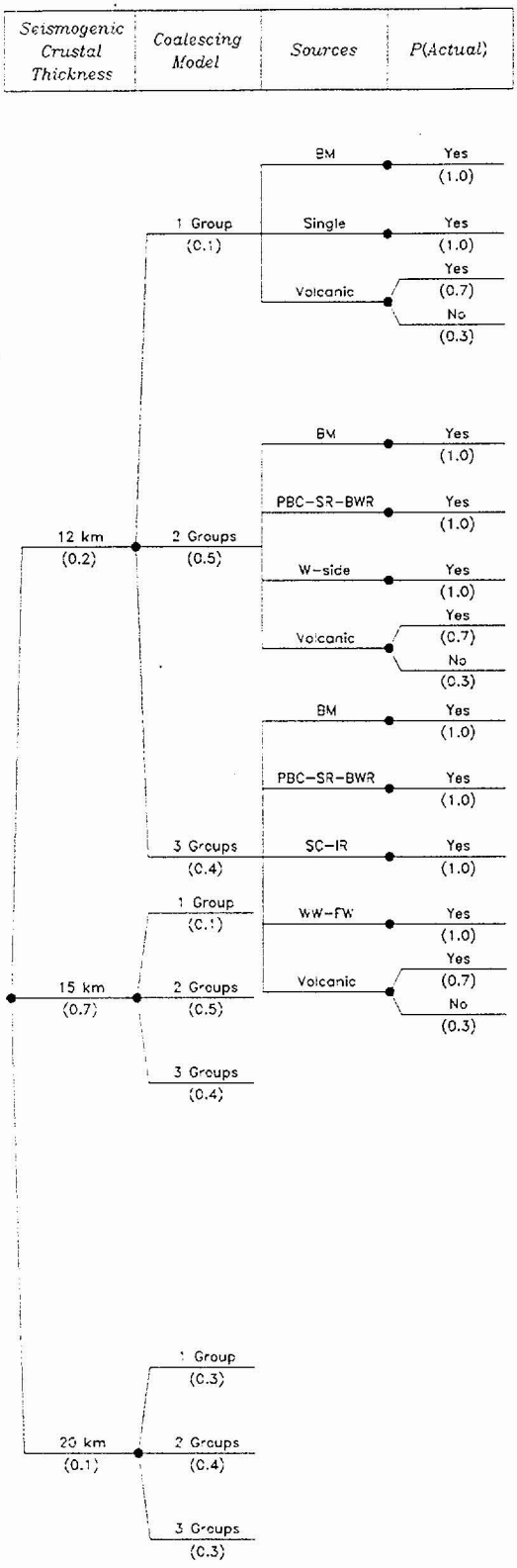

Figure RYA-1b Logic tree for local fault sources

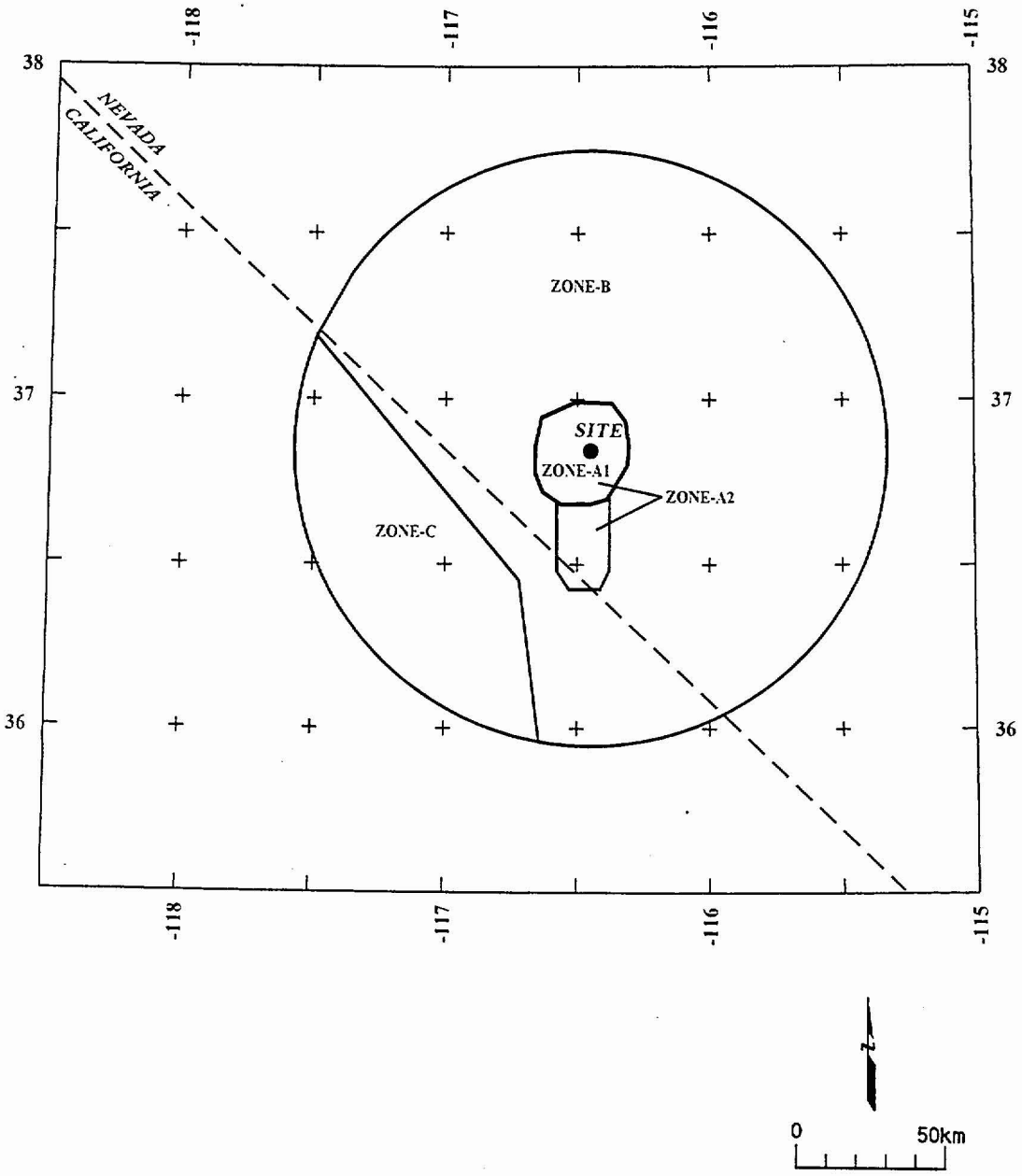

Figure RYA-2 Map showing boundaries of zones used in the seismic source model

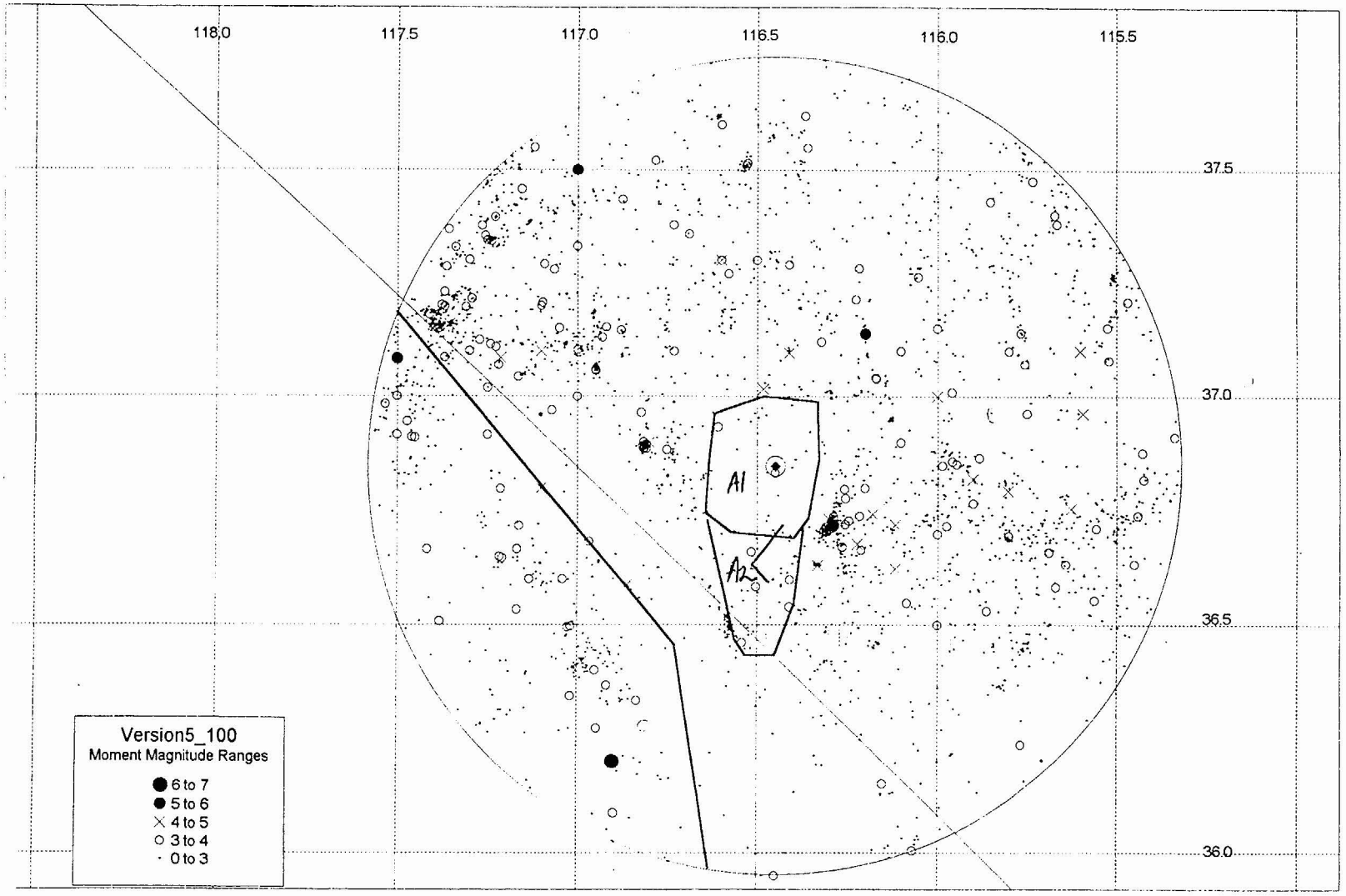

Figure RYA-3 Map showing earthquakes from the version 5 catalog and the background source zones

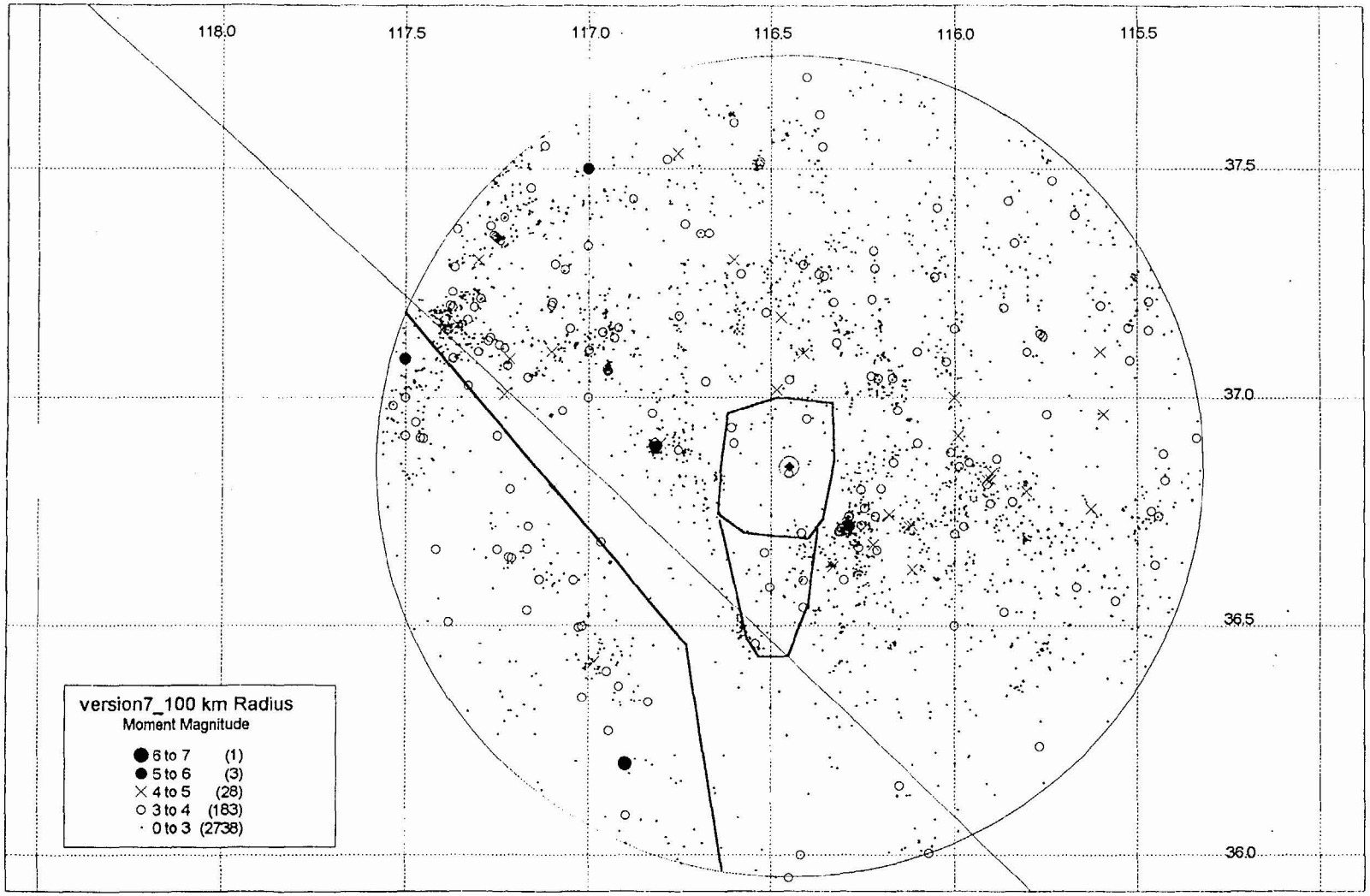

Figure RYA-4 Map showing earthquakes from the version 7 catalog and the background source zones

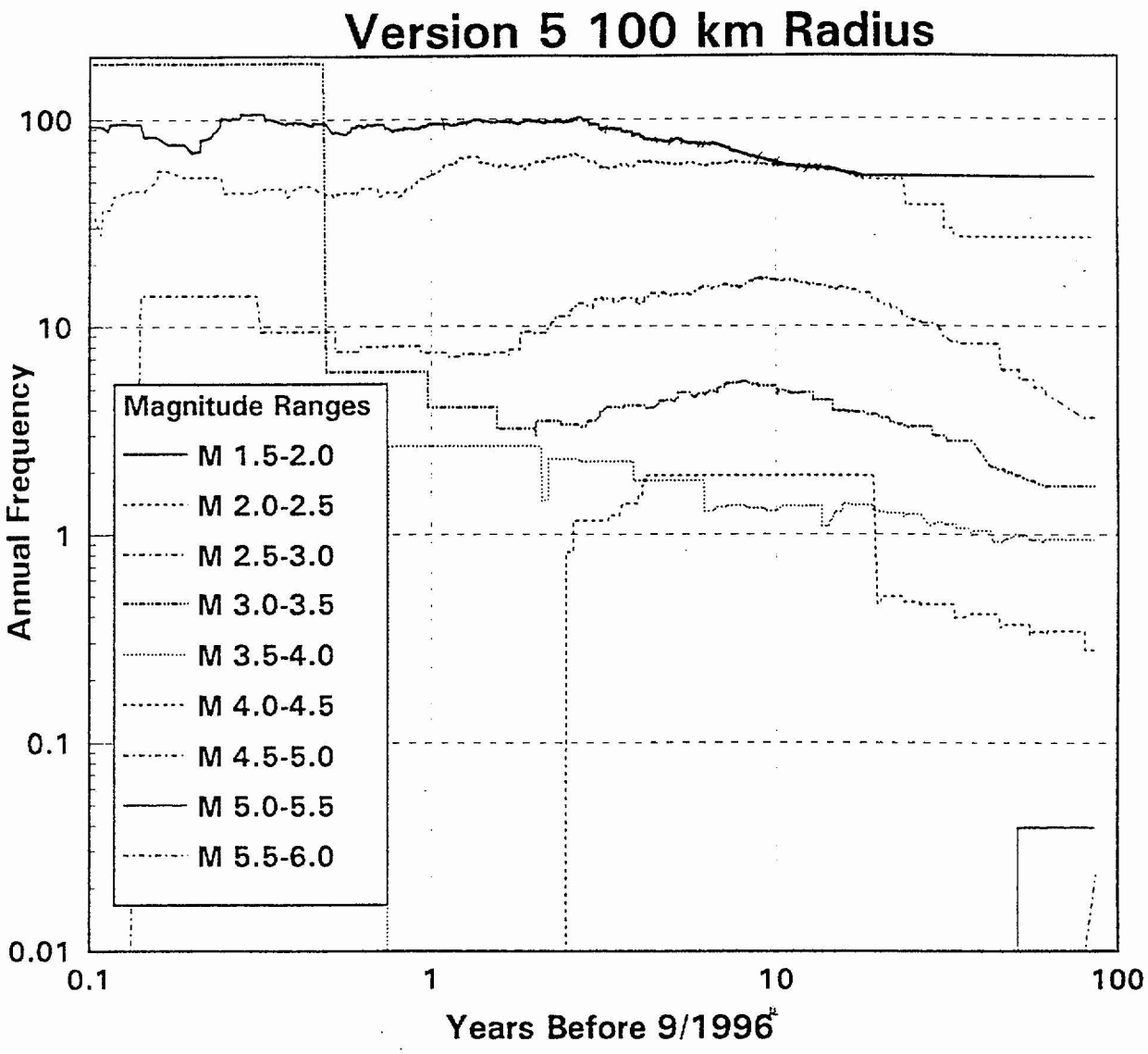

Figure RYA-5 Stepp plot of annual frequency versus years before 9/1996 for individual magnitude bins and the version 5 catalog

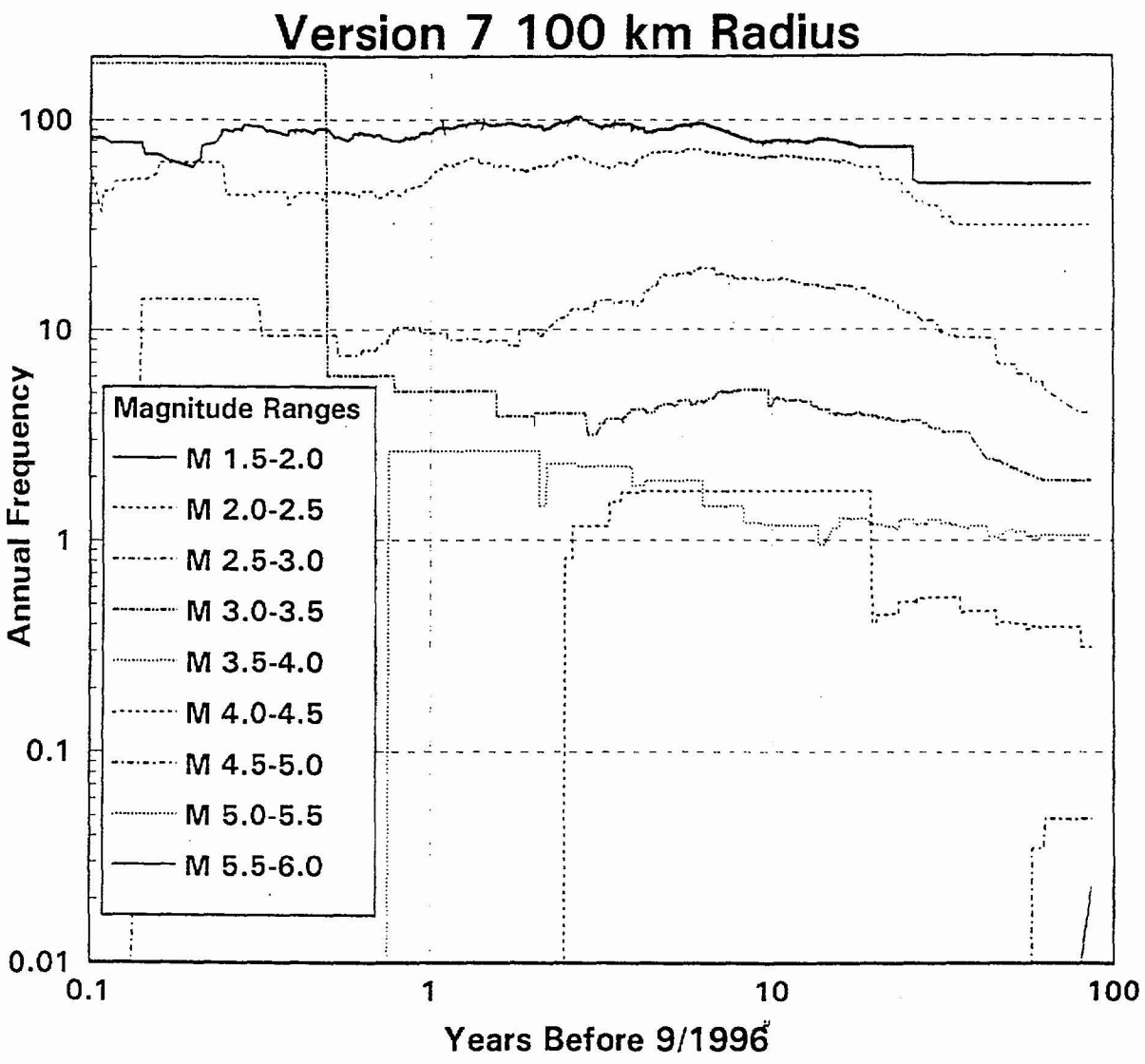

Figure RYA-6 Stepp plot of annual frequency versus years before 9/1996 for individual magnitude bins and the version 7 catalog

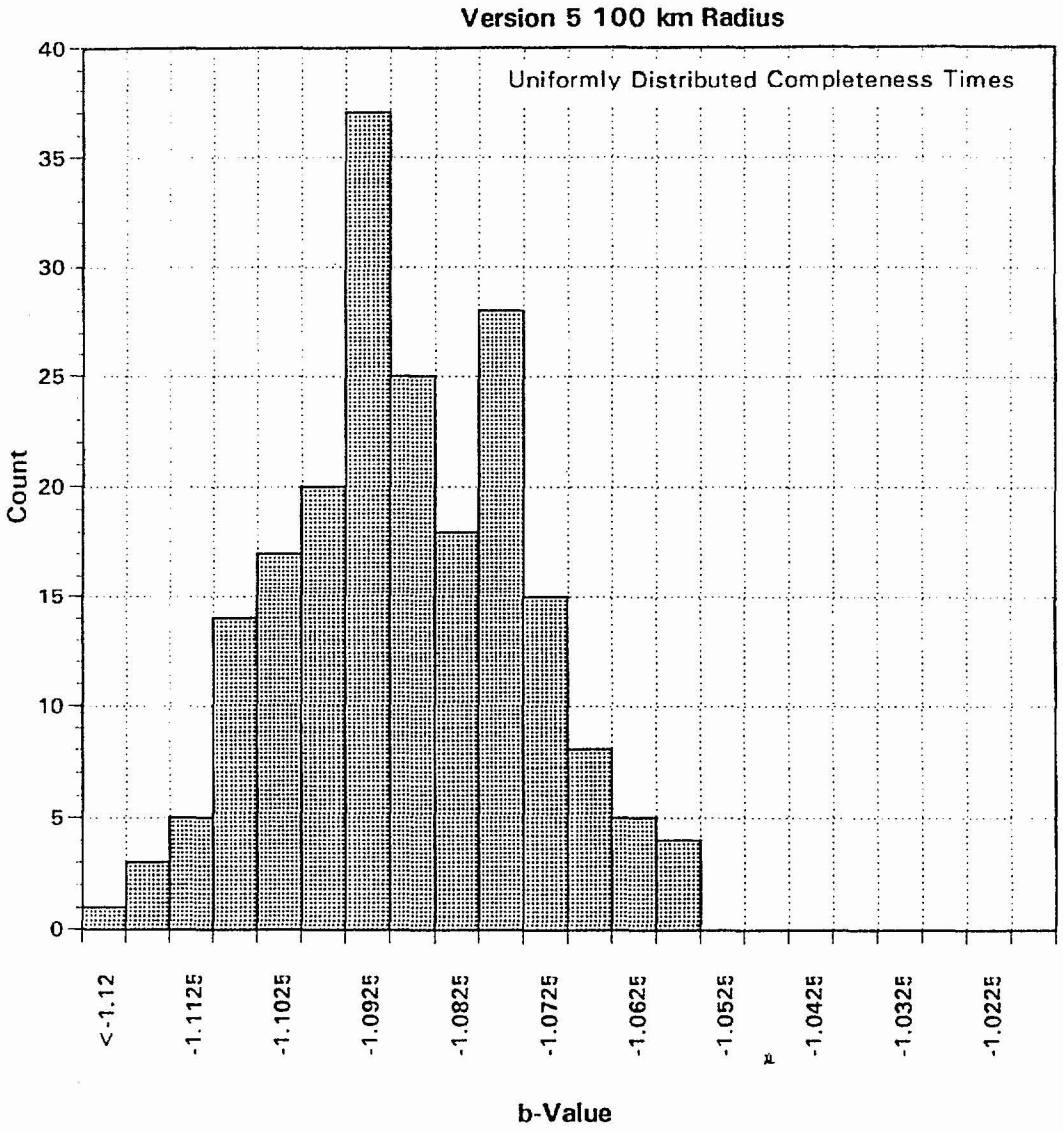

Figure RYA-7 Histogram showing b-values obtained for the version 5 catalog given uniform sampling of completeness times

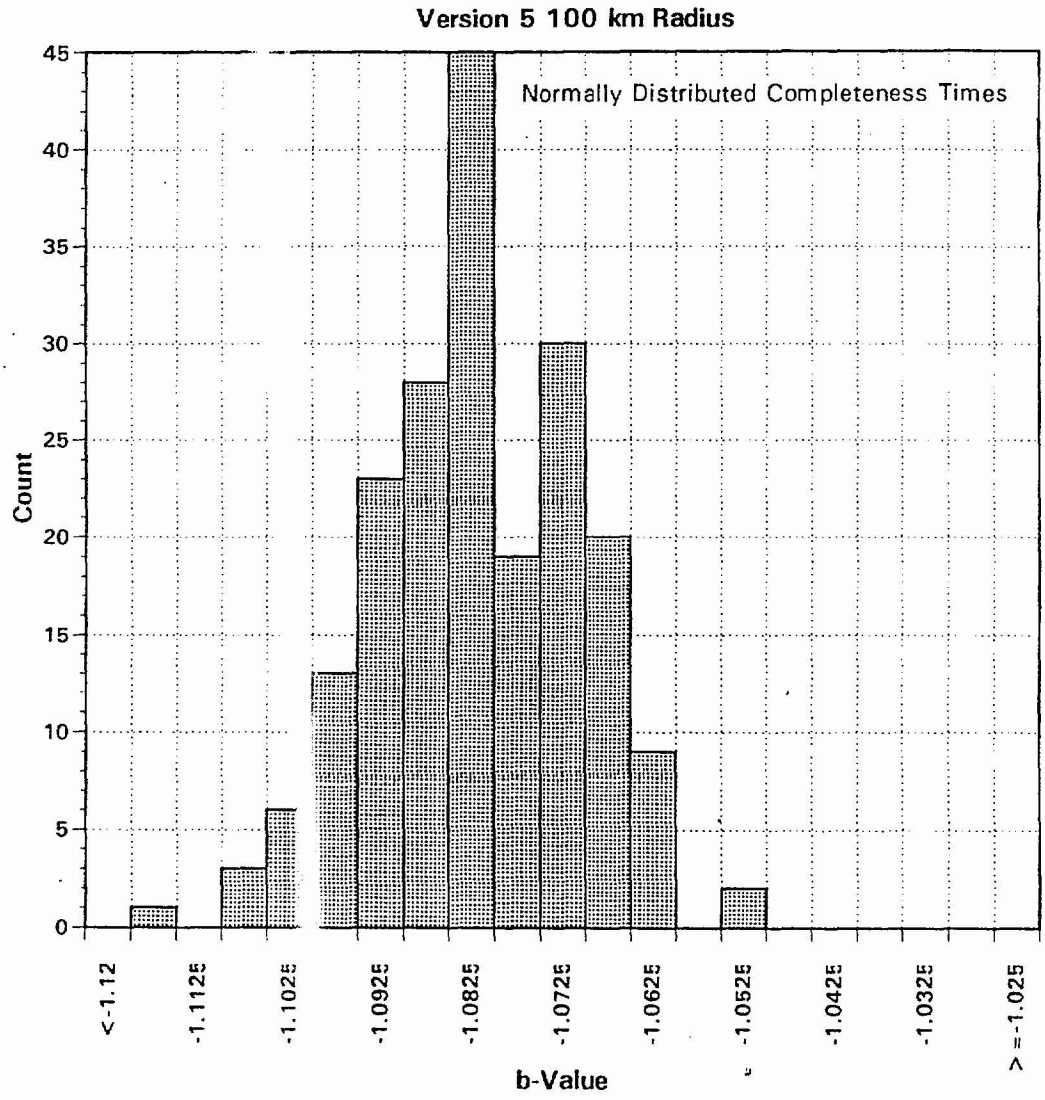

Figure RYA-8 Histogram showing b-values obtained for the version 5 catalog given normal sampling of completeness times

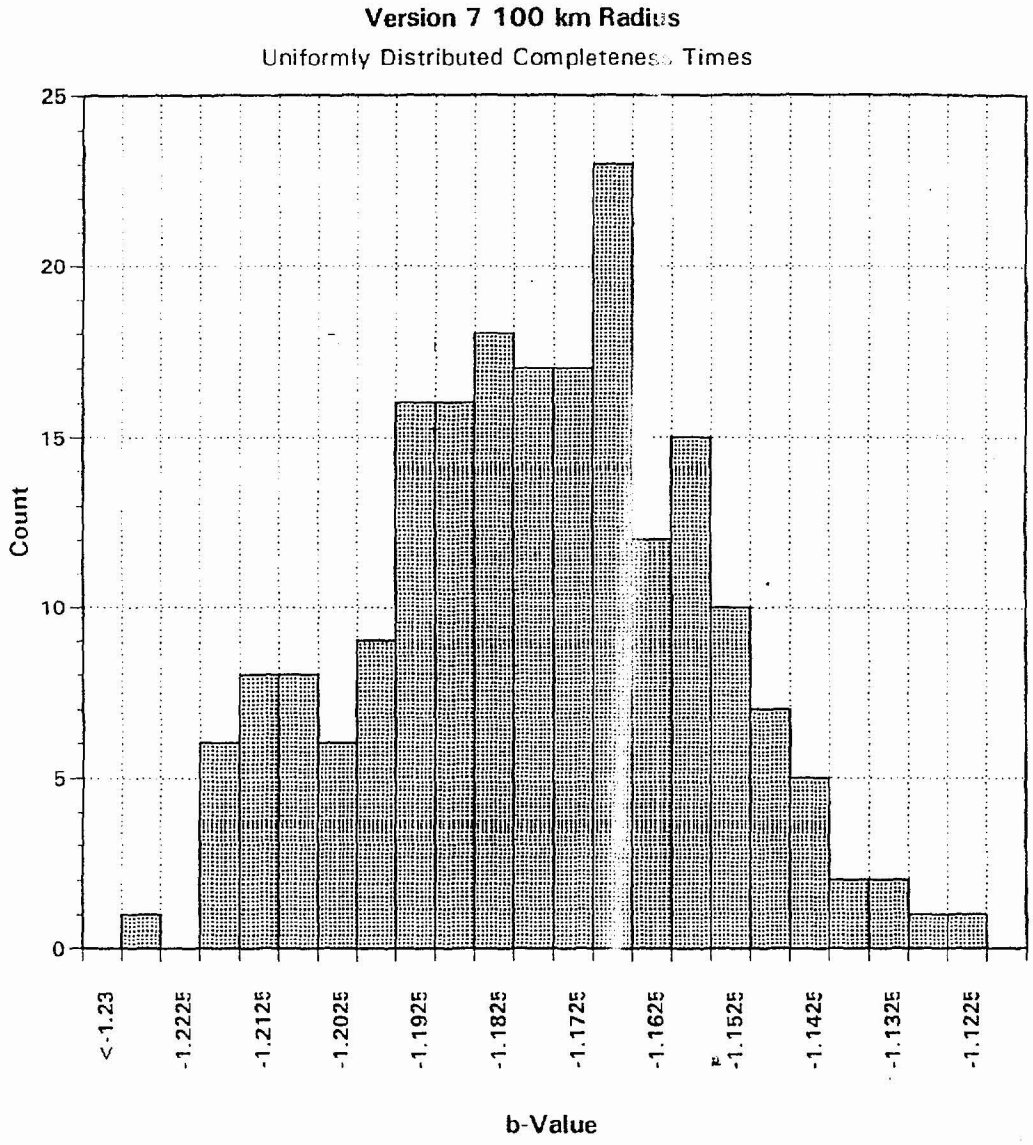

Figure RYA-9 Histogram showing b-values obtained for the version 7 catalog given uniform sampling of completeness times

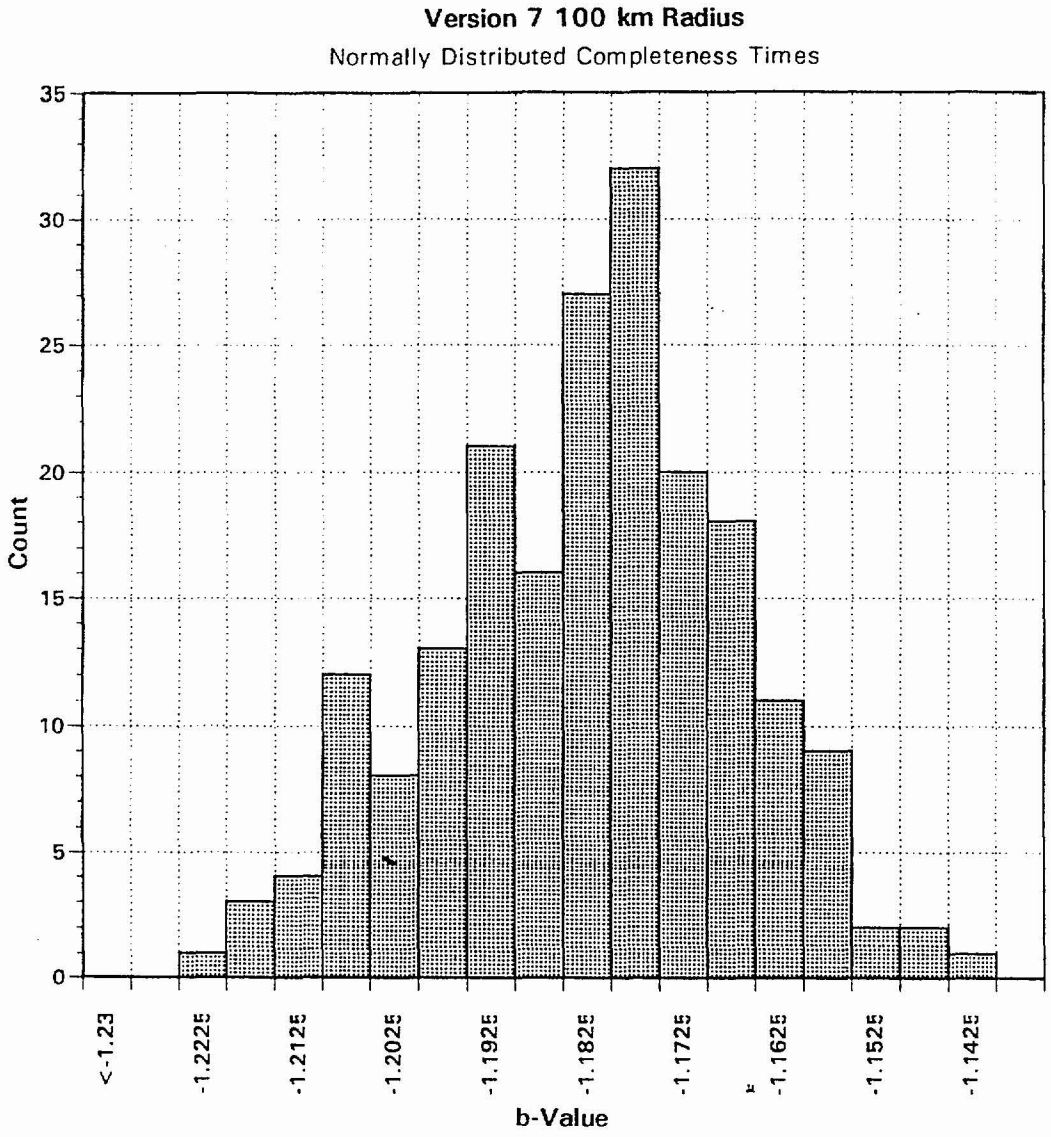

Figure RYA-10 Histogram showing b-values obtained for the version 7 catalog given normal sampling of completeness times

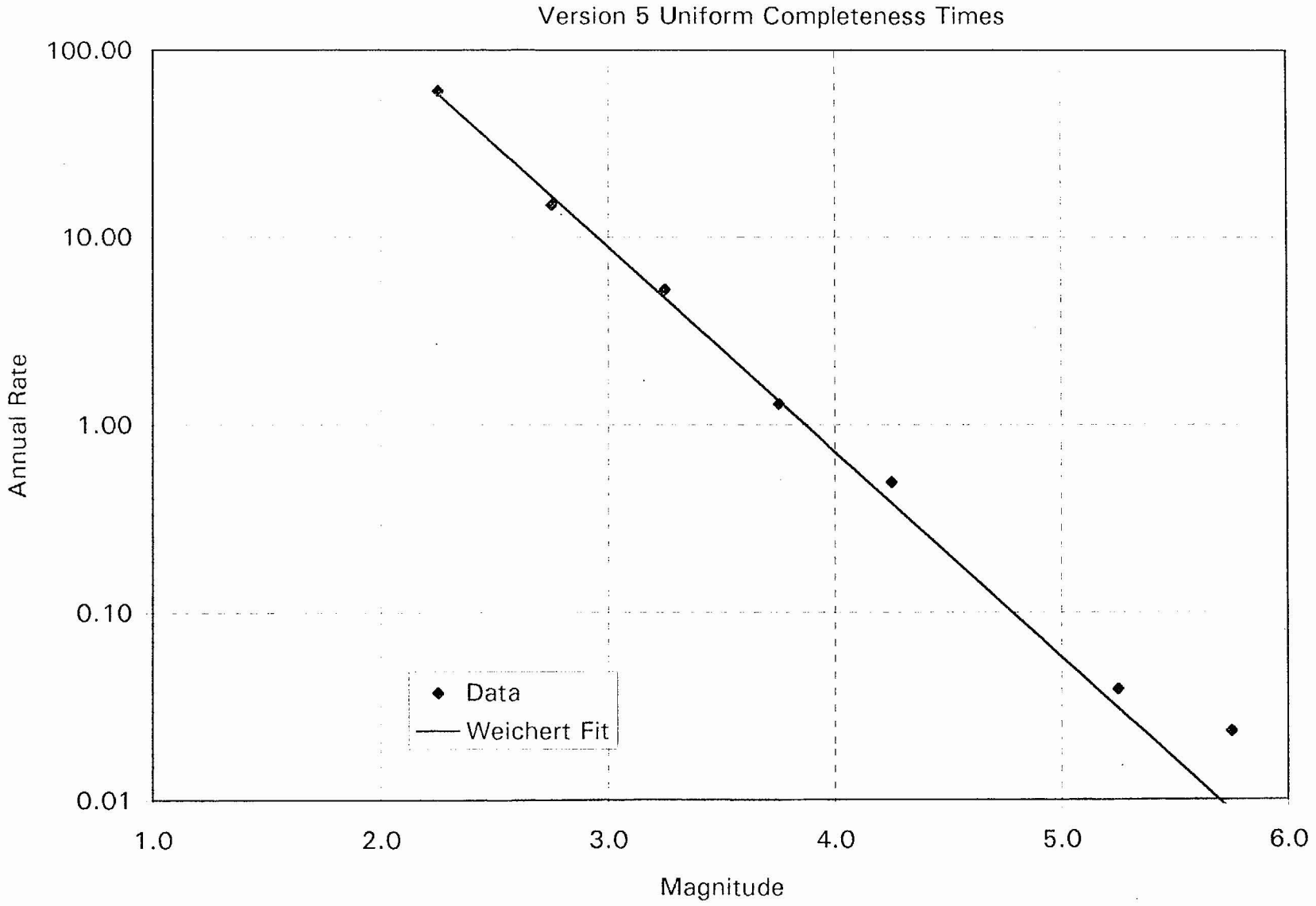

Figure RYA-11 Interval rates for the version 5 catalog that produced the modal b-value 1.09 (Figure RYA-7) and the fit to these data using the Weichert maximum likelihood method

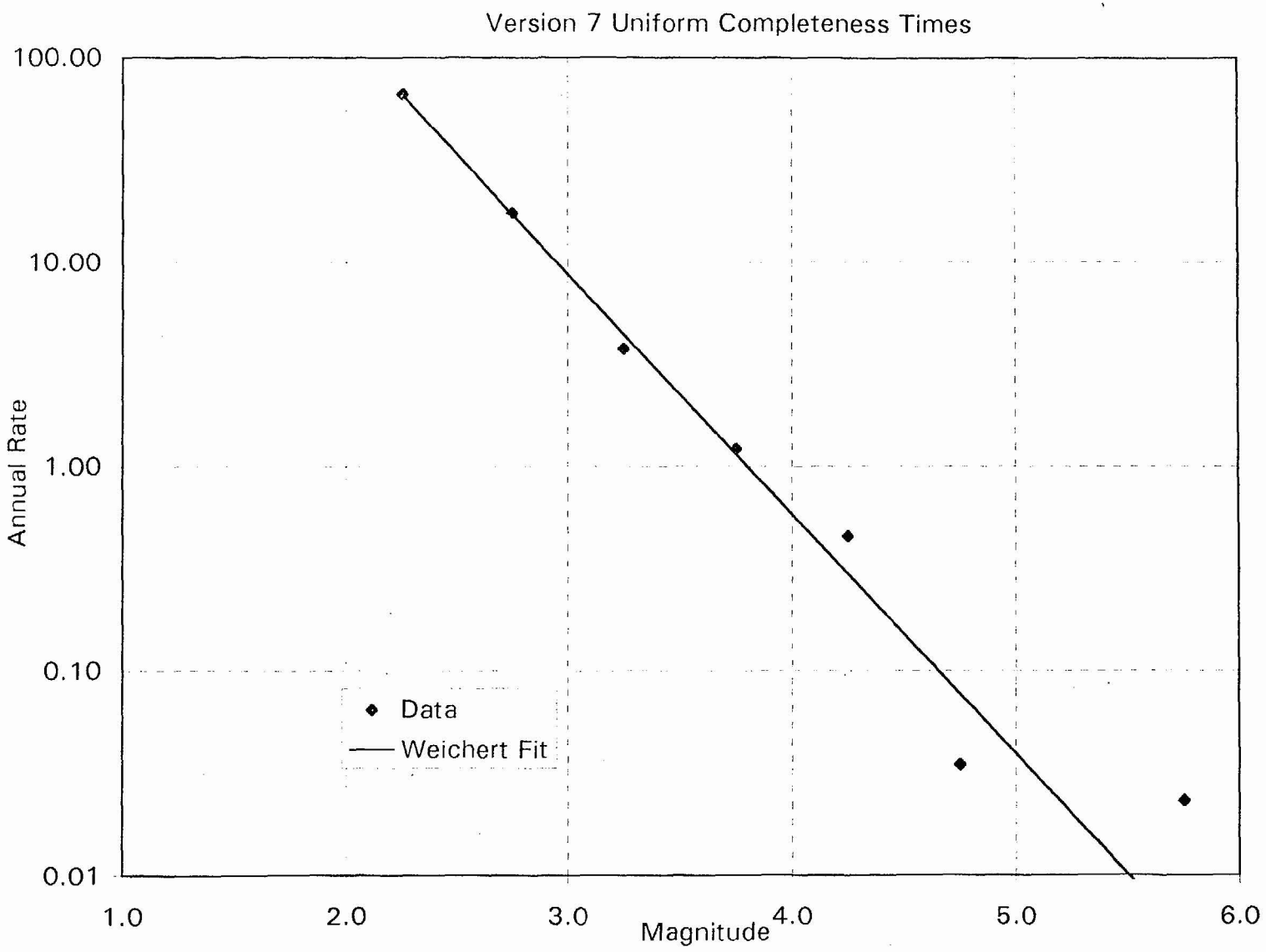

Figure RYA-12 Interval rates for the version 7 catalog that produced the modal b-value 1.17 (Figure RYA-9) and the fit to the data using the Weichert maximum likelihood method

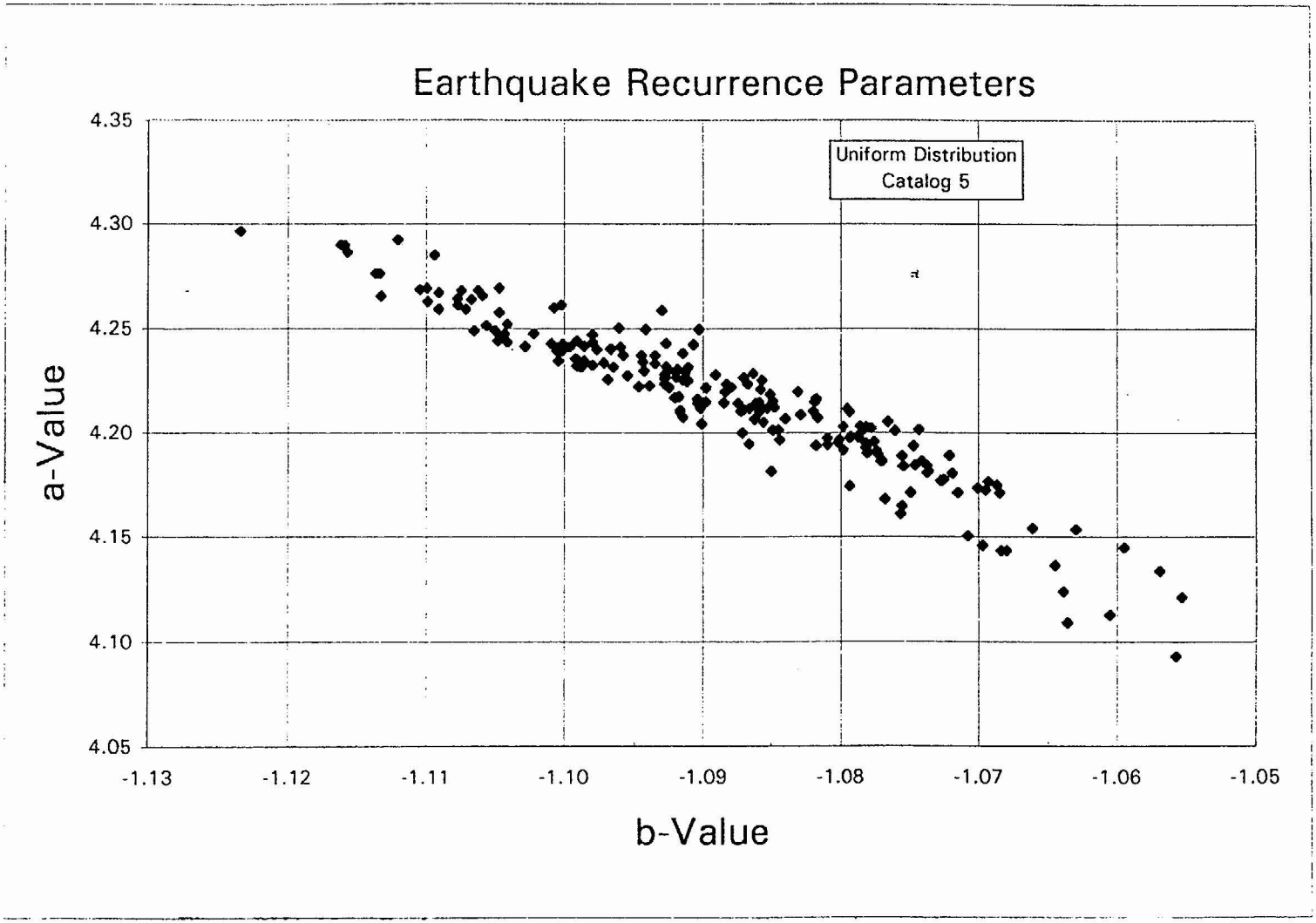

Figure RYA-13 Earthquake recurrence parameters. The paired a- and b-values calculated by uniform sampling from the range of likely completeness times and associated annual rates in the version 5 catalog. This plot shows the correlation between a- and b-values.

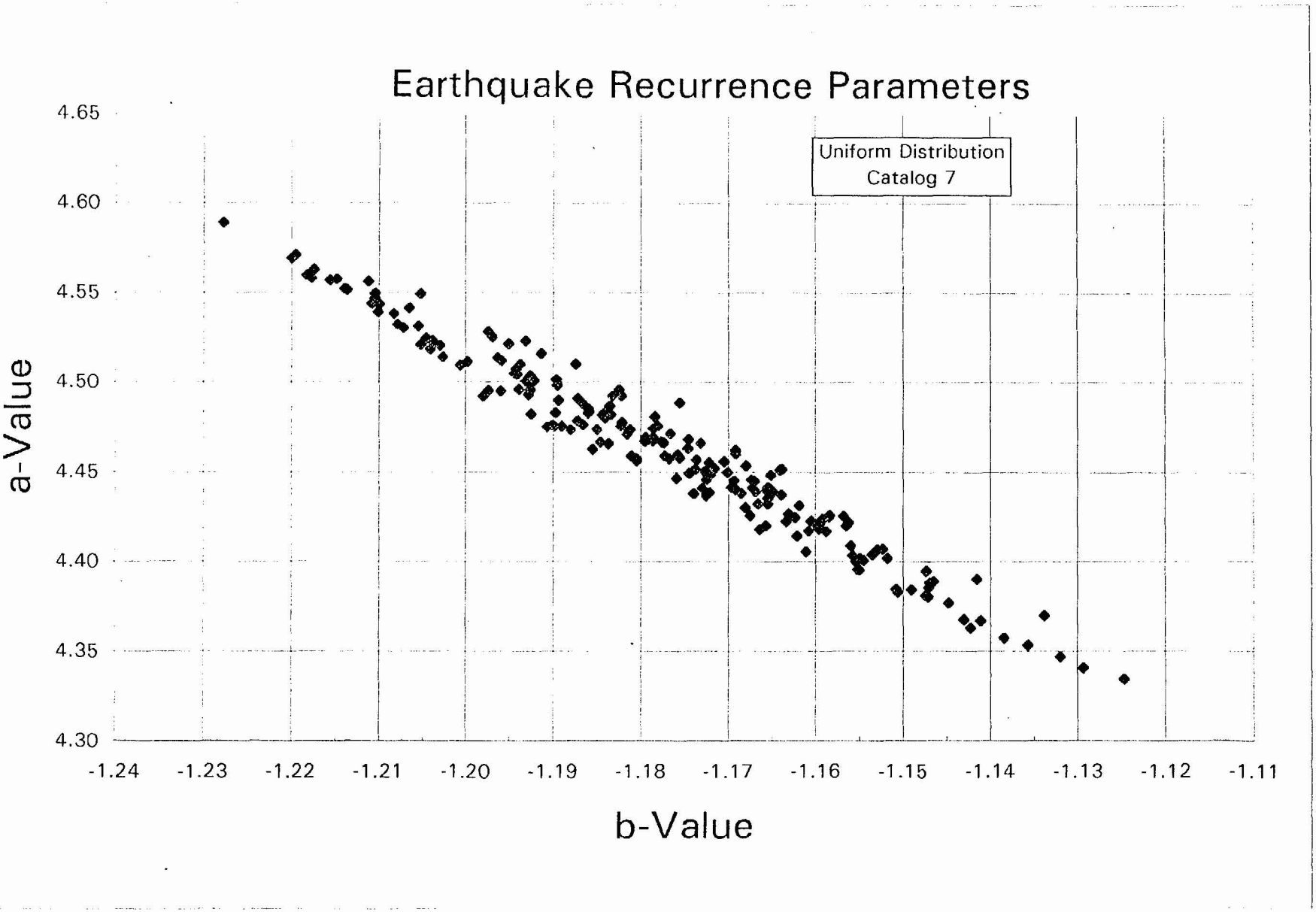

Figure RYA-14 Earthquake recurrence parameters. The paired a- and b-values calculated by uniform sampling from the range of likely completeness times and associated annual rates in the version 7 catalog. This plot shows the correlation between a- and b-values.

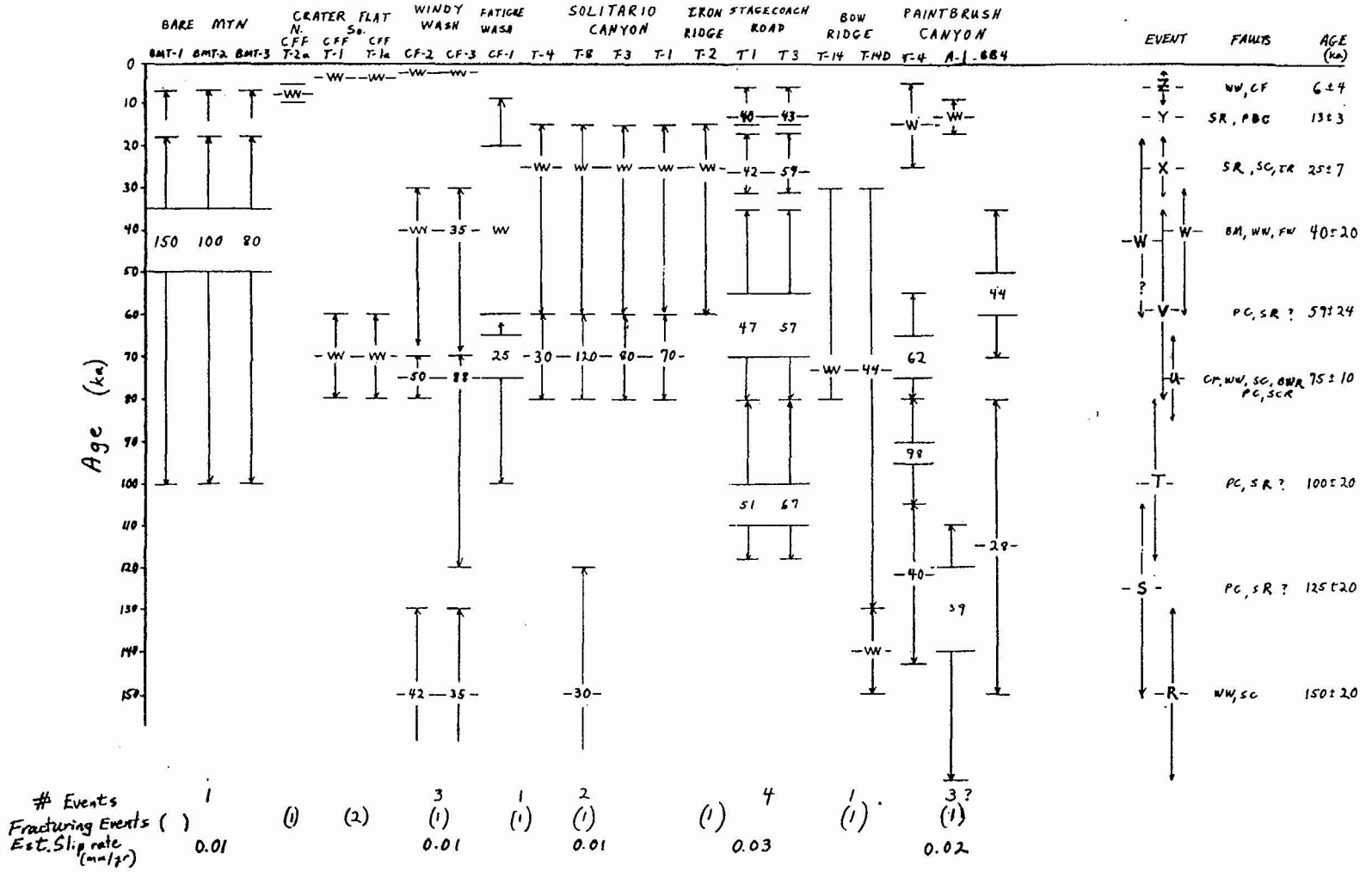

Figure RYA-15 Estimated age and amount (in cm) of late Quaternary displacement for faults in the Yucca Mountain area based on data in USGS (written communication, 1996). Faults are arranged from west to east; trench numbers under each fault are arranged from north to south. Bars and arrows show full uncertainties in estimated age of faulting event at each trench. "w" r represnts fracturing event (displacement < 20 cm). Age on far right of chart shows our best estimate for age of grouped event. See text and tables for fault abbreviations.

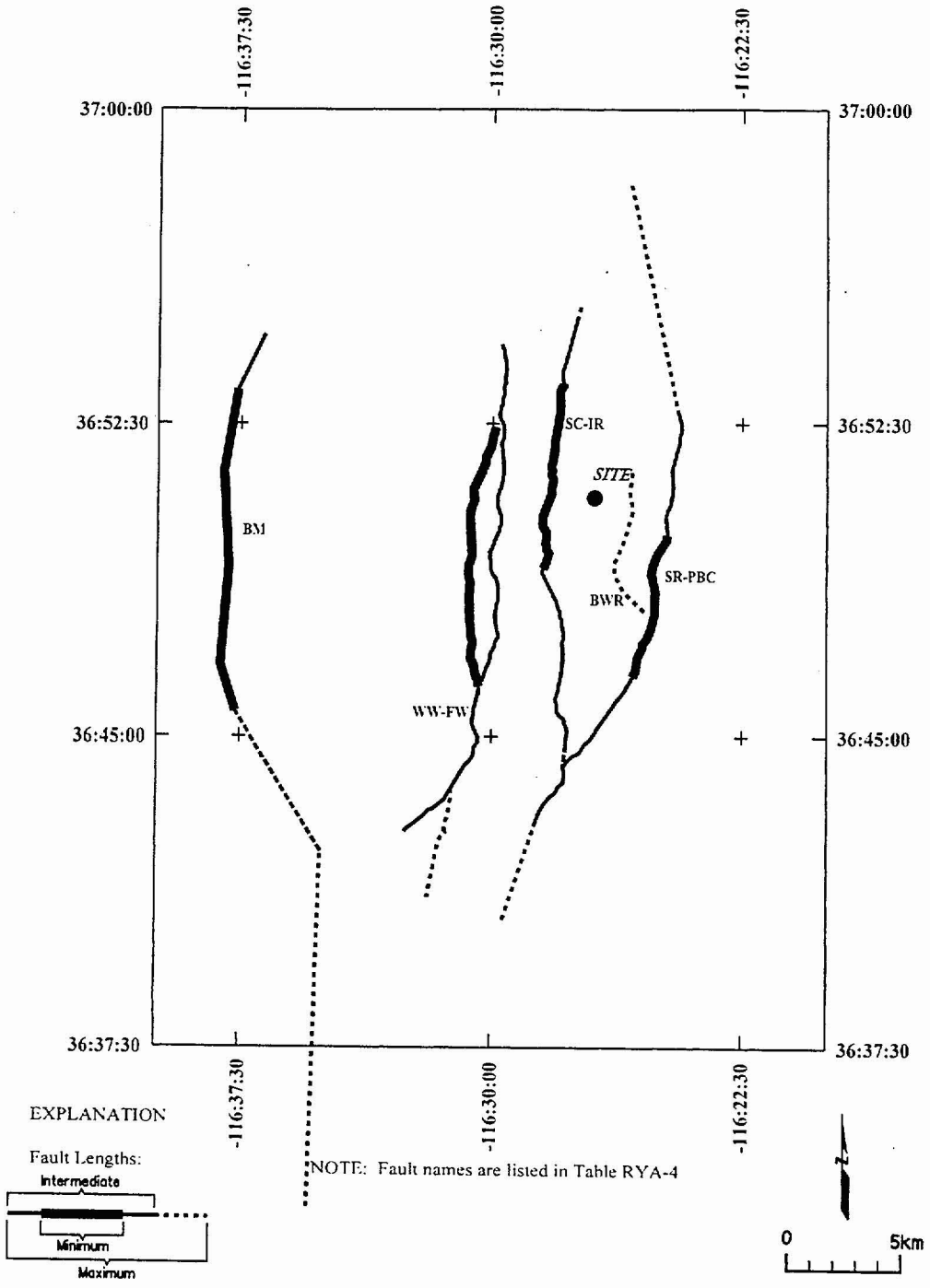

Figure RYA-16 Map showing local fault sources included in the seismic source model

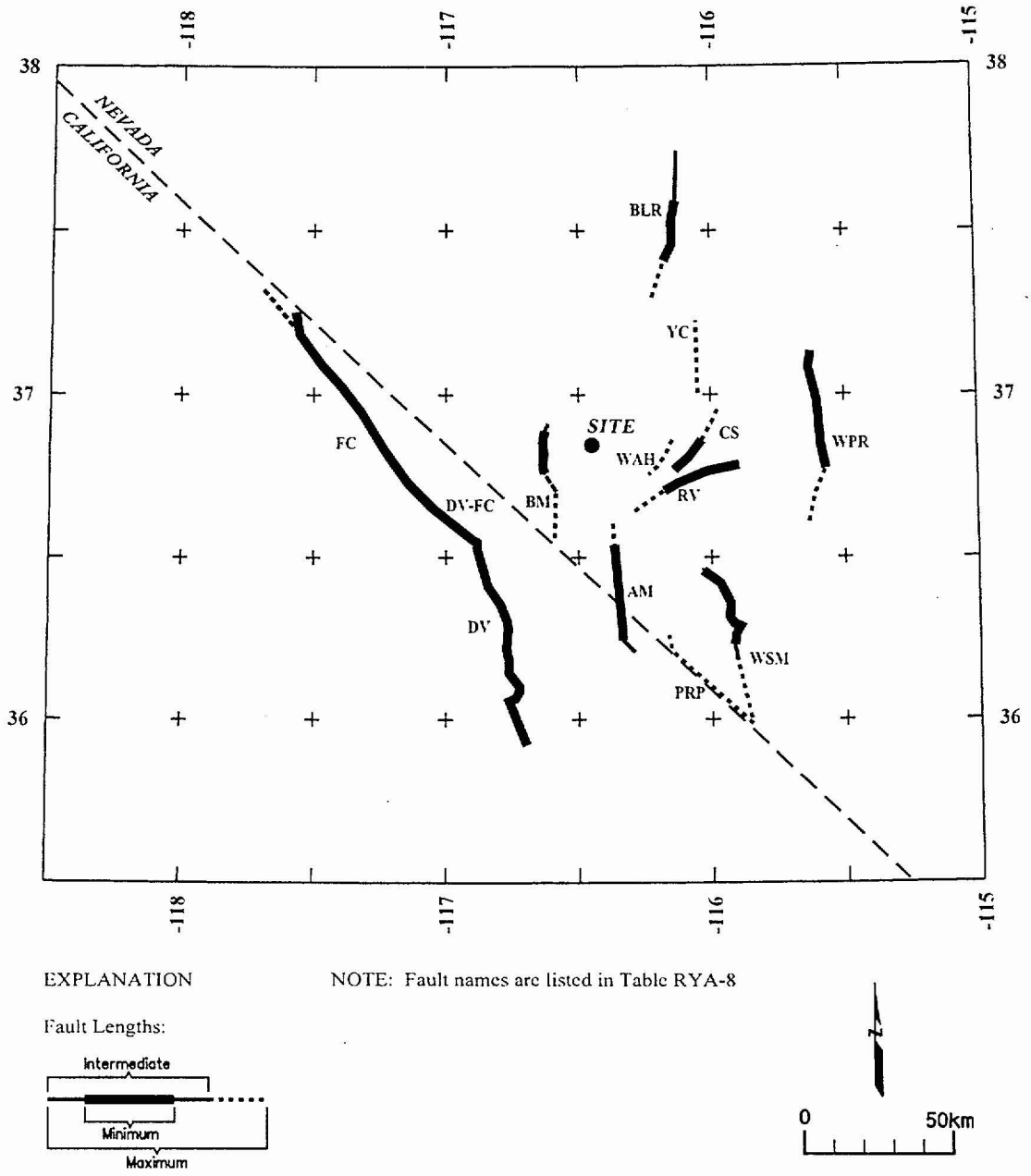

Figure RYA- 17 Map showing regional faults included in the seismic source model.

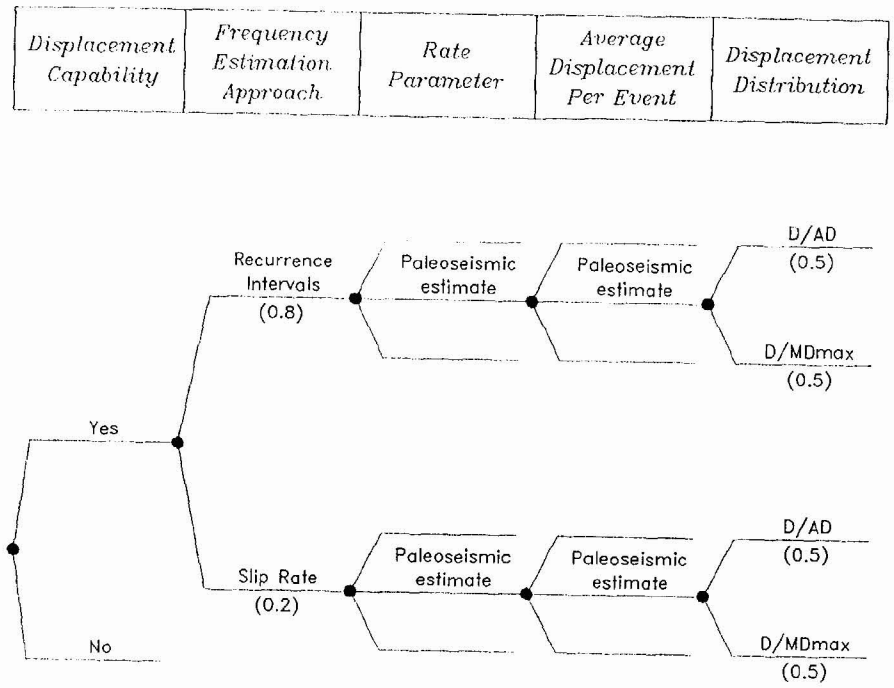

Figure RYA-18 Logic tree used to characterize fault displacement at sites with Quaternary data

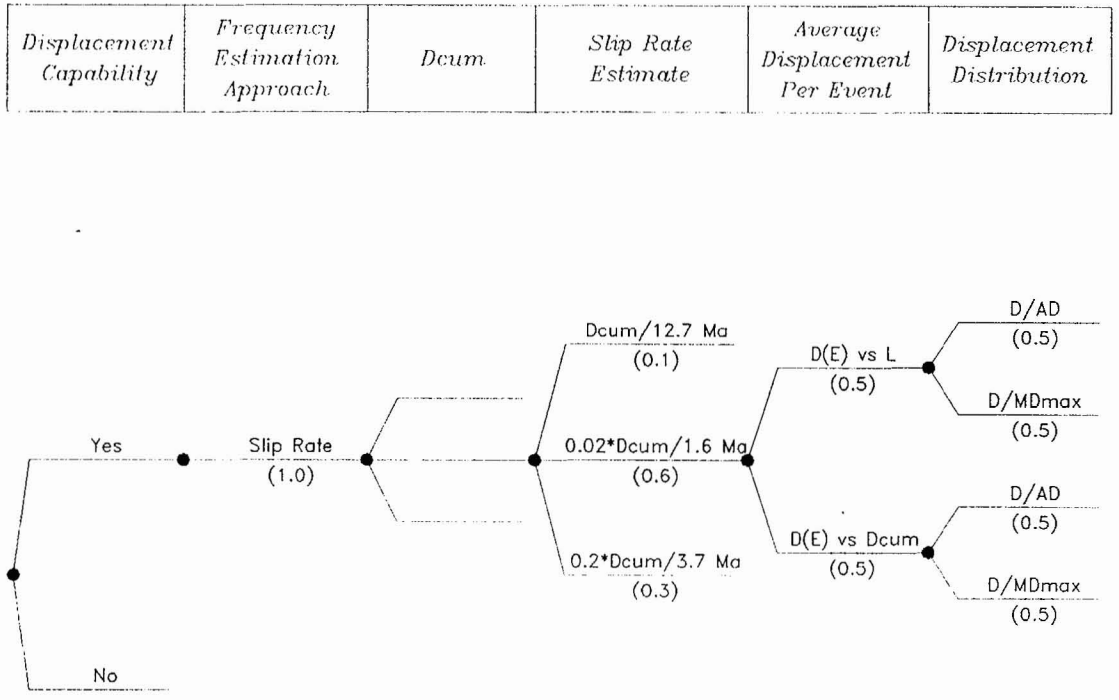

Figure RYA-19 Logic tree used to characterize fault displacement at sites without Quaternary data

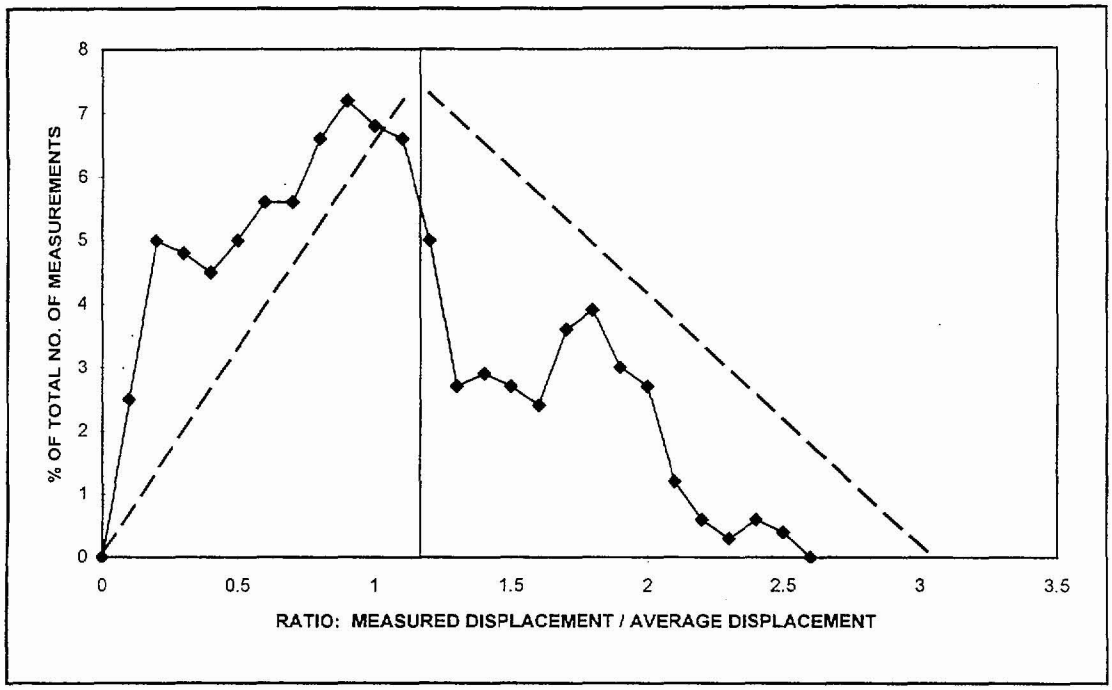

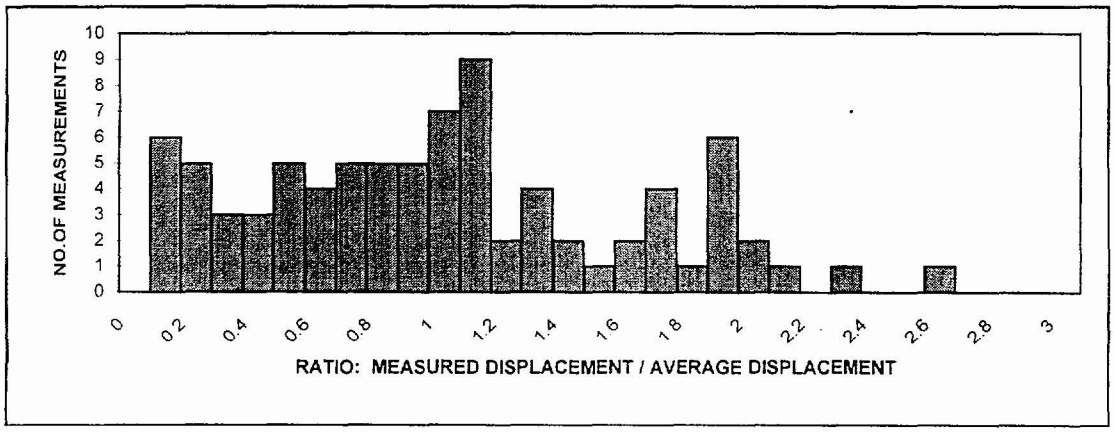

Figure RYA-20 Plots developed by DFS showing event-to-event variability in displacement relative to average displacement per event at a location along a fault based on data from paleoseismic investigations in the Yucca Mountain area

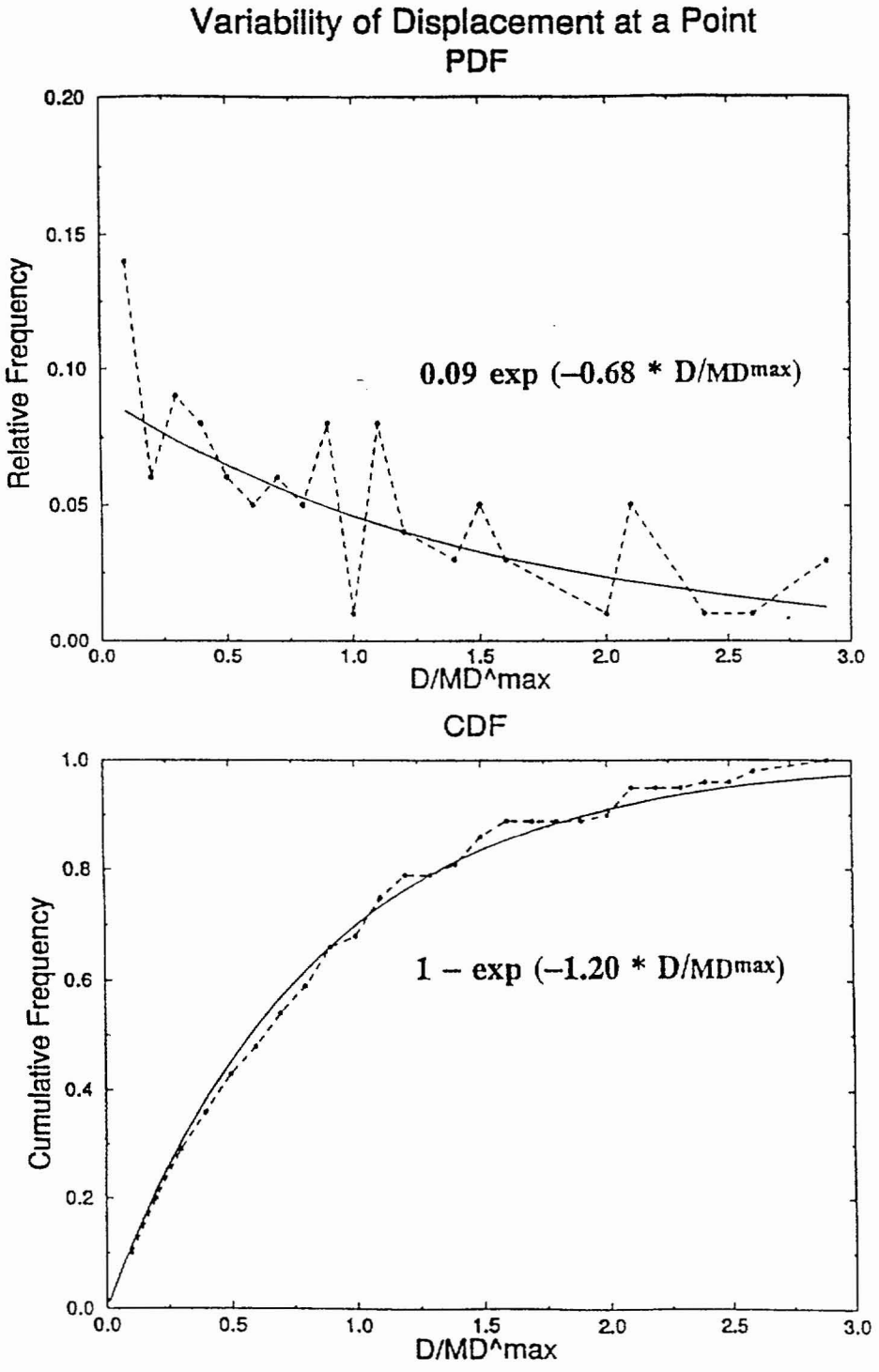

Figure RYA-21 Probability density function (PDF) and cumulative distribution function (CDF) for 80 measurements single-event displacement, normalized to Md^{max} for the corresponding fault, from 19 trenches in the Yucca Mountain area as developed by the AAR team

ELICITATION SUMMARY

KENNETH D. SMITH, RONALD L. BRUHN, AND PETER L.K. KNUEPFER

TABLE OF CONTENTS

TABLE OF CONTENTS

TABLES

FIGURES

TABLE OF CONTENTS

APPENDICES

ELICITATION SUMMARY
KENNETH D. SMITH, RONALD L. BRUHN, and PETER L.K. KNUEPFER

1.0
TECTONIC SETTING AND MODELS

1.1 TECTONIC SETTING

The Yucca Mountain site lies within the Walker Lane tectonic domain (Wright, 1976, 1989; Stewart, 1988) of the southern Great Basin of the Basin and Range province. The site area is slightly more than 300 km (200 miles) from the nearest tectonic plate boundary, the San Andreas fault. The San Andreas fault is the primary structure for strain accommodation between the Pacific and North American tectonic plates. Whereas the San Andreas fault is a transform system, the Basin and Range forms an extensional tectonic regime west of the plate boundary (Wright, 1976, 1989; Stewart, 1978). The extension in the Basin and Range, which began in the late Oligocene and culminated in the Miocene, has been expressed in a variety of deformation mechanisms involving high-angle strike-slip and normal faulting and low-angle normal faulting. Along with Miocene extension came episodes of widespread ignimbrite deposition and associated basaltic volcanism. Little evidence is available in the Yucca Mountain area to evaluate whether low-angle normal faulting remains a primary mechanism for deformation; however, all large historical Basin and Range earthquakes have occurred on moderately to steeply dipping faults (R. Smith, SSC Workshop 4).

Seismogenic faulting, which is distributed throughout the western United States, partly accommodates the relative motion between the North American and Pacific Plates. Global geodetic data and kinematic models indicate that about two-thirds of the total plate motion strain budget of about 48 mm/yr is accounted for on the San Andreas fault system in California and other offshore faults (Minster and Jordan, 1987; Ward, 1990; DeMets *et al.*, 1990; Humphreys and Weldon, 1994). The remaining one-third of the Western United States strain budget is accounted for east of the Sierra Nevada and west of the Colorado Plateau and Rocky Mountains, in the Basin and Range province.

The Sierra Nevada block moves northwestward at a rate of about 12.1 ± 1.2 mm/yr relative to fixed North America east of the Rocky Mountains (Minster and Jordan, 1987; Argus and Gordon, 1991; Dixon *et al.*, 1995). Movements on active faults in the Basin and Range province accommodate this portion of the overall strain budget through a variety of mechanisms. A significant component of lateral slip on faults in the eastern California shear zone is required in these kinematic models and has been measured in geologic and geodetic studies (e.g., Minster and Jordan, 1987; Argus and Gordon, 1991; Dixon *et al.*, 1995). This strain is also accounted for from faulting in the Central Nevada and Intermountain seismic belts (Minster and Jordan, 1987; Argus and Gordon, 1991; Dixon *et al.*, 1995; Smith and Sbar, 1974). Some of these estimates, especially geodetic and Quaternary fault studies, are based on very recent deformation and may not be representative of the total Cenozoic deformation.

The most active fault zones in the Holocene within a 300-km radius of Yucca Mountain mostly are farther than 100 km from the site itself. These faults are located within the Eastern California shear zone (Dokka and Travis, 1990). The Eastern California shear zone is a northwest-trending zone of faults that accommodate right-lateral motion along a north-northwest-trending zone through the Mojave Desert that connects with right-lateral and normal faults along the eastern Sierra Nevada. Geologic and geodetic data from the Mojave Desert indicate a rate of from 5 to more than 8 mm/yr of regional dextral shear that has been active since middle Miocene time (Dokka and Travis, 1990; Savage *et al.*, 1990; Richard, 1992).

East of the Sierra Nevada and north of the Mojave block, the Eastern California shear zone is defined by three major northwest-trending right-lateral fault zones: the Death Valley-Furnace Creek-Fish Lake Valley, the Hunter Mountain-Panamint Valley, and the Owens Valley fault zones. Geologic studies indicate an average late Quaternary slip rate of 1 to 4 mm/yr on the Hunter Mountain-Panamint Valley and Owens Valley fault zones (Burchfiel *et al.*, 1987; Lubetkin and Clark, 1988; Zhang *et al.*, 1990; Beanland and Clark, 1994), and as much as 4 to 8 mm/yr for the Death Valley-Furnace Creek-Fish Lake Valley fault zones (R. E. Klinger and L. A. Piety, written communication, 1996; Reheis and Dixon, 1996; Reheis and Sawyer, 1997). Thus, the Eastern California shear zone accounts for most of the strain budget of the plate boundary system east of the Sierra Nevada, leaving a small portion to be allocated to

faults in central Nevada and western Utah. Known and suspected Quaternary faults east of the Death Valley-Furnace Creek-Fish Lake Valley fault zone and in the Yucca Mountain vicinity have slip rates on the order of 0.001 to 0.01 mm/yr (J. W. Whitney *et al.*, USGS, written communication, 1996b); this is as much as three orders of magnitude less than slip rates on the faults in the Eastern California shear zone (Piety, 1995; W. R. Keefer and S. K. Pezzopane, USGS, written communication, 1996).

1.2 TECTONIC MODELS

Tectonic models are used to constrain fault geometry and behavior and to estimate the characteristics of buried seismogenic sources. First the tectonic model classification scheme of D. W. O'Leary (USGS, written communication, 1996) is discussed and evaluated for completeness. We then modify O'Leary's approach and evaluate the likelihood that each model exists and controls the behavior of active seismic sources. We evaluate the potential for activity of known and inferred faults, and the manner in which the dimensions of these seismic sources may be controlled by structures inherited from geologic history, or formed under the current tectonic regime. We partly follow the terminology of D. W. O'Leary (USGS, written communication, 1996) for clarity and convenience. However, the terms 'pure shear' and 'simple shear' as used by O'Leary to classify tectonic models do not accurately describe the regional tectonics, because these terms are restricted to descriptions of two-dimensional strain fields whereas the strain field at Yucca Mountain is three-dimensional.

1.2.1 Volcanic Models

Several models have been proposed in the literature that relate the development and continuing activity of faults in the Yucca Mountain area (the site fault area discussed later) to volcanic processes. We review the completeness of these models in the following sections. However, we conclude that none of these models explains the nature of active tectonism in the study area.

Caldera Model. Calderas in the Yucca Mountain region formed during Miocene tectonism. Their principal importance today could be in providing insight into the relationship between

the current stress field and the orientation of Miocene structures, which could influence geometry of active faults or help localize background seismicity. Many of these structures that formed in the Miocene also display evidence of Quaternary movement (Fridrich, 1997). The Timber Mountain-Oasis Valley caldera complex in the northern Nevada Test Site (NTS) is the primary source area for the volcanic tuffs that form Yucca Mountain (D. W. O'Leary, USGS, written communication, 1996; written communication, W.C. Day *et al.*, USGS, written communication, 1996e). Carr (1990) proposed that these Miocene calderas extended south of the Timber Mountain complex into Crater Flat. His interpretation was based in part on the presence of basaltic volcanism in Crater Flat, but this volcanism has been shown since to have occurred much later than the Miocene (Geomatrix Consultants, written communication, 1996). Also, faults at Yucca Mountain interpreted by Carr (1990) as caldera ring fracture systems have since been identified as tectonic faults rather than volcanic features (Fridrich, 1997; D. W. O'Leary, USGS, written communication, 1996). Furthermore, Crater Flat has been interpreted from gravity profiling (Langenheim, SSC Workshop 1), magnetic studies (Stamatakos *et al.*, 1997), and geologic investigation (Fridrich, 1997) to be a pull-apart basin filled with interbedded volcanics and sediments. Given this history, we conclude that calderas do not control the active structures in the Yucca Mountain area and assign zero weight to this caldera model.

Rift Model. The north-south-trending Kawich-Greenwater trough (Carr, 1984, 1990) is an older (originated pre-10 Ma) rift structure that likely established most of the regional faulting patterns and may provide the tectonic framework for current activity (Carr, 1990, Figure 8). As proposed by Carr (1984), this rift zone is identified by a nearly north-south-striking gravity low that extends from the northern NTS and the calderas of the Timber Mountain-Black Mountain-Oasis Valley complex, through Yucca Mountain and eastern Amargosa Valley, to end southwest of Death Valley in the Greenwater volcanic center of the Greenwater Range. This rift includes a number of older (15 Ma) silicic volcanic centers as well as younger basaltic cones and flows, including the Crater Flat basalts of Pliocene and Quaternary age. Aeromagnetic data (Majer, SSC Workshop 4) show several additional buried basaltic sources in the proposed rift south of Yucca Mountain near Highway 395 and near Lathrop Wells (Geomatrix Consultants, written communication, 1996; Langenheim *et al.*, 1993; Stamatakos *et al.*, 1997). Other buried volcanic sources south of Lathrop Wells may also be interpreted from the aeromagnetic data (Langenheim *et al.*, 1993). Evidence for

a throughgoing structure associated with these potential field anomalies is also shown by the near similarity in behavior of north to east-northeast faults mapped in Miocene tuffs in the Pahute Mesa area north of Timber Mountain and the faults at Yucca Mountain south of the Miocene caldera complex.

The isostatic gravity data (Ponce, 1993; Majer, SSC Workshop 4; D. W. O'Leary, USGS, written communication, 1996) show a north-south-striking, buried graben structure extending south of Yucca Mountain into Amargosa Valley. This southern part of the Kawich-Greenwater rift zone is named the Amargosa trough by D. W. O'Leary (USGS, written communication, 1996). This graben, which is about 40 km long and about 20 km wide, forms a boundary between regional tectonic domains in southern Nevada (D. W. O'Leary, USGS, written communication, 1996). Quaternary scarps of the Ash Meadows fault system (Piety, 1995) define the east side of the graben. The west edge extends north along the east margin of Bare Mountain and western Crater Flat. The southwest end of the graben parallels the Death Valley fault system, and the southeast end abuts the northern Pahrump Valley fault system near Stewart Valley. The Rock Valley fault zone appears to be truncated along the east margin of the graben, where the north-trending gravity gradient (the so-called Gravity fault) extends into Jackass Flat. The concentration of recent and historical seismicity that parallels the Rock Valley fault zone also is interrupted at this locality (K. Smith, SSC Workshop 2). However, additional northeast-trending scarps in Amargosa Valley to the southwest may be related to the Rock Valley fault (Anderson *et al.*, 1995b). We suggest that in the Miocene the graben structure accommodated strain transferred from the Las Vegas Valley shear, to the east, through the southern Great Basin. From this evidence it can be interpreted to represent a failed rift system. This is one in a family of oblique rift models that we consider to be an integral part of the Yucca Mountain tectonic setting (Figure SBK-1).

Dike Injection. As an alternative to faulting, injection of basaltic dikes may accommodate extension and strain in Crater Flat (Parsons and Thompson, 1991a, b). Thus, periods of volcanism may retard normal faulting in Crater Flat. Given this mechanism of accommodating extension, the strain rates estimated from the fault slip data would tend to underestimate the total local tectonic strain rate. Alternatively, volcanic processes may trigger faulting. For the Scenario U (ash event) of S. K. Pezzopane *et al.* (USGS, written communication, 1996a), several faults in the Crater Flat basin and at Yucca Mountain have

been interpreted to have ruptured concurrently with volcanic activity at about 70 ka. Evidence includes volcanic ash in several trench sites on the Solitario Canyon, Windy Wash, Fatigue Wash, South Crater Flat, and Bow Ridge faults. Elsewhere, subsurface movement of volcanic material has been associated with a series of moderate-sized earthquakes in the Mammoth Lakes-Bishop area of California (Appendix SBK-3). These earthquakes have generated secondary and possibly primary surface faulting and most likely local ground motions on the order of 0.5 g. The presence of Pliocene and Quaternary volcanics in Crater Flat indicates that dike injection accommodates some of the extensional strain in the Yucca Mountain area. A dike injection model may be a mechanism to passively account for strain through emplacement of basaltic material in the lower crust, and it may further trigger, or at least be associated with, earthquakes by movement of volcanics into the shallow (brittle) crust. In our evaluation of tectonic models, we consider it very likely that dike injection affects strain rates (Figure SBK-1); the principal effect of this on seismic source characterization is our treatment of volcanically related sources separately from primary faulting on local sources, as discussed in Section 2.4.1.

1.2.2 Low-Angle Fault Models

All of the low-angle fault models suggested for the Yucca Mountain region include a detachment of some kind. It is possible that an old (Oligocene-Miocene?), currently inactive and deformed, detachment structure underlies the region, with the Bare Mountain fault offsetting it beneath Crater Flat (Scott, 1990; Fridrich, 1997). Large detachments structures most likely operated in the Miocene, as evidenced by the Florspar Canyon fault system (Hamilton, SSC Workshop 3); the evidence of the unroofing of Bare Mountain (Ferrill *et al.*, 1996a); and the presence of middle to lower crustal rocks in metamorphic core complexes. Possible locations of detachments could occur beneath Crater Flat and Yucca Mountain at the Paleozoic-Tertiary contact, the Precambrian-Paleozoic contact, or the mid-crustal brittle-ductile transition (i.e., base of the seismogenic crust).

Wernicke (1995) suggests that detachment faults may be independent seismogenic sources of large lateral extent, and are capable of generating significant earthquakes. However, we do not consider detachment faults to be independent seismic sources at Yucca Mountain because: (1) geologic mapping indicates that the Paleozoic-Tertiary contact in the Yucca

Mountain vicinity is not a regional detachment (Fridrich, 1997; Simonds *et al.*, 1995); (2) there is no evidence for shallow detachments on seismic lines (Brocher, SSC Workshops 2 and 3) or in drill holes; (3) background seismicity in the vicinity shows no evidence for activity on low-angle faults; (4) although detachments occur in the surrounding regions and throughout the Basin and Range, most of these are old (Tertiary); (5) evidence shows that large normal-faulting earthquakes in continental crust occur only on high-angle faults throughout the world (Jackson and White, 1989); and (6) the Little Skull Mountain earthquake occurred on a steeply dipping (60 to 65 degrees) structure (Appendix SBK-2). The evidence indicates that even if a detachment exists under Yucca Mountain, it has a negligible probability of being seismogenic. Thus, we do not model a detachment as a seismogenic source capable of producing earthquakes above the background. In considering the possibility that one or more detachments exist, we use such structures only to constrain down-dip width and fault areas. Specific detachment geometries are discussed in the context of the assessment of dip and area of local faults.

1.2.3 Lateral Shear Models

Lateral shear models propose regional dextral shear along either a buried throughgoing shear zone in the crust or discrete, transcurrent fault populations that are characteristic of the Walker Lane belt (Wright 1976, 1989; Stewart, 1988). In this model, the primary deformation in the southern Great Basin is ultimately driven by the large throughgoing right-slip faults of the Death Valley-Furnace Creek-Fish Lake Valley, Hunter Mountain-Panamint Valley, and Owens Valley fault systems. These latter faults account for most of the approximately 12 mm/yr of the plate motion strain budget in the western Basin and Range of southern Nevada and eastern California. Slip rates on structures east of the Eastern California shear zone are significantly less than those on the primary transcurrent faults. Indeed, the small strain budget east of the high-angle faults of the Eastern California shear zone can be accommodated readily by a combination of high-angle transcurrent, normal, and oblique-normal slip faults, as supported by paleoseismic and seismicity data. This provides further evidence that it is not necessary to invoke low-angle faulting to support our conclusion that no large-area, low-angle normal faults or detachments are active.

Schweickert (SSC Workshop 3) proposed a buried regional shear zone in the Crater Flat area that had some components of the transtensional nappe model of Hardyman and Oldow (1991). This model is given an extremely low weight because: (1) conclusive evidence for offset geologic features along the postulated shear zone is lacking; (2) a 240-km-long shear zone with kilometers of offset should have scarps or other direct evidence at the surface for most of its length, and no such evidence exists.

1.2.4 High-Angle Faulting Model

The tectonic model that we consider best explains present tectonism in the Yucca Mountain region includes a component of lateral shear related to deformation through the Walker Lane belt (Stewart, 1988). The Death Valley-Furnace Creek-Fish Lake Valley fault system accommodates most of the regional strain through a slip rate of 4 to 8 mm per year (R. E. Klinger and L. A. Piety, USBR, written communication, 1996; Reheis and Sawyer, 1997). Slip rates on faults east of the Furnace Creek fault system are 2 to 3 orders of magnitude less. Short-period focal mechanisms (Rogers *et al.*, 1991) show a predominance of high-angle strike-slip faulting (S. K. Pezzopane *et al.*, USGS, written communication, 1996b), although normal mechanisms form a significant percentage of the database. The best evidence for high-angle faulting from a moderate-sized event in which the causative fault plane can be isolated is the 1992 M 5.6 Little Skull Mountain earthquake. It occurred on a steeply dipping structure (60 to 65 degrees; K. Smith, SSC Workshop 2), which is consistent with teleseismic, short-period, and regional faulting mechanisms for the event (K. Smith, SSC Workshop 2). Also, detailed aftershock relocations support the interpretation of faulting on a high-angle structure (K. Smith, SSC Workshop 2). Well-constrained short-period focal mechanisms for earthquakes in the Rock Valley fault zone in 1993, which incorporated supplemental portable instrument data, show high-angle strike-slip faulting, which is consistent with mapping and trenching studies of J. A. Coe *et al.* (USGS, written communication, 1996). Mapping of faults and dips of surface exposures for faults in the Yucca Mountain area also suggest that these are high-angle structures (Simonds *et al.*, 1995).

In the high-angle fault model, structures in the vicinity of Yucca Mountain are interpreted to be planar, and the Rock Valley fault and a buried structure near Highway 95 within the Amargosa trough to the west act as an accommodation zone, which truncates the local Yucca

Mountain faults at their south ends. The Yucca Mountain faults in this model are part of a half-graben, which is bound on the west side by the Bare Mountain fault. The faults are predominantly normal-slip structures having a left-lateral component of displacement that accommodates transtensional strain.

1.3 EVALUATION OF TECTONIC MODELS

The logic tree (Figure SBK-1) simplifies the tectonic models described above, focusing on those elements that may affect the geometric characteristics of other faults or may act as independent seismic sources. We categorize the models of O'Leary (as discussed above) into two classes: (1) oblique rifting and (2) regional dextral shear. The oblique rifting class is preferred (probability 0.99; Figure SBK-1), because it is more encompassing of volcano-tectonic structures in the Yucca Mountain region and includes the possibility of discrete strike-slip faults in addition to oblique-normal-slip and normal-slip faults.

1.3.1 Oblique Rift Models

Oblique rift models focus on the inferred presence or absence of low-angle faults (detachments, and the possibility of rolling-hinge tectonism [Hamilton, SSC Workshop 3]). All of these models include steeply to moderately dipping faults. The logic tree is structured to consider the presence of a detachment fault in two ways: (1) as a structural discontinuity that may control the depth, extent, or geometry (listric or planar) of steeply dipping faults; and (2) as a separate seismic source (active or inactive) to be considered in the seismic sources analysis. Given the lack of evidence for one or more detachment faults acting as a controlling structure in the present tectonic environment, as noted above, we apply extremely low weights (total of 0.01 to the three) to the likelihood of single or multiple detachments or Hamilton's rolling hinge model. In addition, as discussed above, we assign a likelihood of zero that a detachment structure can behave as an independent seismic source.

1.3.2 Regional Dextral Shear Models

These models are divided into two types: those with and those without a low-angle transtensional detachment. Steeply dipping faults are included in both types, but in the

former model (transtensional nappe) there is a large-area, horizontal to subhorizontal detachment fault that transfers strike-slip movement into the middle to upper crust. Given the lack of evidence for the transtensional nappe model of Schweickert (SSC Workshop 3), we assign an extremely low weight (0.01) to this possibility.

1.3.3 Effects of Igneous Dike Injection

Quaternary volcanism may accommodate some of the extension in Crater Flat, and therefore decrease the slip rates on the Bare Mountain and other faults (Parsons and Thompson, 1991a, b). Thus we include dike injection as an element in tectonic models. We do not consider the dike injection model as a separate branch on the logic tree for tectonic models (Figure SBK-1); instead, it is included as an option in both the oblique rift and dextral shear zone models. Given that dike injection has occurred in the Crater Flat area during the Quaternary, it clearly plays a role in any tectonic model. We assign a high likelihood (0.95) that dike injection affects slip rates on the local faults, as we discuss further when considering the seismic potential of volcanic sources. We further consider the significance of volcanic dikes in explaining the low late Quaternary slip rates on the Bare Mountain and possibly the local Yucca Mountain faults as well as acting as a trigger for simultaneous fault ruptures. We also address the question of whether fractures that produce aligned dikes, such as the Crater Flat cones, are also separate seismic sources, perhaps capable of generating earthquakes during magma injection at depth (see discussion of Mammoth Lakes area sequence Appendix SBK-3).

1.3.4 Utilization of Logic Tree for Tectonic Models

We have interpreted a most likely tectonic model—steep to moderately dipping faults in an oblique rift system—consistent with the tectonic history of the Yucca Mountain area and the kinematics of currently active structures. Most other models are given negligible or extremely low weights as descriptors of the active tectonic regime. Furthermore, we consider that the tectonic models principally control down-dip geometry of the local faults. For example, all of the detachment models (single detachment, multiple detachment, rolling hinge) imply that site faults merge at shallow or intermediate crustal depths; the interpretation affects the likelihood that faults coalesce down dip, as well as the width of individual and coalesced faults. Given that this is the only kind of effect we consider credible for the

nonplanar-fault tectonic models (i.e., we do not add additional seismic sources for different models, as discussed below), we do not explicitly incorporate different tectonic models as branches of a logic tree. Instead, our weighting of tectonic models provides a framework for our evaluation of the geometry of local fault sources.

2.0 SEISMIC SOURCES

Seismic source zones are identified throughout the 100-km-radius surrounding the site, as shown on Figures SBK-2 and -3. Regional and local fault sources are identified (Figures SBK-5 and -6); areal seismic source zones (Figures SBK-2 and -3) serve as background zones to these fault sources. The maximum magnitude associated with each seismic source zone is a function of several variables. Within 100 km, the regional and local fault sources that can produce potential maximum earthquakes above the maximum background were identified and are characterized separately. Assigning the maximum background magnitudes for the areal source zones is based on the observations of the largest earthquakes in the Basin and Range that did not have reported primary surface faulting. The largest of these events occurred in Montana in 1925. This event is less relevant to the Yucca Mountain area because of the thinner seismogenic crust in southern Nevada. In the local site vicinity, extensive geologic mapping has identified small-displacement events—as small as cracking events. Because of the enhanced resolution in the local site area (including Yucca Mountain and Bare Mountain), it is interpreted that a fault source comparable to those mapped has not remained undetected. Therefore, a smaller maximum magnitude is assessed for the areal source zone in the local site vicinity. Earthquake recurrence relationships were developed for each areal source zone based on observed seismicity data. For areal sources containing regional and local fault sources, seismicity associated with these fault sources was removed before calculating recurrence parameters for the source zone. Recurrence relationships for regional and local fault sources were developed from fault-specific geologic data.

2.1 THICKNESS OF SEISMOGENIC CRUST

The thickness of the seismogenic crust in the southern Great Basin is assessed both on the depth distribution of seismicity from the earthquake catalog and the record of estimated hypocentral depths for main shocks in the Basin and Range Province (SDO Team, SSC Workshop 4). We use the depth distribution of main shocks in the Basin and Range, an extensional environment, rather than considering California analogs because of the clear difference between the tectonic regimes. We also recognize that there is some variation in the tectonic styles and crustal thickness within the Basin and Range itself (Smith and Sbar, 1974). For example, deformation in the southern Great Basin, dominated by the strike-slip systems of the Death Valley-Furnace Creek-Fish Lake Valley, Hunter Mountain-Panamint Valley, and Owens Valley fault zones (Dixon *et al.*, 1995; Piety, 1995), may be quite different from the tectonics of the Central Nevada Seismic Belt in north-central Nevada and the extension associated with the basaltic volcanics of the Eastern Snake River Plain in the northern Basin and Range. Also, there is some evidence that large main shocks in the Basin and Range ($M > 6.8$) may initiate at greater depth than may be indicated purely by analyzing the depth distribution of earthquakes in the recent period of seismic monitoring (SDO Team, SSC Workshop 5).

Doser and Smith (1989), Doser (1986, 1988), and the SDO Team (SSC Workshops 4 and 5) analyzed the depth of initiation and rupture of the historical, $M > 6.5$ earthquakes in the Basin and Range. These analyses show that earthquakes in this magnitude range may initiate as deep as 20 km. For example, modeling the rupture processes of the Borah Peak earthquake from teleseismic and regional seismograms indicates seismic energy radiating from the fault plane at depths as great as 22 km, whereas the Borah Peak hypocenter has been determined to be at about 16 ± 4 km (R. Smith, SSC Workshop 4). Many of the hypocentral depths for Basin and Range events were calculated from teleseismic recordings (exclusively for the older events), using techniques that require good velocity information in the middle crust to reduce uncertainties in the estimate. Clearly, of the large events in the Basin and Range, the Borah Peak event of October 1983 would provide the best data for evaluating the depth distribution of faulting, yet there were no near-source recordings (< 20 km) for this earthquake.

In contrast, recent moderate-sized earthquakes in the Basin and Range, in particular in the central and southern Great Basin, have shown a shallower depth distribution of aftershock activity and initiation of main shock rupture. The resolution of the estimates of hypocenter depth for many of these sequences is provided by high-quality regional and local data that were not available for the large historical Basin and Range events. Recent moderate-sized earthquakes in the central and southern Basin and Range include the June 1992, M 5.6 Little Skull Mountain, Nevada (Harmsen, 1993; K. Smith, SSC Workshop 3); May 1993, M 6.1 Eureka Valley, California (Peltzer and Rosen, 1995; Massonnet and Feigl, 1995); and July 1986, M 6.3 Chalfant Valley, California, earthquakes (Appendix SBK-3). A sequence of moderate-sized earthquakes in the Mammoth Lakes area of California in the 1980s was well recorded, but its association with the active Long Valley caldera makes it questionable with respect to evaluating seismogenic depth estimates in nonvolcanic areas. The refined hypocentral depths for these moderate sized earthquakes are: Little Skull Mountain, 11.7 km (K. Smith, SSC Workshop 3; Harmsen, 1993; Meremonte *et al.*, 1995); Eureka Valley, 11.8 km (Loper *et al.*, 1993); Chalfant Valley, 12 km (Smith and Priestley, 1997). All of these earthquakes initiated near the base of the local seismogenic zone. This conclusion is based on the assumption that the maximum depth of the well-located aftershock activity defines the local base of the seismogenic zone in these areas.

Earthquakes in the southern Great Basin occur primarily between 5 and 15 km in depth (Appendix SBK-1). The distribution is dominated by the Little Skull Mountain sequence, which represents about 20 to 30 percent of the seismicity catalog for the southern Great Basin in the NTS area (Appendix SBK-1). This sequence was confined primarily between 12 and 6 km depth; the deep distribution peaks near the lower edge of the seismogenic zone. The sequence was particularly well recorded, and depth constraints are good. Rogers *et al.* (1987) showed that seismicity in the southern Great Basin was distributed between about 15 and 2 km, with a gap in activity at about 4 km. This observation has not continued through the period of digital data recording, 1995 through 1997, and may represent mislocations resulting from the misidentification of S-wave arrivals on vertical-component records. Shallow activity has been rare in the recent period but has been observed. The 1993 Rock Valley sequence, an unusually shallow cluster of earthquakes (K. Smith, SSC Workshop 3; Smith and Brune, 1997), generally was confined to less than 3 km depth. These shallow hypocentral depths were confirmed with the installation of near-source (less than one focal

depth), three-component digital recorders. Hypocentral depths of about 2 km from the surface were identified in the Shields *et al.* (1995) study for the 1993 Rock Valley sequence.

Rogers *et al.* (1987) show that most of the seismic energy released in the southern Great Basin occurs at depths less than 12 km, but this observation is based on data from a period (1978-1987) when there was minimal moment release throughout the southern Great Basin. Occasional larger-magnitude earthquakes reportedly nucleated deeper than 15 km; however, many of these events occurred early in the instrumental record, and their hypocenters probably are not well constrained. Nucleation depths of about 16 km have been reported for several major earthquakes in the Basin and Range province: the 1954 Dixie Valley, Nevada; 1959 Hebgen Lake, Montana; and 1983 Borah Peak, Idaho (all from R. Smith, SSC Workshop 4); all were M 7+ range-bounding, normal-faulting events. Critical to the estimation of maximum moment from a structure is whether rupture can propagate to these depths, which would not necessarily have to correlate with hypocentral depth. Also, slip at these depths may not contribute significant ground motion at the surface.

Our weighting of maximum seismogenic thickness allows us to account for the possibility that larger earthquakes may rupture below the depths indicated by the distribution of well-located regional seismicity and the maximum depth of the seismogenic thickness indicated for the three central and southern Great Basin earthquake sequences listed above. Rupture may extend below the brittle seismogenic zone, because the dynamic strain rate during rupture propagation may be high enough to overcome the frictional conditions in the-brittle-to-ductile transition zone that exists in the mid-crust near the base of the seismogenic zone. Under these conditions, rupture propagation may be acceptable in dynamic rheologies that physically do not allow for the initiation of the small- to moderate- sized earthquakes ($M < 6$), which comprise the bulk of the regional seismic catalogs.

The ranges and weightings of seismogenic thickness are interpreted to be the same for all source zones throughout the study area. We define the base of the seismogenic zone as: 12 km, wt. 0.3; 15 km, wt. 0.6; and 17 km, wt. 0.1.

2.2 AREAL SOURCE ZONES

Four primary source zones were delineated for non-fault-specific seismic sources within 100 km of the site (Model A - Figure SBK-2). These are the West Walker Lane, the East Walker Lane the Basin and Range, and a Local Zone within the site area that was not characterized by local faults. These source zones were chosen based on a review of the seismicity reports for the southern Great Basin (Appendix SBK-1) and an interpretation of the seismotectonic implications of the distribution of seismicity in the historical catalog (Appendix SBK-2). These seismotectonic interpretations also affected our evaluation of tectonic models, particularly with regard to neotectonic deformation (Appendix SBK-2). These zones represent those areas that remain after the areas of regional fault sources have been removed. These areas include the location of potential maximum background and other earthquakes not associated with particular fault sources. The maximum background earthquake and the rate of recurrence for this event are assessed from the activity rates estimated from the recurrence rates of the declustered seismicity in these areas.

In addition, a subregion in the East Walker Lane (Rock Valley) is defined to account for regional variability in seismicity (Model B - Figure SBK-3). The region is defined on the bases of tectonic, geologic, and seismicity rate criteria, as described below. The branch of the logic tree that includes this subregion is assigned a weight of 0.3 (Figure SBK-4), with 0.7 assigned with the interpretation of no subregion.

The Death Valley-Furnace Creek-Fish Lake Valley fault zone defines the boundary between the West Walker Lane and East Walker Lane areal source zones. Defining the western zone as the West Walker Lane is not strictly correct, as it is more appropriately termed the Eastern California shear zone, but we use this terminology. This area includes the active faults and deformation west of the Furnace Creek system. Given that seismic network coverage in this region has been sparse throughout the history of seismic monitoring, we cannot rely on the quality of earthquake locations and hypocentral depth estimates as much as we can for other areas that have denser network coverage and thereby more accurate hypocenter locations.

The East Walker Lane zone is defined on the west by the Furnace Creek system and on the east by a change in tectonic style to a dominantly range-bounding, normal-fault environment

(Figures SBK-2 and -5). We include the generally northeast-striking faults of the Sarcobatus Flat region within this source zone, although this particular fault is characterized separately (Figure SBK-5). We attribute the high level of seismicity in this zone to deformation associated with the high slip rate on the Death Valley-Furnace Creek-Fish Lake Valley fault system. Also included in this source zone is the seismicity and northeast-striking faults in the southern and central NTS region, as well as the extension of the Rock Valley fault zone east into the Spotted Range east of NTS. This zone continues south in a general northwest-southeast orientation, with its eastern border defined by the Las Vegas Valley shear zone. We also defined this zone to include only tectonic, or tectonically triggered, earthquakes, avoiding the seismicity catalog problems related to the Basin and Range source zone to the east, where nuclear testing has been isolated. The East Walker Lane zone accounts for much of the seismicity that trends outboard, to the east, from the Furnace Creek system, as well as most of the northeast-striking fault systems that we interpret to represent neotectonic deformation most likely driven by the strain in the Eastern California shear zone. The most prominent concentration of seismicity in this zone is that associated with the Rock Valley fault zone (Appendix SBK-2). We have also defined the Death Valley area as a subzone within the East Walker Lane zone in our optional configuration (Figure SBK-3). We believe that this subzone may be more likely to produce earthquakes that may cause ground motion on the order of 0.1 g at Yucca Mountain; this is evidenced by the 1992 Little Skull Mountain earthquake. Also, several $M > 3.5$ events have taken place in the Rock Valley fault zone during the past several years, and a general concentration of seismicity is associated with the fault zone. Given this difference in activity during the past tens of years in this subzone as compared to the East Walker Lane zone as a whole, the separation as a subzone enables us to address the possible stationarity of seismicity, although we cannot establish whether this subzone will be a persistent source of activity during a 10,000-year interval.

The Basin and Range zone was established to capture the north- to north-northeast-striking, predominantly low strain rate, range-bounding fault systems within 100 km of the site. We also included the nuclear testing areas of the northern and eastern NTS in this areal source in order to contain explosion-triggered recurrence bias exclusively to the Basin and Range source zone. A subzone was established around Pahute Mesa and Yucca Flat to account for the fundamental problem of separating tectonic earthquakes from explosion-triggered seismicity. These nuclear testing areas may tend to overestimate the hazard by including

seismicity that is directly triggered by explosions. Although the triggered earthquakes ultimately may have occurred without underground testing, including them could overestimate the long-term activity rate. That is, the seismicity in this subzone during the period of nuclear testing may not be representative of the long-term tectonic strain rate in the area. To account for this interpretation, we computed activity and b-values only for the periods that preceded nuclear testing. We consider any increase in seismicity in this region during the recent period of testing to be directly related to the testing, but we also recognize that any attempt to remove all of the dependent events would not be representative of the activity rate. Indeed, attempts were made to separate natural from explosion-triggered seismicity in the catalog compilation, yet we are unconvinced that this can be done adequately. Furthermore, the explosion-triggered seismicity could be a manifestation of tectonic strain, with the explosions representing a triggering stress just as the Landers earthquake was a trigger for the Little Skull Mountain earthquake. To address the uncertainty of adequately accounting for the effect of explosion-triggered seismicity in the NTS we consider two options. The first option is that the aftershock removal process has adequately removed seismicity triggered by the NTS explosions and no adjustment is necessary. This option is assigned a weight of 0.6 (Figure SBK-4). The second alternative is to adjust for the effect of the NTS explosions by removing seismicity within the NTS region post 1950 from the calculation of seismicity rates within the Basin and Range Province. A Pahute Mesa-Yucca zone was defined (Figure SBK-3) that encompasses the area of NTS explosions. All seismicity post 1950 was removed from this area in the calculation of the seismicity rate. This option was assigned a weight of 0.4 (Figure SBK-4).

We also consider the possibility of a background earthquake within the local (site) area. This Local Zone includes the volume not characterized by the recurrence estimates for the local faults themselves: central Crater Flat and the footwalls of the Bare Mountain and Paintbrush Canyon faults. Because the local faults account for most of this volume, we consider the size of the maximum background earthquake in the Local Zone to be less than that for the other areal source zones. This is based simply on the observation, particularly from the distribution of faulting and aftershock activity for the 1986 M 6.3 Chalfant earthquake (our model background earthquake; Appendix SBK-3), that earthquakes of only a limited size could occur in the remaining volume without being accounted for in the recurrence estimates for the local faults. It would be double counting to apply the same magnitude distribution for the

maximum background earthquake from the other areal source zones. The weighting for the maximum background earthquake for the Local Zone is: M 6.2, wt. 0.2; M 6.0, wt. 0.6; M 5.6, wt. 0.2.

2.2.1 Catalogs and Declustering

We have used the 100-km catalog developed for this project to assess recurrence (a- and b-values) for areal source zones. Two declustering algorithms were applied to the 100-km combined catalog. Weighting was applied relevant to the stability of the b-value estimates for the subregions. The algorithms, from Veneziano and van Dyck (1985) and Youngs *et al.* (1987), apply different assumptions in determining the definition of a foreshock or aftershock and therefore behave differently for different regions. The Veneziano and van Dyck (1985) method establishes a baseline activity rate within a given distance from a main shock, then uses this baseline activity to define the local rate. The Youngs *et al.* (1987) method removes dependent events based on several time and distance criteria. The activity rates and completeness levels range significantly within the 100-km region. We consider that earthquakes within the 100-km region follow a power-law distribution in magnitude. The declustering algorithm that returned a distribution that better represented this power-law scaling was considered more efficient in removing dependent events for that region. The Veneziano and van Dyck algorithm appeared to be more stable when applied to the Little Skull Mountain aftershock zone and therefore was weighted higher in the East Walker Lane zone, whereas the Youngs and others method generated smoother recurrence curves when applied to sparse background regions. The weighting listed below and shown in Figure SBK-4 reflects our assessment of the b-value estimates. For the West Walker Lane zone, we weight the Youngs and others declustering algorithm at 0.7, assigning 0.3 weight to the Veneziano and van Dyck algorithm. Our weighting is the opposite for the East Walker Lane zone, for reasons noted above. However, we weight the Youngs and others approach more heavily for the Rock Valley subzone (Youngs *et al.*, 0.7; Veneziano and van Dyck, 0.3). The Basin and Range zone receives weights of 0.4 for the Youngs and others algorithm and 0.6 for the Veneziano and van Dyck approach; identical weights are assigned in the Pahute Mesa-Yucca Flat subzone.

The catalog completeness intervals that we have adopted for assessing earthquake recurrence parameters are based on review of those developed by I.G. Wong (handout to team seismologists at SSC Workshop 4) and on examining the seismicity of the region. The adopted intervals are: **M** 2.5 to <3.5, 1979 to date; **M** 3.5 to <4, 1961 to date; **M** 4 to <5, 1934 to date; **M** 5 to <6, 1900 to date; **M** ≥ 6, 1880 to date. Furthermore, we considered earthquakes that occurred in close proximity to the regional faults to be associated with those faults. These events were not counted in computing the seismicity rate for the regional zones.

A truncated exponential fit using the maximum likelihood method of Wiechert (1980) was applied to all magnitude distributions. A minimum magnitude of 2.5, where this magnitude was above the completeness level, was used to determine the b-values and activity rates, otherwise the minimum completeness level was applied.

2.2.2 Maximum Background Earthquake

We define a background earthquake as any earthquake in a non-fault-specific zone that does not display primary surface rupture. Primary surface rupture is defined as surface faulting taking place on the actual fault plane that radiated the seismic energy at depth. DePolo (1994) reported on the maximum background earthquake for the Basin and Range. There is a range of earthquake magnitudes over which primary fault rupture has been observed in the Basin and Range (S. K. Pezzopane and T. E. Dawson, USGS, written communication, 1996). Distinguishing primary from secondary faulting from the historical data base (S. K. Pezzopane and T. E. Dawson, USGS, written communication, 1996) is difficult because of the variability of instrumental seismicity throughout the historical period and the details of the observations following many of these earthquakes. Actually, isolating the fault plane at depth may require a detailed analysis of the aftershock zone. Also, some interpretation is involved in distinguishing primary from secondary surface faulting based on field data.

The principal factor that affects the development of primary surface faulting is the distribution of seismic moment release with depth. For example, primary surface displacement was observed for the 1950 M 5.6 Fort Sage, California, earthquake, but no primary or secondary surface faulting was mapped following the 1992 M 5.6 Little Skull Mountain earthquake; events of the same magnitude. Although no instrumental record of

sufficient quality to resolve the moment release at depth was available for the Fort Sage event, we consider that faulting must have been shallow, based on its surface expression. This is in contrast to the 1992 Little Skull Mountain earthquake, for which faulting was confined to between 12 and 6 km depth (K. Smith, SSC Workshop 2). It is not surprising for such depth ranges that there was no expression of surface faulting for this earthquake. Therefore, there is a range of earthquake magnitudes over which primary faulting may occur, but above which primary faulting will always be seen. If primary rupture has occurred on faults of Quaternary age, then we assume that these structures have been identified in our assessment of specific fault sources described below, and listed in Tables SBK-2 and -4. Our weighting of the magnitude of the maximum background event is developed to account for the distribution of magnitudes over which no primary surface rupture is observed and for the incompleteness of the historical record and the subjectivity in the interpretation of primary versus secondary surface faulting.

The largest earthquake exhibiting no primary surface faulting in the historical record in the Western United States was the 1925 M 6.6 Clarkston, Montana, event (dePolo, 1994). This earthquake, which occurred in an area having a greater crustal thickness than does the southern Great Basin, is anomalous in the compiled record of background earthquakes (dePolo, 1994). We have taken the possibility for this event into account by assigning a low probability for an M 6.6 maximum event for our areal source zones, although we consider the tectonic and structural environment of the Montana area to be quite different from that of the southern Great Basin. We further consider that the 1986 M 6.3 Chalfant Valley earthquake is a better analog for a maximum background earthquake in the southern Great Basin (Appendix SBK-3). This earthquake produced significant surface faulting, but none that can be considered to have occurred on an extension of the causative fault plane from seismogenic depth to the surface; we interpret that no primary faulting occurred. Although right-lateral offsets of as much as 10 cm were observed along the White Mountains fault zone, a major Holocene fault zone (Lienkaemper *et al.*, 1987), the Chalfant main shock rupture did not occur on this fault. Some of the fault slip, particularly small-event slip, seen in trench data for the local site faults at Yucca Mountain, may represent this type of secondary faulting.

Another moderate-sized earthquake in the southern Great Basin that we consider an analog for the background earthquake is the M 6.1 May 1993 Eureka Valley, California, earthquake.

Although smaller than the Chalfant event, it also produced surface displacements that were most likely not primary surface faulting. In contrast to strike-slip faulting during the Chalfant earthquake, the Eureka Valley earthquake showed nearly pure normal slip on a structure oriented north-south (Peltzer and Rosen, 1995; Massonnet and Feigl, 1995). Given the similarity in faulting style, this earthquake is considered more representative of the surface expression of moderate-sized, normal-faulting earthquakes ($M < 6.5$) that may occur in the site area.

The maximum background earthquakes for the West Walker Lane, East Walker Lane, Basin and Range, Rock Valley, and Pahute Mesa-Yucca Flat zones and subzones are: M 6.6, wt. 0.1; M 6.4, wt. 0.2; M 6.3, wt. 0.5; and M 6.2, wt. 0.2. The maximum background earthquake for the Local Zone is: M 6.2, wt. 0.2; M 6.0, wt. 0.6; M 5.6, wt. 0.2.

2.3 REGIONAL FAULT SOURCES

Fault sources within 100 km of Yucca Mountain were identified based on Piety (1995), Anderson *et al.* (1995a, b), H. L. McKague *et al.* (CNWRA, written communication, 1996), W. R. Keefer and S. K. Pezzopane (USGS, written communication, 1996), and S. K. Pezzopane (USGS, written communication, 1996). Of the faults identified as relevant to ground shaking hazard (S. K. Pezzopane, USGS, written communication, 1996), potentially seismogenic faults were identified as those showing evidence of displacement since mid-Quaternary time (730 ka) or associated with historical seismicity (Table SBK-1). In many cases, only a small part of a potentially seismogenic fault is identified as having middle or late Quaternary slip; however, in assessing maximum magnitude, we treat the entire mapped fault as a seismogenic zone. We did not characterize as seismic fault sources a number of structures identified as Type I faults (H. L. McKague *et al.*, CNWRA, written communication, 1996). These are summarized in Table SBK-2, along with our bases for not including them. The areal extent of a fault source was estimated based on the uncertainties of the fault dip (see below) and the potential combinations of related local structures that may be included in the recurrence for that source. For example, we combined the Buried Hills and Emigrant Valley South faults for analysis. We also consider multiple combinations of behavior of the Death Valley-Furnace Creek-Fish Lake Valley faults, as discussed below.

The uncertainty in the length and down-dip width of the regional fault sources was established to account for any uncertainty in the locations of small-magnitude earthquakes in the regional catalog, which could be removed before estimating the background seismicity rates.

The location and extent of each fault source are given on Figure SBK-5; data on each fault source are compiled in Table SBK-1, with sources and annotations to clarify the bases for interpretations included in the table. Uncertainties in fault extent are included in the fault lengths in Table SBK-1. One example of a fault length that involves considerable uncertainty is the northern extent of the Ash Meadows fault zone. The fault is shown by Piety (1995) as extending north to the vicinity of the Rock Valley fault. However, the Ash Meadows fault is collinear with the so-called Gravity fault (Fridrich, 1997) to the north, and the inferred sense of downthrow is consistent, suggesting continuity of the structures. North of the Rock Valley fault the gravity anomaly continues, but the scarps that characterize the Ash Meadows fault are not present. Therefore, two alternative models for the northern extent of the Ash Meadows fault are considered in the analysis, with the longer fault (100 km) incorporating the Gravity fault north of the Rock Valley fault. Given the lack of evidence for Quaternary slip on this part of the possible fault, we assign a low weight (0.1) to this total fault length.

Approaches to evaluating maximum magnitude and recurrence for these regional fault sources follow. Detailed notes regarding individual faults are included with Table SBK-1. Many long faults, such as the Death Valley and Furnace Creek sources, probably rupture only in part during individual earthquakes (i.e., are segmented, either in a persistent or non-persistent manner). However, we find insufficient data to adequately characterize or model segmentation explicitly on these structures. The Southern Death Valley, Death Valley, Furnace Creek, and Fish Lake Valley faults form a nearly continuous zone of right-lateral shear with a total length on the order of 300 km. It is possible that the fault system behaves as a coherent unit, comparable to portions of the San Andreas fault, although it is much more likely that the constituent faults rupture independently. In considering the combined faults, we recognize the Death Valley normal fault as a pull-apart structure within a right-lateral shear system (which we will call the Death Valley system for simplicity). We assess possible combinations of faults explicitly in our analysis. Although there is mapped continuity among all of the faults of the Death Valley system (e.g. Jennings, 1994), it is extremely unlikely that

they rupture together (R. E. Klinger and L. A. Piety, USBR, written communication, 1996). First, the faults have distinct structural and geomorphic signatures (R. E. Klinger and L. A. Piety, USBR, written communication, 1996); second, the connection between the Furnace Creek and Fish Lake Valley faults has not ruptured in the Holocene (Reheis and Sawyer, 1997), suggesting these two faults have not ruptured continuously; and third, there is no historical analog where a strike-slip fault has ruptured through a major pull-apart of the dimensions of Death Valley. Thus we assign a probability of 0.01 to a single linked fault system. We next consider possible sub-linkages, including the Death Valley-Southern Death Valley fault (0.05 likelihood the faults rupture together, again because of lack of historical analogs and distinct geomorphic signature) and the Furnace Creek-Fish Lake Valley system (0.05 likelihood they rupture together, given the large step-over between them and the apparent difference in timing of paleoseismic events, from studies of Reheis and Sawyer, 1997, and R. E. Klinger and L. A. Piety, USBR, written communication, 1996). These two linked fault zones are not conditional; that is, Death Valley and Southern Death Valley can behave as linked faults in our model regardless of the behavior of the Furnace Creek and fish Lake Valley faults, and vice versa. Most weight (0.94 for each fault), however, is assigned to the faults rupturing independently. Details of assessments for each fault are shown in Table SBK-1.

2.3.1 Maximum Magnitude

For regional fault sources, we used various approaches for estimating maximum magnitudes based on various fault rupture parameters (Table SBK-1). These included regression relations based on surface rupture length, surface rupture area, maximum displacement, and average displacement (Wells and Coppersmith, 1994). Approaches were weighted on a fault-specific basis depending on the input needed and the data available for each fault.

Fault length is based principally on the total mapped length of a fault. In many cases, only part of the fault has documented Quaternary slip (e.g., Pahrump fault has Quaternary slip on about 18.5 km of a 50- to 65-km-long fault; Table SBK-1). We treat these faults by placing a low weight on the Quaternary section and a higher weight on the total fault length, reasoning that the *maximum* magnitude would be produced by a rupture of the entire fault, even if that apparently has not happened in the middle to late Quaternary. For the Pahrump fault, then,

we assign a weight of 0.3 to the short, Quaternary fault length, and a weight of 0.7 to the longer, total fault length (which is uncertain between 50 and 65 km).

Fault area is computed by multiplying fault length by down-dip width. We compute down-dip width from the fault dip and the thickness of the seismogenic zone. We lack specific information on dip for most of the regional faults. Thus, we assign fault dip based on type of faulting: normal faults (45 degrees weighted 0.1, 60 degrees weighted 0.8, and 70 degrees weighted 0.1); strike-slip faults (70 degrees weighted 0.2, 90 degrees weighted 0.8); and oblique-slip faults (60 degrees weighted 0.2, 70 degrees weighted 0.6, and 90 degrees weighted 0.2). Our assessment of the thickness of the seismogenic crust was discussed in section 2.1.

We obtain displacement values from surface fault studies appropriate to the individual faults. In general, we use data from paleoseismic studies (trenches, mapping) to identify the largest single-event displacement reported along a fault in estimating maximum (surface) displacement. Given that the regressions used to compute magnitude from displacement are based on surface observations (Wells and Coppersmith, 1994), use of surface data is appropriate. Although one cannot be certain that trenches have identified the true maximum coseismic surface displacement on a fault, the fact that trenches generally are sited at locations that show evidence of large displacement supports our use of these data. Average displacement is obtained from the along-fault variations in slip during a particular event, rather than from measurement of average displacement during repeated ruptures at a site, because it is the former that is the basis of the regression equations. We require at least 5 points, preferably more, along a fault to estimate average displacement, following the observations of Hemphill-Haley and Weldon (1996).

2.3.2 Recurrence

Earthquake recurrence for fault sources is assessed based on the slip rate on the fault as converted to seismic moment rate using fault area and from estimates of paleoseismic return times when available. The slip rate approach generally is preferred because of significant uncertainties in interval data, both because of dating uncertainties and because the paleoseismic events documented on each of the faults for which we can adequately assess

return periods are not all equal in size. For example, one event may have an interpreted displacement of 1.5 m, whereas others at the same trench site show 0.2 to 0.5 m. It is quite likely that not all of these paleoseismic events are the size of the maximum earthquake (*characteristic earthquakes* in the sense of Schwartz and Coppersmith, 1984). In particular, the return periods may overestimate the frequency of occurrence of maximum earthquakes. Quaternary slip rates are preferred over longer-term Tertiary slip rates because the stress regime has changed for many of the structures, especially at and near Yucca Mountain. However, even slip-rate data are unavailable for some of the faults, such as the Buried Hills-Emigrant Valley South fault. In these cases, we constrain the order of magnitude of the slip rate by comparing the topography of the range along which the fault is found with the topography of other ranges in the Basin and Range for which slip rates of bounding faults are known. We further constrain the slip rate if information is available that alluvial geomorphic surfaces of a certain age (for example, middle Quaternary) are or are not displaced. All slip rate estimates are applied to the fault as a whole, even if the estimate comes from a single point; in general, we have insufficient data to characterize the regional faults in more detail.

Both the characteristic (Youngs and Coppersmith, 1985) and truncated exponential (Berrill and Davis, 1980) recurrence models are used to model the relative frequency of various size earthquakes for a given slip rate. We assign a higher weighting to the characteristic type of distribution for range-bounding faults, reasoning that these faults are most analogous to the Wasatch fault and other major faults that fit characteristic distributions. We apply a higher weighting to the truncated exponential distribution for faults that comprise numerous, discontinuous surface traces, reasoning that these are not the continuous kinds of structures on which characteristic earthquakes generally have been recognized. We assign the weighted average b-value obtained for the areal source in which a fault is located to the recurrence curves derived for faults, as there are insufficient earthquakes associated with individual regional fault sources to compute meaningful local b-values. These assessments are listed in Table SBK-1.

In developing recurrence relationship for the local sources we assume that the maximum magnitude assessments described in Section 2.3.1 are the central value for the characteristic magnitude interval (e.g. Youngs *et al.*, 1987). The characteristic events are assumed to be uniformly distributed in the magnitude range M_{max}±¼, such that the upper limit of the

recurrence relationship is M_{max}+¼. For the exponential recurrence model the upper limit is also set at M_{max}+¼. When the overall rate of earthquake occurrence is specified by the recurrence interval of surface-rupturing earthquakes, this recurrence rate was assumed to apply to earthquakes of magnitude greater than or equal to M_{max}-¼.

2.4 LOCAL FAULT SOURCES

We consider faults within the Crater Flat domain of D. W. O'Leary (USGS, written communication, 1996) separately. Data are summarized in Table SBK-3 for all faults and fault combinations to which we assign non-zero weights as being independent seismogenic structures. These include Bare Mountain, North Crater Flat, South Crater Flat, Windy Wash, Fatigue Wash, Solitario Canyon, Iron Ridge, Bow Ridge, Paintbrush Canyon, and Stagecoach Road faults as well as the hypothesized Highway 95 fault (we refer to all but the Bare Mountain and hypothesized Highway 95 faults as the Yucca Mountain—YM—faults).

One issue concerning the Bare Mountain fault that emerged during the PSHA workshops is that the late Quaternary slip rate is less than the summed slip rates across the YM faults. If the Bare Mountain fault is the master structure, and the YM faults are antithetic or secondary, then the slip rate on the Bare Mountain fault should equal or exceed the sum of slip rates on the YM faults. This is a paradox only if one assumes that the 120-kyr of record on the Bare Mountain fault is representative of the average slip rate during the 500 kyr or more of record on the YM faults. However, additional events on the Bare Mountain fault during a 100-kyr period would increase its slip rate to a level comparable to or even greater than the YM faults. With faults such as these, which have extremely long recurrence intervals, one may need 500 kyr or more of paleoseismic record to represent the average slip rate; this is not available for the Bare Mountain fault. Second, some percentage of the extension across the master fault in this area may be accommodated by volcanism and dike injection in the lower crust in Crater Flat, which we consider a very likely scenario (as discussed in the section on tectonic models). This would reduce the slip rate across the master fault, although it may not reduce the slip rate across the antithetic faults. Clearly, several Quaternary volcanic events have accommodated extension in this area. Third, much of the slip on the YM faults occurred during the "ash event," which apparently did not rupture the Bare Mountain fault. If

it was, indeed, tied to volcanism, which we interpret as the most likely explanation, then perhaps this unique event should be subtracted from the tectonic strain rate represented by the YM faults for comparison with the Bare Mountain fault. In that case, the slip rates are comparable.

We also evaluated the following mapped faults in terms of the likelihood they generate independent seismic events: Abandoned Wash (no Quaternary displacement, although some secondary cracking possible); Drill Hole Wash (no Quaternary slip); Dune Wash (no Quaternary slip); Ghost Dance (no primary Quaternary slip); Midway Valley (no primary Quaternary slip); Sundance (no Quaternary slip); and Yucca Wash (no evidence for existence). In several cases we interpret faults as having produced no primary Quaternary slip. The Ghost Dance fault is particularly important in this regard. E. M. Taylor *et al.* (USGS, written communication, 1996a) describe paleoseismic studies along the Ghost Dance fault, and additional information was made available to us during SSC Workshops 2, 3, and 4. We interpret the results of these studies as follows: evidence for ground cracking during the Quaternary is equivocal along the Ghost Dance fault: if there has been ground cracking, it produced minimal or zero surface displacement; net displacement across the fault in the middle and late Quaternary has been undetectable, based on the detailed mapping by W. C. Day *et al.* (USGS, written communication, 1996a), which shows no surface scarps or offsets, and the evidence from surface-exposure dating of Whaleback Ridge that indicates exceptionally low rates of surface erosion. Thus we believe that the likelihood is negligible that the Ghost Dance fault produces independent seismic events above the maximum magnitude assigned to the Local Zone. Our arguments regarding other mapped faults not included in Table SBK-3 are similar.

Several other structures are hypothesized to exist in the Yucca Mountain vicinity; these were discussed by various experts during SSC Workshop 5. We evaluated each of these possible structures, and concluded either that the hypothesized structure does not exist, or that the maximum earthquake would be within the range of activity defined for the areal source zones. These include a volcanic seismic source (except for the possible link between volcanism and the ash event, considered below); a buried fault that aligns along the cones of Crater Flat; and a cross fault trending northwest across Crater Flat. The former involves earthquakes directly caused by basaltic fissure development and extensional events. We use

the evidence of Smith *et al.* (1996) to argue that such volcanic sources produce maximum earthquakes (M ~5.5) below the maximum magnitude we have assigned to the Local Zone. There is no evidence that a buried fault controls the alignment of Black, Red, and Little Cones in Crater Flat. Given the detailed mapping that has been carried out to describe tectonic activity and identify Quaternary fault scarps in Crater Flat, we would expect that if a north-northeast-trending fault existed and were active it would be recognized. No such fault has been recognized, although it is hypothesized in the Rift Model discussed above. We conclude that it cannot be any more active than the cones themselves, indicating no activity in middle or late Quaternary (post the ca. 1 Ma age of the cones). Finally, no evidence supports a hidden or buried strike-slip fault trending northwest across Crater Flat. Little space is available for this or any other structure to be hidden among or beneath the Yucca Mountain faults. Lacking surface expression, such a fault, if it exists, must produce earthquakes below the threshold of surface faulting. We conclude that we have captured all such earthquakes within the magnitude distribution for the Local Zone, and by including a smaller maximum background earthquake to account for such an event in the site area.

2.4.1 Fault Combinations and Simultaneous Ruptures

The possibility that some faults are linked or coalesce at depth and could rupture together during individual earthquakes is considered for the local fault sources based on similarities in rupture behavior or deformation patterns and possible along-strike or down-dip linkages. These are shown on Figure SBK-6 (Table SBK-3). The possible ruptures of the Yucca Mountain faults with each other and with the Bare Mountain fault constitute one group of such linkages. The chance that all local faults (Bare Mountain and YM faults) rupture together is considered, but given a negligible weight, because there is no paleoseismic evidence for simultaneous events involving the Yucca Mountain faults and the Bare Mountain fault. Indeed, the available stratigraphic and geochronologic evidence is inconsistent with simultaneous ruptures on Bare Mountain and all the other faults. Because of likely down-dip structural linkages among the faults, a rupture linkage cannot be precluded, and we note that at least one Bare Mountain rupture also may have involved minor movement on two or more of the block-bounding faults (event W of S. K. Pezzopane *et al.*, USGS, written communication, 1996a). However, combinations of Bare Mountain and other faults are not explicitly assessed in our analysis, because the rupture of other faults appears to

have been secondary, and we consider the simultaneous rupture of all local faults to be a negligible possibility.

We define terms as follows.

A. Coalesced faults. These are faults that branch upward from a common master fault at seismogenic depths. The geometries of coalescence were summarized by Fridrich during SSC Workshop 5; we adopt his approach with minor modifications. We consider a single coalesced master fault for simplicity; we deal with other combinations through our analysis of down-dip area.

B. Linked faults. These are faults mapped as independent structures (with distinct names) and separated by generally short intervals without mapped surface traces, yet having sufficient geometric continuity to make it reasonable to infer that they are linked below the surface as throughgoing structures. We consider three combinations: Paintbrush Canyon + Stagecoach Road + Bow Ridge; Solitario Canyon + Iron Ridge; and South Crater Flat + Windy Wash + Fatigue Wash. Another interpretation of the Solitario Canyon fault is that it can be linked with the Stagecoach Road fault for a few events (within S. K. Pezzopane *et al.* [USGS, written communication, 1996a] scenarios), but the potential seismic contribution already is encompassed by other combinations considered explicitly.

C. Simultaneous rupture. This is a rupture on more than one fault (as mapped at the surface) that occurs either as the result of a single earthquake or, more likely, as subevents during an earthquake that teleseismically would be considered a single event. In effect, a simultaneous event is one in which ground motion is contributed by the subevents, but they are spaced so closely in time as to be contained within the same seismogram. In our analysis this concept is applied principally to the so-called ash event, Scenario U.

Having resolved that all the YM faults and Bare Mountain fault do not rupture simultaneously in an earthquake, we next address fault coalescence and simultaneous ruptures. First, we consider whether all local faults (except Bare Mountain) are cut off by an active detachment. The evaluation is dependent on the tectonic model. We assign zero weight to the possibility of a shallow detachment as an active seismogenic structure and to a deeper detachment as an active seismogenic structure, even though one or both of these may exist within the present tectonic regime. Our reasoning is that, Wernicke's (1995) argument notwithstanding, all major earthquakes in the Basin and Range have occurred on crustal-penetrating faults, even if shallow structures were inferred in the vicinity from seismic

reflection profiling. Thus, in our evaluation, these hypothesized detachment structures affect only down-dip fault extent, which we address separately.

Next we evaluate the likelihoods that all the YM block-bounding faults are coalesced, linked, or independent (Figure SBK-7). The first possibility is that all sole into a detachment between 5 km and the base of the seismogenic crust, a model-driven possibility to which we assign a likelihood of 0.01, in keeping with our evaluation of tectonic models discussed above. Although the seismic reflection data of lines YMP-1 and -2 do not resolve structure at that depth (Brocher *et al.*, 1996), and the best substantiation for a moderate-depth detachment comes from the cross sections produced by Ferrill *et al.* (1996a), the geophysical data provide little evidence to support such a structure.

The second possibility is that all of the YM block-bounding faults are planar or near-planar but coalesce at depth, in either one or two master faults. This is more allowable than the detachment models, given surface fault geometries and dips. However, lacking any direct evidence of fault coalescence, we consider this possibility still very unlikely; we assign it a weight of 0.09.

We distribute the remaining likelihood between two end members--four linked block-bounding planar faults (assigned a weight of 0.4) and planar faults behaving independently (assigned a weight of 0.5). For each fault considered individually, we further assess whether the fault acts as an independent primary source. We assign likelihoods less than 1 for both the Iron Ridge (assigned a weight of 0.1 as an independent seismic source) and Bow Ridge (assigned a weight of 0.4 as an independent seismic source) faults, as discussed in Table SBK-3. In evaluating the alternatives of linked or independent faults, our preferred approaches were to consider fault geometries and the history of linked ruptures (i.e., is it possible that two colinear faults, such as Paintbrush Canyon and Stagecoach Road, have ruptured together some or all of the time?). Most of the scenarios described by S. K. Pezzopane *et al.* (USGS, written communication, 1996a) argue for complex interactions among faults in terms of overlapping ages of rupture events. Many combinations of behavior are possible, and independent activity is the most likely behavior (although complex linkages are considered). We simplify the possibilities by restricting ourselves to the two end members and assigning a slightly higher weight to independent fault ruptures. The front part